BIOACTIVITY OF KAFFIR LIME (*CITRUS HYSTRIX* DC.) LEAF EXTRACT ON GINGIVITIS

WATUNYOO BUAKAEW

A Thesis Submitted to the Graduate School of Naresuan University
in Partial Fulfillment of the Requirements
for the Doctor of Philosophy in Biomedical Sciences
2022

BIOACTIVITY OF KAFFIR LIME (*CITRUS HYSTRIX* DC.) LEAF EXTRACT ON GINGIVITIS

WATUNYOO BUAKAEW

A Thesis Submitted to the Graduate School of Naresuan University
in Partial Fulfillment of the Requirements
for the Doctor of Philosophy in Biomedical Sciences
2022

Thesis entitled "Bioactivity of Kaffir lime (*Citrus hystrix* DC.) leaf extract on gingivitis"

By WATUNYOO BUAKAEW

has been approved by the Graduate School as partial fulfillment of the requirements for the Doctor of Philosophy in Biomedical Sciences of Naresuan University

Oral Defense Committee

..... Chair
(Professor Paul James Brindley, Ph.D.)

..... Advisor
(Associate Professor Kanchana Usuwanthim, Ph.D.)

..... Co Advisor
(Assistant Professor Supaporn Sangouam, Ph.D.)

..... Co Advisor
(Chanai Noysang, Dr.rer.nat.)

..... Co Advisor
(Rungnapa Sranujit, Ph.D.)

..... Internal Examiner
(Assistant Professor Yordhathai Thongsri, Ph.D.)

..... External Examiner
(Wannaporn Ittiprasert, Ph.D.)

Approved

.....
(Associate Professor Supawitoo Sookpeng, Ph.D.)

Dean of the Graduate School

Title BIOACTIVITY OF KAFFIR LIME (*CITRUS HYSTRIX* DC.) LEAF EXTRACT ON GINGIVITIS

Author WATUNYOO BUAKAEW

Advisor Associate Professor Kanchana Usuwanthim, Ph.D.

Co-Advisor Assistant Professor Supaporn Sangouam, Ph.D.
Chanai Noysang, Dr.rer.nat.
Rungnapa Sranujit, Ph.D.

Academic Paper Ph.D. Dissertation in Biomedical Sciences, Naresuan University, 2022

Keywords Citrus hystrix DC., Candida albicans, Macrophage, Gingivitis, Proteomics

ABSTRACT

Gingivitis is an inflammatory condition of the gingival tissue. The treatment focuses on both reducing inflammation and removing dental plaque. Chlorhexidine mouthwash is one of the effective choices used as anti-plaque in dental care. However, long-term usage can cause several side effects. This study aimed to develop a safer mouthwash containing *Citrus hystrix* DC. (kaffir lime, KL) leaf extract, and elucidate the mechanism of action in terms of anti-inflammatory and anti-*Candida* activities. This study identified the active compound, lupeol that can inhibit the production of pro-inflammatory cytokines (IL-1β, IL-6, and TNF-α), the expression of NF-κB- and NLRP3-associated genes (*NOS2*, *NFKB1*, *IL1B*, *IL18*, *NLRP3*, and *PYCARD*) and proteins (COX-2, phospho-IκBα, and NF-κB p65) in macrophages. Additionally, the proteomic analysis revealed proteins that might be involved in the anti-*Candida* activity under β-citronellol treatment, including oxidative stress response (Sod1p, Gst2p, and Ddr48p), cell wall (Als2p, Rbt1p, and Pga4p), and ATP synthesis-associated proteins (Atp3p, Atp7p, Cox1p, and Cobp). Finally, the mouthwash containing KL leaf extract was developed, and the efficacy was evaluated in 47 participants with mild-to-moderate gingivitis. The reduction of GI, PI scores, and the colony counts of *Staphylococcus* spp. and *Candida* spp. were found after 14-day usage. From the results, the mouthwash showed the potential to be used in conjunction with proper oral hygiene to help alleviate gingivitis.

ACKNOWLEDGEMENTS

This thesis could not have been accomplished without the financial support from Research and Researchers for Industries (RRI) Ph.D. Scholarship (PHD60I0053), Thailand Science Research and Innovation (TSRI), and Khaolaor Laboratories Co., Ltd. I would like to express my deepest appreciation to my thesis advisor, Associate Professor Dr. Kanchana Usuwanthim, for allowing me to pursue my doctorate and providing invaluable guidance throughout this thesis. Besides my advisor, I would like to thank the rest of my thesis committee, Dr. Rungnapa Sranujit, Dr. Chanai Noysang, Assistant Professor Dr. Supaporn Sangouam, and Assistant Professor Dr. Yordhathai Thongsri, for their assistances, encouragements, and comments.

I would like to thank Assistant Professor Dr. Nungruthai Suphrom and Dr. Witsanu Sonyot for their assistances with the chemical structure identification, as well as Mr. Sucheewin Krobthong, and Mr. Yodying Yingchutrakul, for helping me with the proteomic analysis. This thesis would not have been feasible without their counsel and cooperation.

I would also like to give special thanks to my thesis external examiners, Professor Paul Brindley and Dr. Wannaporn Ittiprasert Tanno, for allowing me to be part of an interesting project at George Washington University, leading me to expand my research knowledge and experience.

Finally, words cannot express how grateful I am to my parents, family, and friends for their unending love and support, as well as for pushing me to be the best in all of my endeavors.

WATUNYOO BUAKAEW

TABLE OF CONTENTS

Page

List of tables

Page

List of figures

Page

Chapter I

Introduction

Background and significance of the study

Gingivitis is the inflammation of the soft-tissue area of the gingival epithelium and connective tissue which is most commonly bacterial induced. The characteristics of gingivitis are redness, swelling, and bleeding of the gum (1). According to the periodontal disease survey in Thailand (2017) conducted by the Department of Health, gingivitis is the most common periodontal disease among people 15 years and older (2). Generally, gingivitis is a reversible inflammation that can be achieved with good oral hygiene protocol, such as regular brushing and dental flossing, and improper oral care practice or lack of adequate treatment for gingivitis may increase the risk of developing periodontitis, the severe form of periodontal inflammation that affects the supporting structure of the gingiva. Uncontrolled periodontitis results in attachment loss, alveolar bone destruction, increased tooth mobility, and ultimately tooth loss (3).

Several microbes have been reported to be associated with gingivitis, particularly the bacteria in the species of *Streptococcus*, *Fusobacterium*, *Actinomyces*, *Veillonella*, and *Treponema* (1). There have also been reports of two distinct microbes, *Staphylococcus aureus* (4-6) and *Candida albicans* (7-9), involved in the pathogenesis of gingivitis and periodontitis. The colonization of microbes triggers an immune response in the gingiva through microbial products called pathogen-associated molecular patterns (PAMPs) (10). PAMPs can be recognized by macrophages, phagocytes residing in the gingival tissue, via the receptors, called pattern recognition receptors (PRRs) (11). Another group of molecules derived from host cells that PRRs recognize is damage-associated molecular patterns (DAMPs). DAMPs are also produced along with the inflammatory response and tissue injury (12). The binding of PAMPs and DAMPs by PRRs activate signal transduction via a variety of signaling pathways, including nuclear factor kappa B (NF-κB) (13, 14) and NOD-like receptor protein 3 (NLRP3) inflammasome (15, 16). The activation promotes the release of pro-inflammatory cytokines, such as tumor necrosis factor-alpha (TNF-α), interleukin 1β (IL-1β), and interleukin 6 (IL-6).

Generally, reducing inflammation is one of the primary objectives in the treatment of gingivitis, along with the removal of dental plaque deposits (1). It has also been suggested to use chlorhexidine mouthwash in addition to brushing to reduce the dental biofilm formation (17). However, long-term usage of chlorhexidine mouthwash can cause various side effects, such as tooth staining, dry mouth, and alteration of taste sensations (18). Therefore, developing a mild and gentle mouthwash would be beneficial for gingivitis treatment.

Several studies have been conducted to seek a new source of active compounds from medicinal plants with anti-inflammatory and antimicrobial activities. Kaffir lime (*Citrus hystrix* DC.) is a tropical plant that has been used in Thai traditional medicine for anti-inflammatory therapy. Numerous research projects have been conducted to determine both the anti-inflammatory and antimicrobial properties of the various parts of the kaffir lime plant, including the peel and leaves. The study

by Lertsanitthanakorn et al. (2006) reported that kaffir lime essential oil has an anti-inflammatory effect on inhibiting the 5-lipoxygenase activity with an IC_{50} value of 0.05 g/ml (19). Kidarn et al. (2018) identified an active compound, furanocoumarins, from the peel of the kaffir lime, which suppressed the level of pro-inflammatory mediators, such as nitric oxide (NO), inducible nitric oxide synthase (iNOS), and COX-2 in macrophages (20). For the antimicrobial activity, a study by Kooltheat et al. (2016) showed that kaffir lime leaf crude water extract inhibited the production of *S. mutans* biofilms with a MIC value of 6,250 mg/mL (21). The effect of kaffir lime leaves against *S. aureus* has been reported (22, 23), as well as anti-*Candida* activity (24, 25). However, data on the protein involved in the mode of action of kaffir lime leaf extract in killing *C. albicans* are currently limited and there is a lack of evidence on the NLRP3 inflammasome signaling pathway.

As a result, finding a novel active compound with anti-inflammatory and antimicrobial activities to control microbial biofilm formation and alleviate the inflammation at an early stage would be beneficial in preventing the development of periodontitis. The objectives of this research, therefore, were to investigate the anti-inflammatory and anti-NLRP3 inflammasome activities of kaffir lime leaf extract in macrophages, and, additionally, to elucidate the proteins involved in the mode of action on anti-*Candida* activity using the proteomics approach. We also developed and evaluate the efficacy of a herbal mouthwash containing kaffir lime leaf extract on participants with gingivitis.

Objectives of the study

1. To extract and identified active compound of kaffir lime leaf.
2. To investigate the effect of kaffir lime leaf extract on NF-κB and NLRP3 inflammasome mediated inflammation in human monocyte-derived macrophages.
3. To evaluate the anti-*Candida* activity, as well as identify the protein involved in the mode of action on *C. albicans* using a proteomic approach.
4. To develop a mouthwash-containing kaffir lime leaf extract, and investigate the anti-gingivitis efficacy in gingivitis participants.

Scope of the study

The scope of this study was to develop a mouthwash that contains kaffir lime leaf crude extract to control gingivitis and to discover the biologically active compounds that have anti-inflammatory and anti-*Candida* properties. The experiments were divided into 4 parts: (1) extraction and identification of active compounds from the crude extract using GC-MS analysis, (2) assessment of the identified chemical compound's anti-inflammation and anti-NLRP3 inflammasome activities in human macrophages, (3) investigation of anti-Candida activity using proteomics approach, and (4) development of mouthwash containing kaffir lime leaf extract and evaluation of the efficacy on the subject with mild-to-moderate gingivitis.

Chapter II

Literature review

Inflammation

Inflammation is the body's immune response to pathogens (pathogen-associated molecular patterns, PAMPs) or stress signals (danger-associated molecular patterns, DAMPs). The cellular response is mediated by a range of distinct leukocytes. As illustrated in **Figure 1**, the outcome of inflammation varies according to the inducers. Inflammatory inducers activate the physiological processes that result in diverse forms of inflammation. For instance, an inflammatory response to an infection can stimulate immune cells to defend against microbes, but this mechanism can result in tissue damage, sepsis, and the development of autoimmune disease (26).

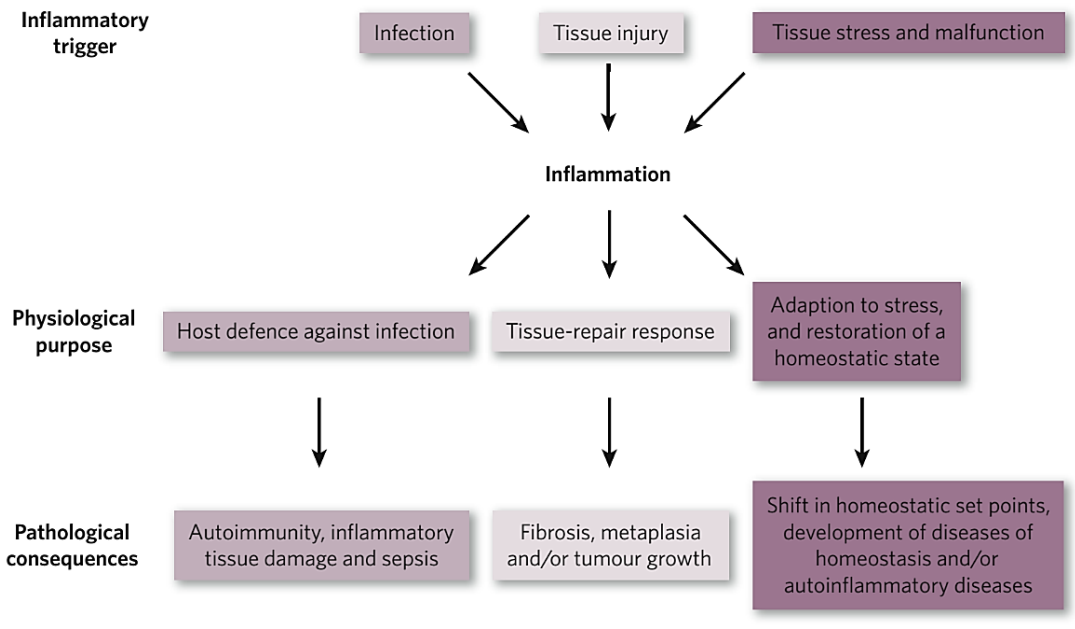

Figure 1 Causes, a physiological response, and the outcome of inflammation (26). The different inflammatory inducers lead to the several ways of host cells' responses to restore homeostasis. However, the uncontrolled inflammatory response can also contribute to various types of pathological consequences.

PAMPs or DAMPs can be recognized or captured by host cells via specific receptors on the cell membrane. The binding results in the stimulation of a variety of pro-inflammatory cytokines and mediators that support the inflammatory process. This is achieved by increasing the ability of phagocytes to eliminate foreign molecules via phagocytosis and by increasing leukocyte recruitment from blood vessels to the site of infection. Following pathogen clearance, the host cell

environment attempts to reestablish homeostasis and progresses to the resolution phase, which ultimately results in tissue repair.

1.1 Inflammatory components

As illustrated in **Figure 2**, inflammation is composed of four components: inducer, sensor, mediator, and effector. Inducers are molecules that can initiate an inflammatory response. The source of exogenous inducers can be derived from both microbial and non-microbial components. On the microbial structure, inducers such as PAMPs can be found. Among them is lipopolysaccharide (LPS), which is found primarily in the cell wall of gram-negative bacteria. Non-microbial inducers include allergens and foreign molecules such as plant pollen. Endogenous inducers, or DAMPs, originate in the body or cells and include tissue damage, tissue stress, and malfunction, as well as endogenous crystals such as monosodium urate crystal (26).

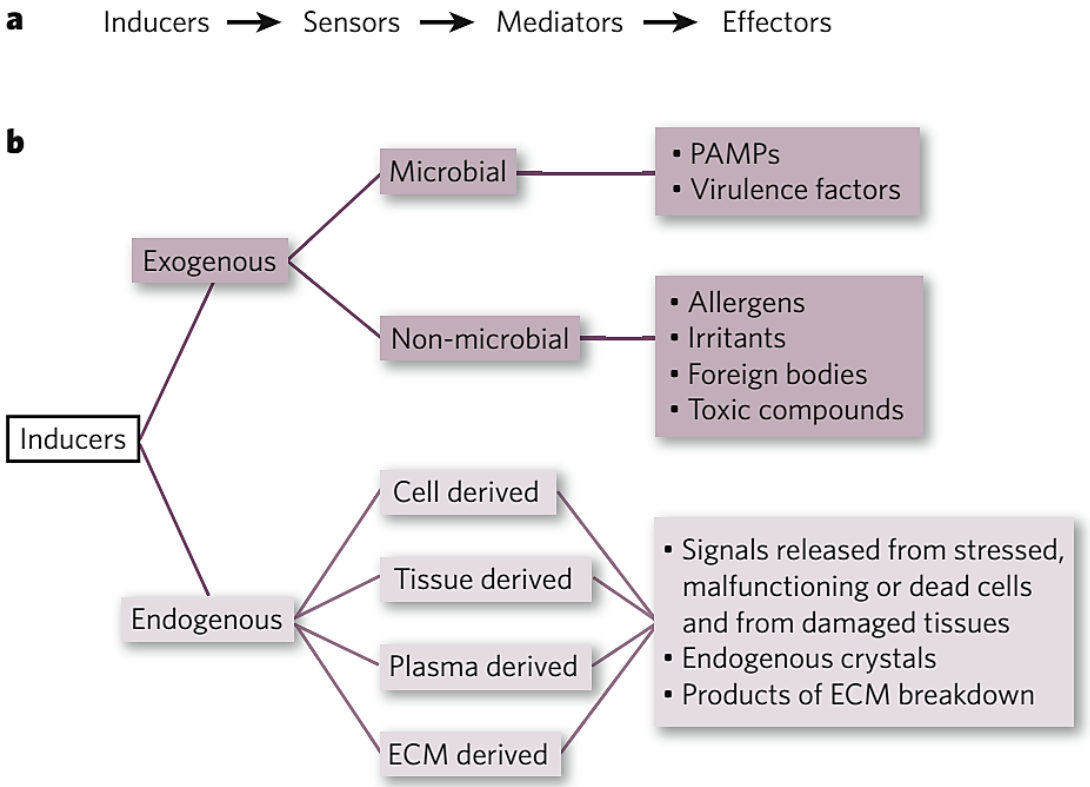

Figure 2 Schematic representative of inflammatory components (26). The four components of inflammation (a), and the different sources and example molecules of inflammatory inducers (b).

The term "sensors" refers to a type of receptor that is capable of recognizing and binding to various types of inducers. For instance, Toll-like receptor 4 (TLR4) is located on the cell membrane of a variety of different types of phagocytes, including monocytes and macrophages. This sensor can bind specifically to LPS and initiate inflammatory responses by stimulating the production of pro-inflammatory cytokines, such as TNF-α, IL-6, and IL-8, and releasing them, as well as increasing the production of COX-2, which contributes to an increase in the level of other lipid mediators during inflammation.

The term "mediators" refers to the chemical components that are released by inflamed cells and tissues. Pro-inflammatory cytokines such as IL-6, IL-8, and TNF-α, pro-inflammatory enzymes such as COX-2, and lipid mediators such as prostaglandin E2, are only a few of the mediators. These mediators can assist the inflammatory process in a variety of different ways, such as enhancing vascular permeability, vasodilation, and the adhesion molecule on the vascular endothelium, which promotes leukocyte extravasation to the infection site. As a result, all mediators are capable of acting on effector cells.

Effectors are tissues and cells which can interact with inflammatory mediators. Numerous leukocyte types, particularly macrophages, can detect inflammatory cytokines via specific receptors and trigger the inflammatory process. Furthermore, vascular endothelial cells can respond to mediators, leading to an increase in vascular permeability. As a result, inflammatory responses differ according to the inducers, sensors, mediators, and effectors, as shown in **Table 1**.

Table 1 The example of inflammatory response in different inducers.

Inducers	Sensor	Mediators	Effectors
Lipopolysaccharide	TLR4	IL-6, TNF-α, and PGE_2	White blood cells and endothelial cells
Allergens	IgE	Vasoactive amines	Endothelial cells and smooth muscle cells
Monosodium urate crystal	NALP3	IL-1β	White blood cells and endothelial cells
Collagen	Hageman factor	Bradykinin	White blood cells and endothelial cells

1.2 Monocytes

Monocytes are white blood cells that comprise 10% of the nucleated blood cells. The major functions of these cells are antimicrobial activity and cytokine production. The cells begin as pluripotent stem cells in the bone marrow and differentiate into colony-forming cells with a high proliferative potential (HPP-CFC) cells upon activation of numerous cytokines. HPP-CFC cells develop into granulocyte-macrophage progenitor cells that generate colony-forming units (CFU-GM). As illustrated in **Figure 3**, the CFU-GM cells differentiate into colony-forming units of macrophage progenitor (CFU-M) cells and mature to monocytes upon activation with a variety of cytokines, including IL-3, granulocyte-macrophage colony-stimulating factor (GM-CSF), and colony-stimulating factor 1 (CSF-1) (27).

Monocytes may be categorized into three subsets based on their LPS receptor (CD14) and Fc gamma receptor III (CD16) expression. The classical monocyte ($CD14^{+}CD16^{-}$) population is the most prevalent (85%). The second subset is non-classical monocytes ($CD14^{dim}CD16^{+}$), which comprised 10% of the population. Intermediate monocytes ($CD14^{+}CD16^{+}$) were a minor subset, accounting for 5% of total monocytes (28, 29).

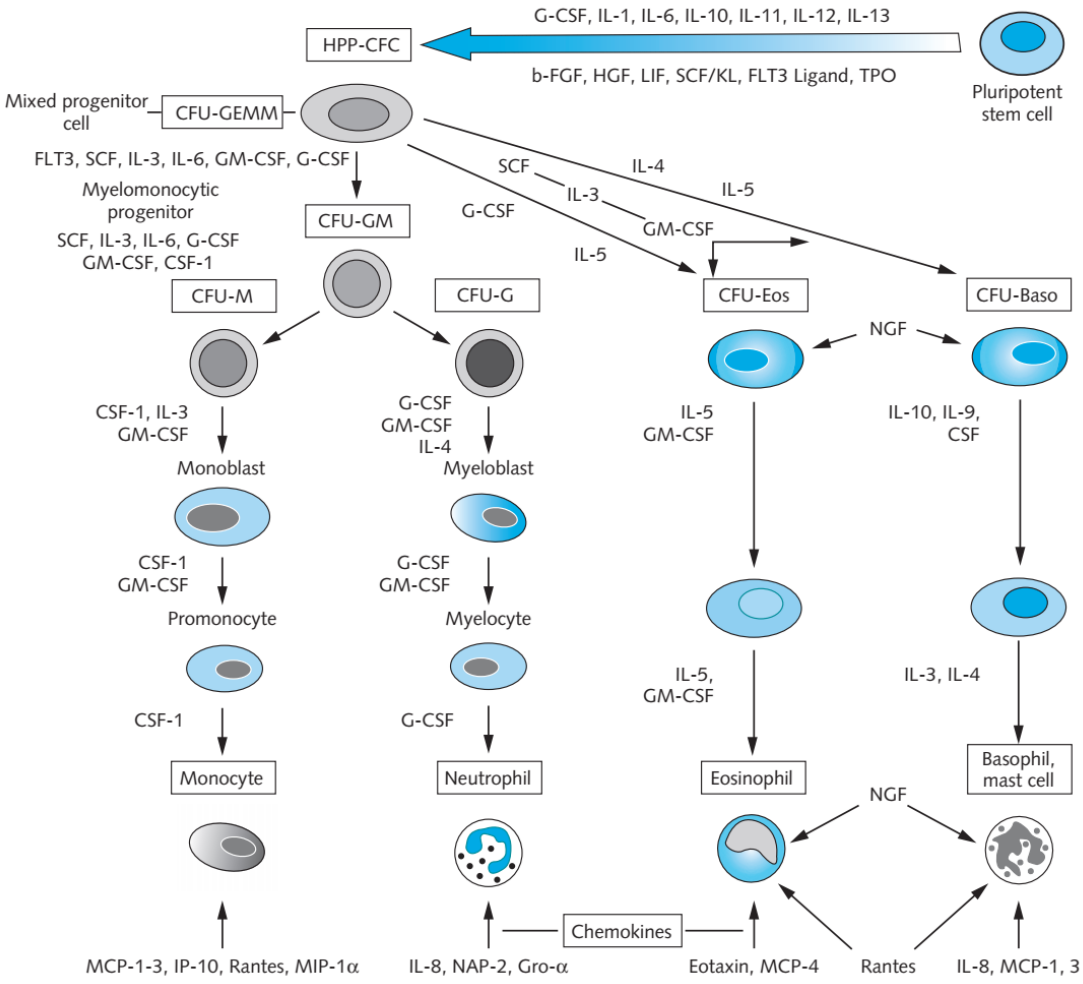

Figure 3 Schematic of hematopoiesis (27).
Monocytes are differentiated from colony-forming unit-granulocyte, erythrocyte, monocyte, megakaryocyte (CFU-GEMM), followed by CFU-GM, and CFU-M in the bone marrow through the activation of several set of cytokines.

1.3 Macrophages

Macrophages are myeloid immune cells that exhibit phagocytosis. Together with monocytes and dendritic cells, these cells were classified as mononuclear phagocytes. Macrophages originate in the bone marrow, as seen in **Figure 4**. Granulocyte/macrophage precursor (GMP) cells mature into macrophage (monocyte)/dendritic cell precursor cells (MDP). MDPs differentiate into common

dendritic cell precursors (CDPs) or common monocyte progenitors (cMoPs), which are the direct precursors of Ly6C^{hi} monocytes. Monocyte extravasation into the bloodstream is reliant on the C-C motif chemokine receptor 2 (CCR2). Inflammatory circumstances activate monocytes to perform pro-inflammatory effector activities or boost DC-like capabilities such as antigen presentation and migration to lymph nodes. Monocytes develop into restorative macrophages during the resolution phase and contribute to tissue restoration. Continuous homeostatic inflammation or remodeling of the tissue enables the growth of monocyte-derived macrophages without passing through the pro-inflammatory effector monocyte stage. Additionally, monocytes differentiate into tumor-associated macrophages that aid in tumor growth and metastasis (30).

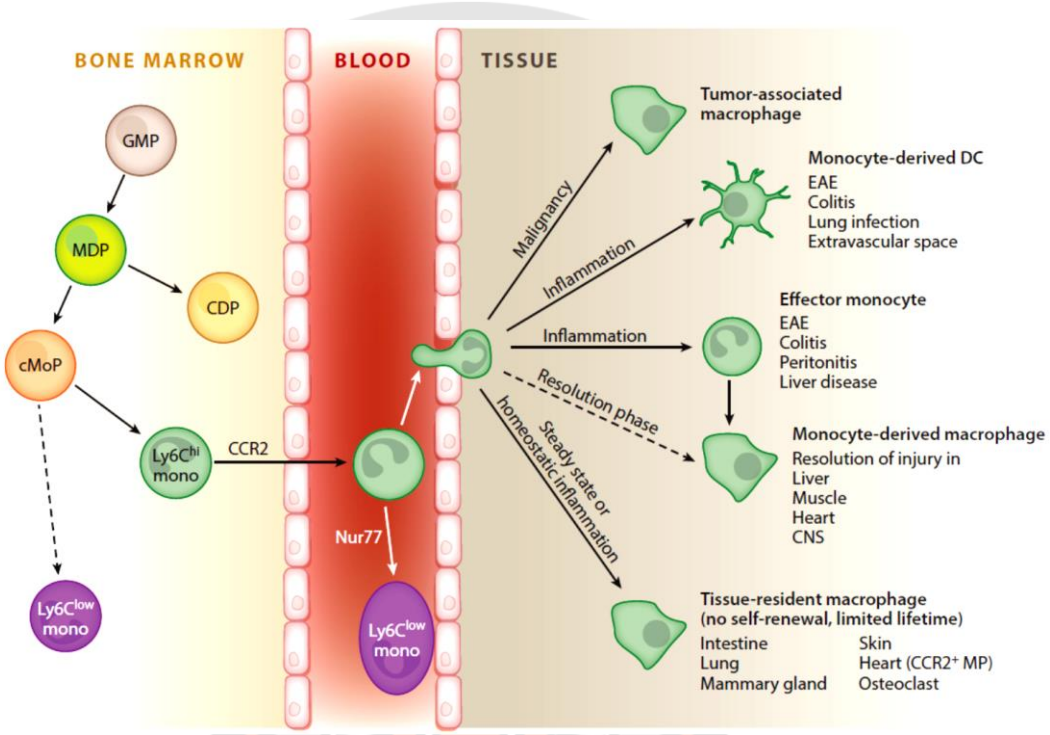

Figure 4 Monocytes-derived macrophages differentiation fates (30).
Macrophages from the bloodstream can be differentiated into different types of specific macrophages depending on the location of tissue and organ.

Macrophages are cells that can become polarized in response to their environment. As a result of their polarization, macrophages are classified into four distinct categories, as seen in **Figure 5** (31).

1. Classical M1 macrophages: these macrophages are derived from inflammatory inducers such as LPS and interferon-gamma (IFN-γ). M1 macrophages contribute to inflammation by producing pro-inflammatory cytokines (e.g., IL-1, IL-6, and TNF-α) and by increasing their capacity for phagocytosis, which results in the

clearance of inflammatory inducers. Various biological markers are expressed by this cell type, including CD80, CD86, and toll-like receptor 4 (TLR4).

2. Alternative M2 macrophages: the cells have the opposite role of M1 macrophages, as M2 macrophages contribute to the anti-inflammatory condition, and can be differentiated by IL-4 and IL-10-induced polarization. This cell type expresses a significant number of cell surface markers, including CD163 and CD206. Additionally, M2 macrophages may be classified into four subgroups.

2.1 M2a (activated by IL-4 and IL-13)

2.2 M2b (activated by immune complexes or TLR agonist)

2.3 M2c (activated by IL-10)

2.4 M2d, this subtype is characterized by the pattern of expression of IL-10^{high} IL-12^{low} profile with tumor-associated macrophages (TAMs) features (31).

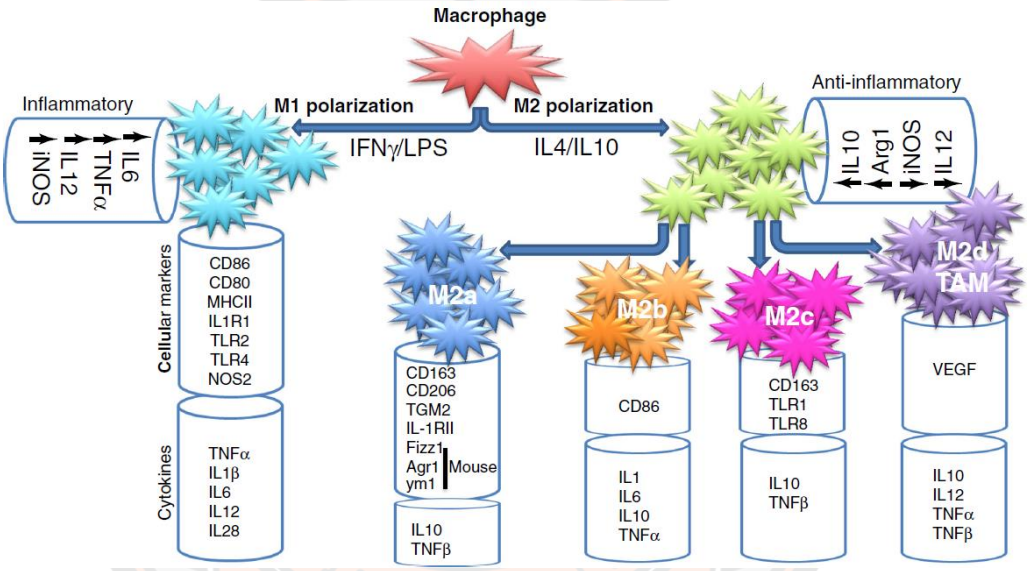

Figure 5 Macrophages subtypes and specific markers (31).
Four subtypes of anti-inflammatory macrophages (M2) have been identified with different cellular markers and cytokine production.

1.4 Toll-like receptor-mediated inflammatory response

Toll-like receptors are type I transmembrane proteins which consist of leucine-rich repeats (LRRs) and are capable of recognizing bacterial and viral PAMPs in the extracellular environment. The extracellular TLRs include TLR1, TLR2, TLR4, TLR5, TLR6, and TLR11. Some types of TLRs are expressed on endolysosomes, such as TLR3, TLR7, TLR8, TLR9, and TLR10. TLRs rely on a cytoplasmic Toll/interleukin (IL) 1 receptor (TIR) domain as a docking site for TIR-containing cytoplasmic adaptor proteins to transmit signals (32). TLRs bind to a variety of ligands, as seen in **Table 2**. Each receptor contributes to the cellular response uniquely. For example, TLR4 binds to LPS. The interaction initiates an inflammatory

signaling cascade inside the cells. The activation leads to the production of pro-inflammatory cytokines and chemokines which enhance the inflammatory response.

Table 2 Toll-like receptors and their ligands (32).

Toll-like receptors	Ligands
1/2	Triacyl lipopeptides
2/6	Diacyl lipopeptides
3	dsRNA
4	Lipopolysaccharide
5	Flagellin
7	ssRNA
8	ssRNA in humans; unclear in mice
9	CpG DNA, malarial hemozoin
10[a]	Unknown
11[b]	Uropathogenic bacteria, *Toxoplasma gondii* profilin-like protein
12[b]	Unknown
13[b]	Unknown

a = Expressed only in humans.

b = Expressed only in mice.

TLR4 activation has been extensively investigated in terms of signaling cascades globally since this receptor is located on most phagocytes and plays a role in the inflammatory process. TLR4 is composed of two domains: the extracellular domain, which forms a heterodimer with MD-2, a ~14-kDa secreted glycoprotein, and the ligand-binding component, as shown in **Figure 6**. The hydrophobic pocket in MD-2 is occupied by LPS, which interacts with TLR4 to relay the signal into the cytoplasmic domain. For the intracellular domain, a set of signaling molecules known as the Myddosome complex is used. As shown in **Figure 7**, the myddosome is composed of six myeloid differentiation primary response 88 (MyD88) death domains, four interleukin-1 receptor-associated kinase 4 (IRAK4) death domains, and four interleukin-1 receptor-associated kinase 2 (IRAK2) death domains (33).

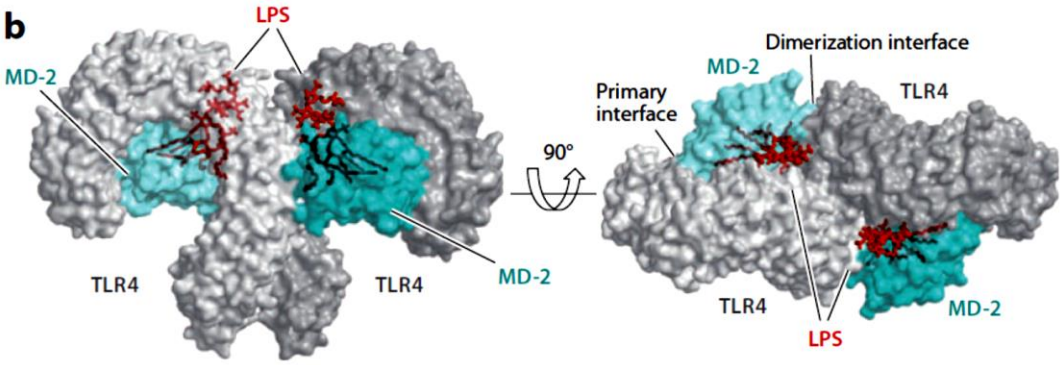

Figure 6 Crystal structure of TLR4-MD-2 complex (33).
TLR4, MD-2, and LPS are in gray, cyan, and red, respectively.

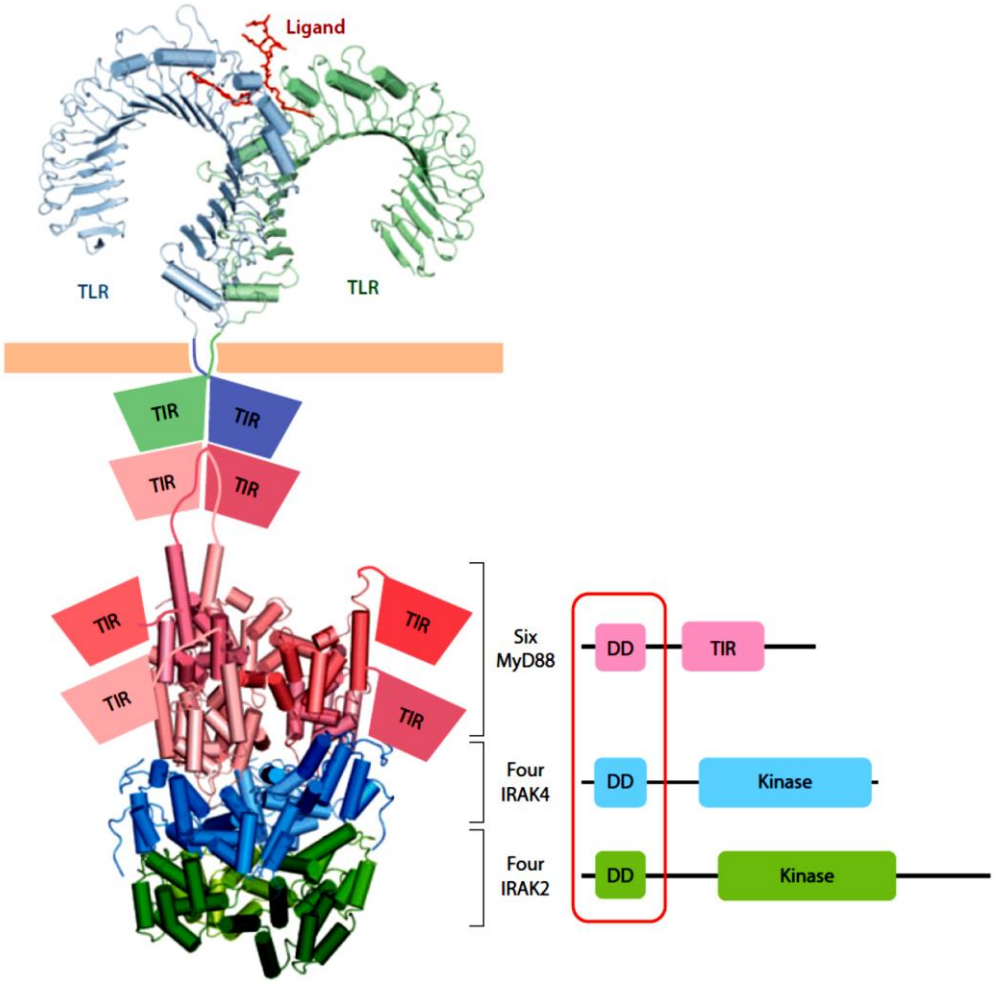

Figure 7 Structure of the Myddosome complex (33).
Six MyD88, four IRAK4, and four IRAK2 death domains make up the myddosome. The parallelogram-shaped TIR domains are illustrated. On the right, a schematic representation of the domain configurations of MyD88, IRAK4, and IRAK4 is presented. Abbreviations: TIR, Toll/IL-1R homology; TLR, Toll-like receptor; DD, death domain.

TLR4 is expressed on a wide variety of cell types but is particularly abundant on leukocytes such as monocytes and macrophages. TLR4 recognizes LPS derived from bacterial components and activates transcription factors such as nuclear factor kappa beta (NF-kB) and mitogen-activated protein kinase (MAPK). The activation leads to an increase in the encoding of inflammatory genes. All of these inflammatory genes are translated into a variety of inflammatory cytokines that are released by inflammatory cells in response to bacterial infection.

LPS binds to TLR4, and the coreceptor MD-2 initiates interactions between the TLR4 cytoplasmic domain and the toll/IL-1 receptor (TIR)-containing adaptor proteins, which include myelin and lymphocyte protein (Mal), MyD88, and TIR-domain-containing adapter-inducing interferon-β (TRIF)-related adaptor molecule

(TRAM). MyD88 interacts with IRAK4 and requires its kinase activity to interact with IRAK1 and IRAK2. Further, the MyD88–IRAK complex interacts with the ubiquitin ligase TRAF6 to form polyubiquitin chains that activate the IKK complex for transcription of NF-κB and ERK-dependent genes. Ubiquitin ligases (cIAP1 and cIAP2) recruited to the TLR4 signaling complex govern signaling component translocation to the cytoplasm, where activation of transforming growth factor beta-activated kinase 1 (TAK1) begins a MAPK cascade that increases gene expression. TLR4, which is activated at the plasma membrane, is endocytosed but can signal within the endosomal compartment via the adaptors TRAM and Toll/IL-1 Receptor (TIR)-domain-containing adapter-inducing interferon-β (TRIF). As shown in **Figure 8**, the kinase and ubiquitin ligase combination of receptor-interacting serine/threonine protein kinase 1 (RIP1) and pellino E3 ubiquitin protein ligase 1 (Peli1) activate NF-kB by interacting with TRIF, whereas TANK binding kinase 1 (TBK1) and TRAF3 stimulate IRF3-dependent transcription.

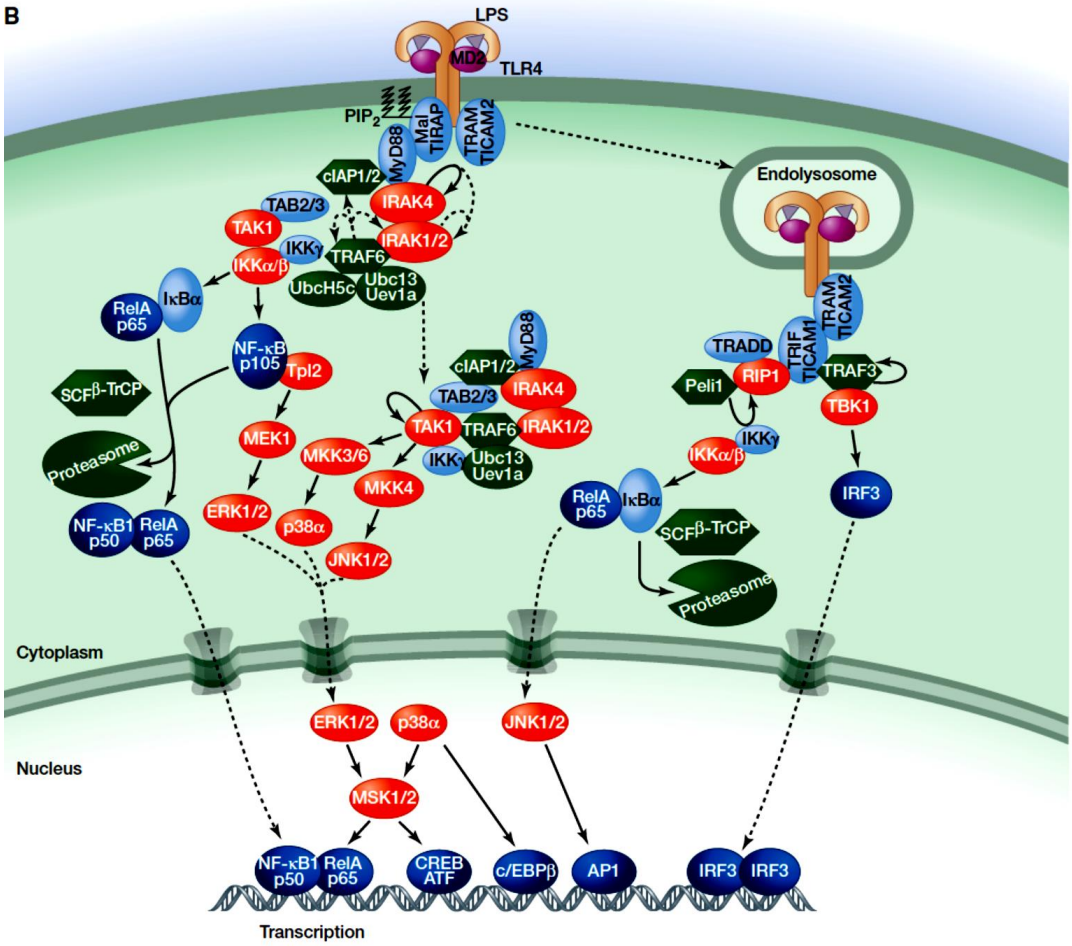

Figure 8 Signaling pathway of TLR4 (32).
The binding of LPS to TLR4 triggers the interaction of signaling molecules, leading to upregulated pro-inflammatory gene expression. Red: a molecule with kinase activity, light blue: molecule containing carboxy-terminal leucine rich repeat, dark blue: transcription factor, green: other molecules without kinase activity.

As shown in **Figure 9** activation of the TLR4-MD2 complex results in the upregulation of several genes within the cells, most notably the pro-inflammatory cytokines, as well as enzymes involved in the production of pro-inflammatory mediators. Furthermore, activation of TLR4 signaling results can lead to an increase in the expression of additional genes implicated in the inflammatory process, including those involved in leukocyte recruitment, cell adhesion, and vascular consequences. As a result, signal transmission in the TLR4 pathway may be a potential target for identifying anti-inflammatory strategies (32).

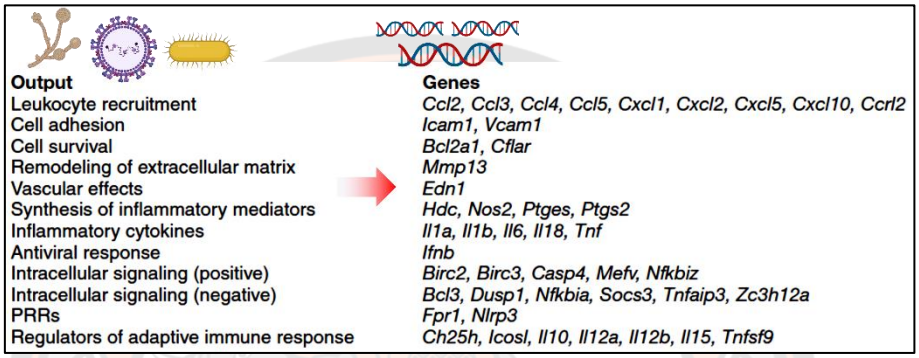

Figure 9 Genes associated with TLR4 signaling activation (32).

1.5 Cytokines

Cytokines are small proteins that cells produce to interact with or affect other cells. Cytokines can function in a variety of ways: they can be secreted and have an impact on secreted cells (autocrine), they can be released and have an effect on adjacent cells (paracrine), or they can have an effect on distant cells (paracrine). Numerous cell groups create cytokines, but the primary makers are helper T cells (Th) and macrophages (34).

1.5.1 Pro-inflammatory cytokines

Pro-inflammatory cytokines are primarily generated by macrophages in promoting inflammation. Numerous studies have shown that pro-inflammatory cytokines such as IL-1β, IL-6, IL-18, and TNF-α play a critical role in the pathophysiology of inflammatory-related conditions.

1) IL-1β

IL-1β is expressed in a broad variety of tissues and cells, including macrophages. IL-1β is synthesized as a 269-AA precursor protein and is processed to the C-terminal 153-AA mature form by caspase-1, which is activated in inflammasomes. Two IL-1 receptors are found on the cell surface: IL-1 type 1 receptor (IL-1R1) and IL-1 type 2 receptor (IL-1R2). The binding of IL-1β to IL-1R1 required the forming of a heterodimer with the IL-1 type 3 receptor (IL-1R3) (also known as IL-1RAcP), along with IRAK and MyD88. IL-1R1 induces inflammatory responses and has been demonstrated as being expressed on the cell surface of T cells, fibroblasts, epithelial cells, and endothelial cells. Another receptor, IL-1R2, is found

to be expressed in hematopoietic cells, including B cells, mononuclear phagocytes, polymorphonuclear leukocytes, and bone marrow cells (35).

2) IL-6

IL-6 can be produced by several cell types, including mononuclear phagocytes, T-cells, B-cells, fibroblasts, endothelial cells, keratinocytes, hepatocytes, and bone marrow. IL-6 communicates via binding to the IL-6 receptor (IL-6R) chain (gp80, CD126) and the signaling component gp130 (CD130). The function of IL-6 includes the acute phase response, B cell proliferation, and thrombopoiesis. In addition, its synergistic effect on T cells when combined with IL-1 and TNF.

3) IL-18

IL-18 is critical for host defense against a variety of pathogenic microbes because it significantly increases the production of IFN-γ, nitric oxide (NO), and reactive oxygen species (ROS) in phagocytes. IL-18 exerts its effects through its receptor, IL-18R, which is a member of the IL-1R family. The receptor is comprised of two parts; an IL-18R chain (IL-18R1, IL-1Rrp) and an IL-18R accessory protein (IL-1RAcPL). The intracellular region contains a TIR domain in common with TLR, MyD88 binds to TIR and activates to deliver a signal into the cell (36).

4) TNF-α

Several types of cells can produce TNF-α, including, macrophages, monocytes, T cells, mast cells, natural killer cells (NK cells), and fibroblasts. TNF-α transmits its signal through one of two receptors: TNFR1 (CD120a) or TNFR2 (CD120b). TNFR1 is expressed on a variety of cell types, whereas TNFR2 is mostly found on leukocytes and endothelial cells. TNF-α performs a variety of functions, including initiating inflammation, cell death, and pain (37).

1.5.2 Anti-inflammatory cytokines

Anti-inflammatory cytokines are a class of immunomodulatory cytokines that are engaged in regulating or suppressing inflammation and re-establishing immunological homeostasis.

1) IL-10

IL-10 is an anti-inflammatory cytokine that inhibits the inflammatory response by several pro-inflammatory cytokines. Although macrophages, dendritic cells, B cells, and T cells can all release IL-10, the primary source of IL-10 is T cells. IL-10 transmits the signal through the IL-10R1 and IL-10R2 receptors. IL-10 functions by inhibiting the synthesis of pro-inflammatory cytokines and inhibiting the expression of MHC and co-stimulatory molecules, both of which are necessary for cell-mediated immunity (38).

2) Transforming growth factor (TGF)-β

TGF-β is composed of five distinct isoforms (TGF-β1 to TGF-β5). TGF-β produces cells including lymphocytes, monocytes/macrophages, and

platelets. TGF-β has many functions, including suppressing the synthesis of pro-inflammatory cytokines, inhibiting the activity of macrophages and T cells, and antagonizing macrophage nitric oxide production. TGF-β transmits the signal via attaching to its serine and threonine kinase receptors on the cell membrane, the type II (TRII) and type I (TRI) receptors (39).

1.6 Cyclooxygenases

Cyclooxygenases (COX; prostaglandin G/H synthase) are the enzymes that catalyze the bis-dioxygenation of arachidonic acid (AA) and subsequent reduction to prostaglandin (PG) G2 and PGH2. COX-1 and COX-2 are the two isoforms of cyclooxygenases. COX-1 and COX-2 are 576 and 581 amino acid homodimers, respectively. Both enzymes include three oligosaccharides with a high mannose component, one of which assists in protein folding. A fourth oligosaccharide found only in COX-2 controls its degradation. Considering the 60% sequence similarity between COX-1 and COX-2. COX-1 is produced constitutively in most tissues, and its role is to produce PGs that are required for homeostasis activities, including gastric cytoprotecting and hemostasis. COX-2 is primarily involved in the creation of PGs during the inflammatory process and carcinogenesis (40).

1.7 Inflammasome

The inflammasome is defined as a multicomplex protein that is located in the cytoplasm of the cells. The inflammasome signaling pathways play a critical part in an inflammatory response and coordinate the host's defensive mechanism against invading microorganisms. Inflammasome signaling is assembled in response to a broad variety of PAMPs and DAMPs. Pattern-recognition receptors (PRRs) involved in inflammasome activation include the nucleotide-binding oligomerization domain (NOD), the leucine-rich repeat (LRR)-containing protein (NLR) family members NLRP1, NLRP3, and NLRC4, as well as the proteins missing in melanoma 2 (AIM2) and pyrin. These receptors are some of the PRRs that perceive the signals that activate the inflammasome through caspase-1; known as the canonical inflammasome. By contrast, the activation of the inflammasome mediated by caspase-11 in mice and caspases-4/5 in humans is classified as a non-canonical inflammasome. The activation of the inflammasome leads to an inflammatory response mediated by caspases and the release of the key cytokines; interleukin-1β (IL-1β) and interleukin-18 (IL-18). Eventually, the inflammasome signaling cascade can result in pyroptosis cell death (41).

1.7.1 NLRP3 inflammasome

NLRP3 (NOD-, LRR-, and pyrin domain-containing protein 3) is a sensor located on macrophages, monocytes, dendritic cells, and splenic neutrophils. As shown in **Figure 10**, NLRP3 is composed of two components: a sensor and an effector. The sensor is a tripartite protein composed of three subunits: an amino-terminal pyrin domain (PYD), a central NACHT domain, and a carboxy-terminal leucine-rich repeat domain (LRR domain) (42). An apoptosis-associated speck-like protein containing a caspase-recruitment domain (ASC) has two protein interaction domains: a PYD at the amino terminus and a caspase recruitment domain at the

carboxy-terminus (CARD). The NACHT domain has ATPase activity, which is required for the self-association and function of NLRP3. By folding back onto the NACHT domain, the LRR domain is considered to produce autoinhibition. Caspase-1 is the effector component, consisting of an amino-terminal CARD, a central large catalytic domain (p20), and a carboxy-terminal small catalytic subunit domain (p10) (43).

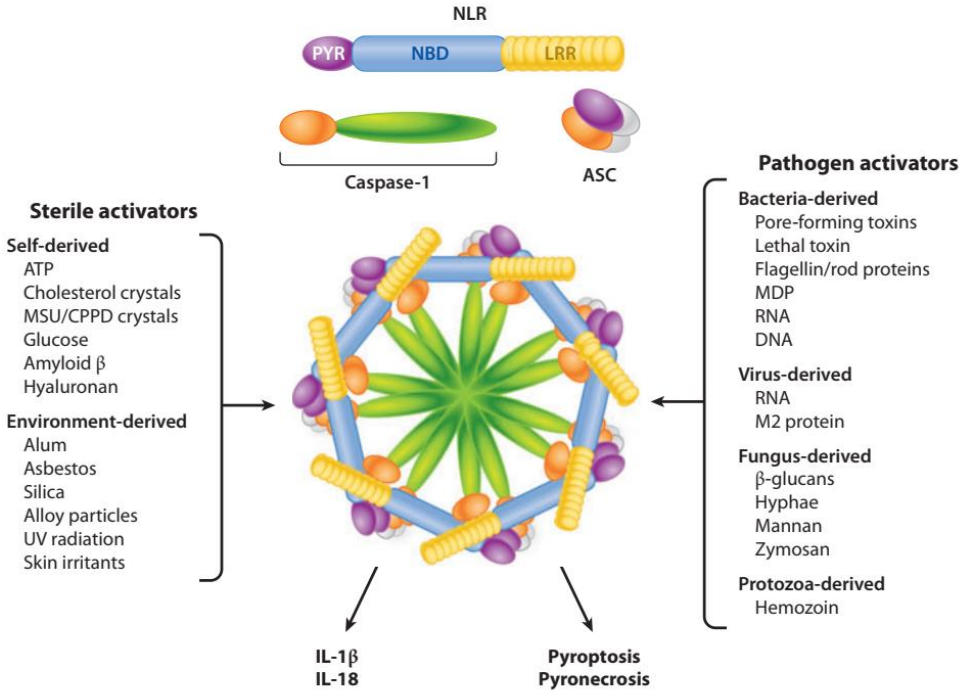

Figure 10 The structure of the inflammasome and its inducers (42).
Sterile and pathogen activators are the two main categories of inflammasome activators. Self-derived or DAMPs, such as ATP and glucose, are examples of sterile activators. PAMPs, also known as pathogen activators, can be produced by bacteria, viruses, fungi, and protozoa. The inflammasome's activation results in the release of IL-1β and IL-18 as well as the cell death processes pyroptosis and pyronecrosis.

The activation of the NLRP3 inflammasome requires two steps, as seen in **Figure 11**. The priming signal can be derived from cytokines, PAMPs, and DAMPs molecules, such as LPS, particulates, crystals, and ATP. Through the NF-κB signaling pathway, the binding of inducers and receptors results in the overexpression of NLRP3 inflammasome components such as pro-IL-1β, pro-IL-18, NLRP3, and caspases. These inducers initiate downstream signaling processes such as K^+ efflux, Ca^+ flux, lysosomal disruption, mitochondrial reactive oxygen species (mtROS) generation, cardiolipin relocalization to the outer mitochondrial membrane, and the release of oxidized mitochondrial DNA (Ox-mtDNA). Viral RNA is another inducer that can activate NLRP3 via the mitochondrial antiviral signaling protein (MAVS) on the outer membrane of the mitochondria. Following these processes, the

inflammasome oligomerizes and activates caspase-1 which, when activated, begins cleaving pro-IL-1β, pro-IL-18, and Gasdermin D into mature forms (GSDMD). The N-terminal GSDMD molecule inserts into the cell membrane, generating a pore and inducing pyroptosis, which is described as cytoplasmic swelling, early plasma membrane rupture, nuclear condensation, and internucleosomal DNA breakage. The cytoplasmic material is excreted into the extracellular space, where it is believed to enhance inflammatory and repair responses (43).

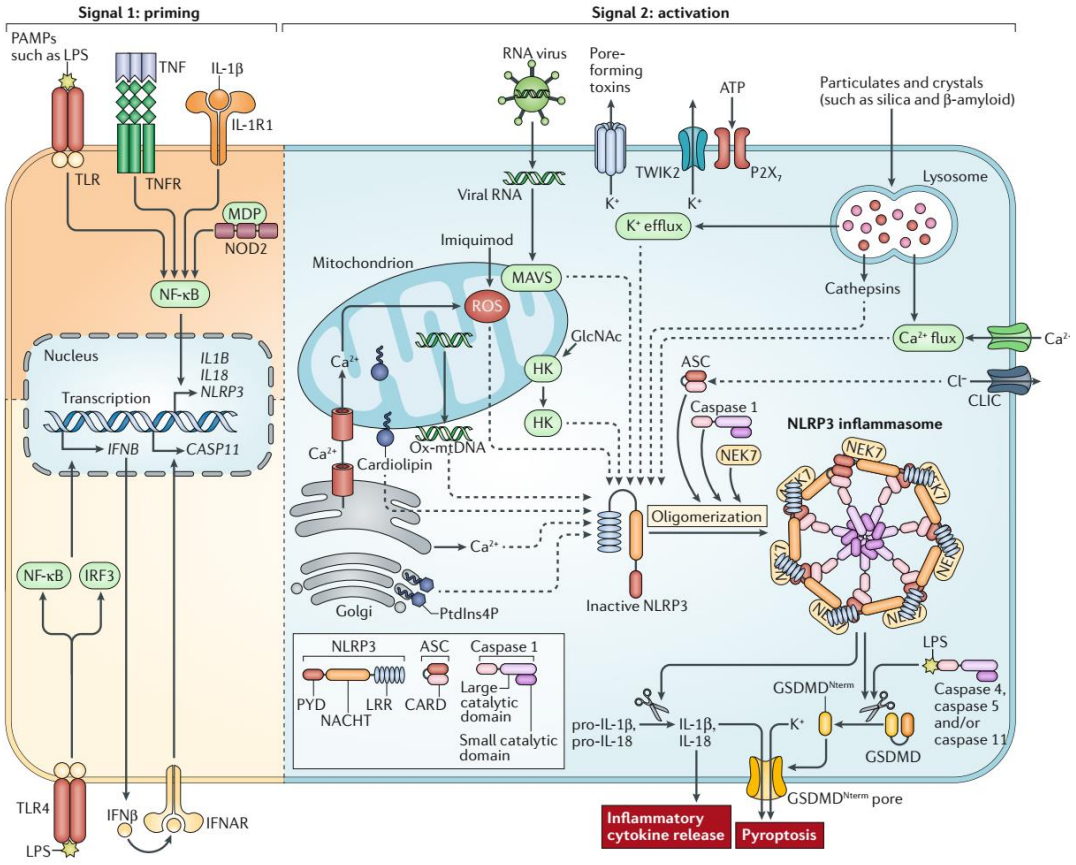

Figure 11 NLRP3 inflammasome signaling pathway (43).

The activation of NLRP3 requires two signals: priming and activation signals. The priming signal is provided by PAMPs or cytokine, leading to the upregulation of NLRP3 inflammasome-associated genes. The activation signal provided by various sources, including DAMPs (ATP, particulates, and crystal), the efflux of K^+ and Ca^+, RNA virus, and ox-mtDNA, resulting in oligomerization of NLRP3 inflammasome. The formation of inflammasome activates caspases to cleave immature form of cytokines and GSDMD into a mature form. The formation of GSDMD pore can eventually induce the pyroptosis cell death. CARD, caspase recruitment domain; CLIC, chloride intracellular channel protein; GlcNAc, N-acetylglucosamine; GSDMDNterm, GSDMD amino-terminal cell death domain; HK, hexokinase; IFNAR , IFNα/β receptor ; IL-1R1, IL-1 receptor type 1; LRR , leucine-rich repeat; MDP, muramyl dipeptide; NEK7 , NIMA-related kinase 7; NF-κB, nuclear factor-κB; P2X7

, P2X purinoceptor 7; PtdIns4P, phosphatidylinositol-4-phosphate; PYD, pyrin domain; TNFR, tumor necrosis factor receptor; TWIK2, two-pore domain weak inwardly rectifying K^+ channel 2.

Oral microbiome

Oral microbial communities vary from those identified at other body sites and are among the most diversified in terms of community composition. Firmicutes, Proteobacteria, Actinobacteria, and Bacteroidetes are the dominant phyla discovered, with various degrees of representation in distinct ecological niches inside the oral cavity, with the most distinct variation being between shedding epithelial (oral mucosa) and non-shedding surfaces (tooth-adherent biofilm). Over 600 common taxa have been described in the oral cavity at the species level. Interestingly, tooth-adherent microbial communities are among the most diverse and abundant and have been found to create sophisticated structurally organized biofilms (11).

Due to the diversity of bacteria found in the oral cavity, bacteria can be classified approximately into two groups: gram-positive and gram-negative bacteria. The essential distinction between these two groups is in the cell wall structural component, as illustrated in **Figure 12**. Gram-positive bacteria have thick peptidoglycan coatings ranging in thickness from 30–100 nm. Additionally, gram-positive bacteria contain numerous different compounds such as lipoteichoic acid, teichoic acid, and lipoprotein. While gram-positive bacteria have a simpler cell wall structure, gram-negative bacteria have a more complicated cell wall structure. Gram-negative bacteria have an exterior membrane composed of lipopolysaccharide with a thin layer of peptidoglycan connecting the inside and outer membranes through lipoprotein (44).

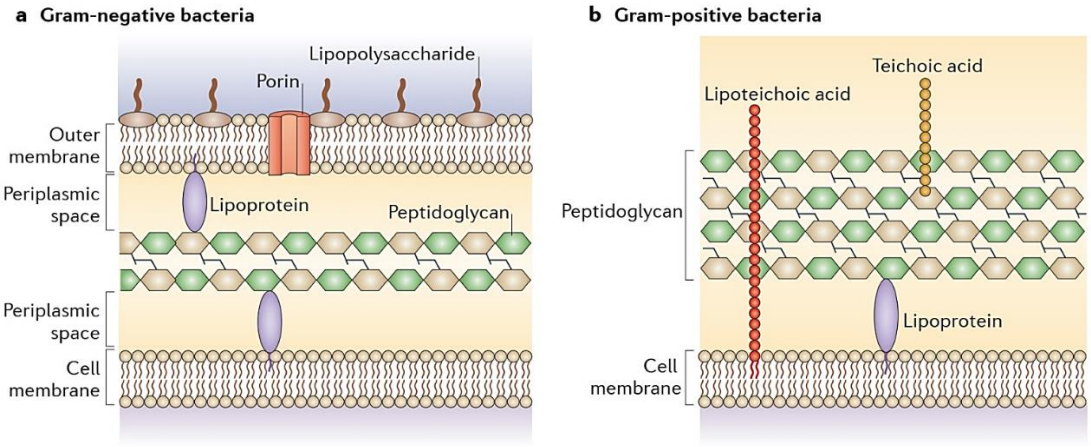

Figure 12 The structure of the cell walls of Gram-positive and Gram-negative bacteria (44).

The cell wall of Gram-negative bacteria consists of a thin layer of peptidoglycan in the periplasmic space between the inner and outer lipid membranes (a), and Gram-positive bacteria have a single lipid membrane surrounded by a cell wall composed of

a thick layer of peptidoglycan and lipoteichoic acid, which is anchored to the cell membrane by diacylglycerol (b).

Although the oral cavity is home to a great diversity of microorganisms, the distribution of microflora is not random. The majority of species prefer certain sites over others due to the unique local environment provided by certain regions, such as the anaerobic environment provided by the periodontal pocket. As illustrated in **Figure 13** (45), several bacterial species populate various parts of the mouth cavity. *Streptococcus* species appear to be found in all sites, including the hard palate, tongue, and saliva. *Streptococcus* spp., along with *Actinomyces* spp., *Haemophilus* spp., *Capnocytophaga* spp., *Veillonella* spp., and *Neisseria* spp., is one of the major pioneering bacteria species that adhere to the tooth surface. Bacterial species that colonize early aid other bacterial species in occupying space and gaining an advantage in subsequent competition with other species. As a result, bacteria communities in the oral cavity develop biofilms, which are described as oriented aggregations of microorganisms connected or to a surface and coated in extracellular polymeric substances (EPS) produced by the bacteria themselves. This biofilm can shield microorganisms from potentially harmful conditions, such as antibiotics.

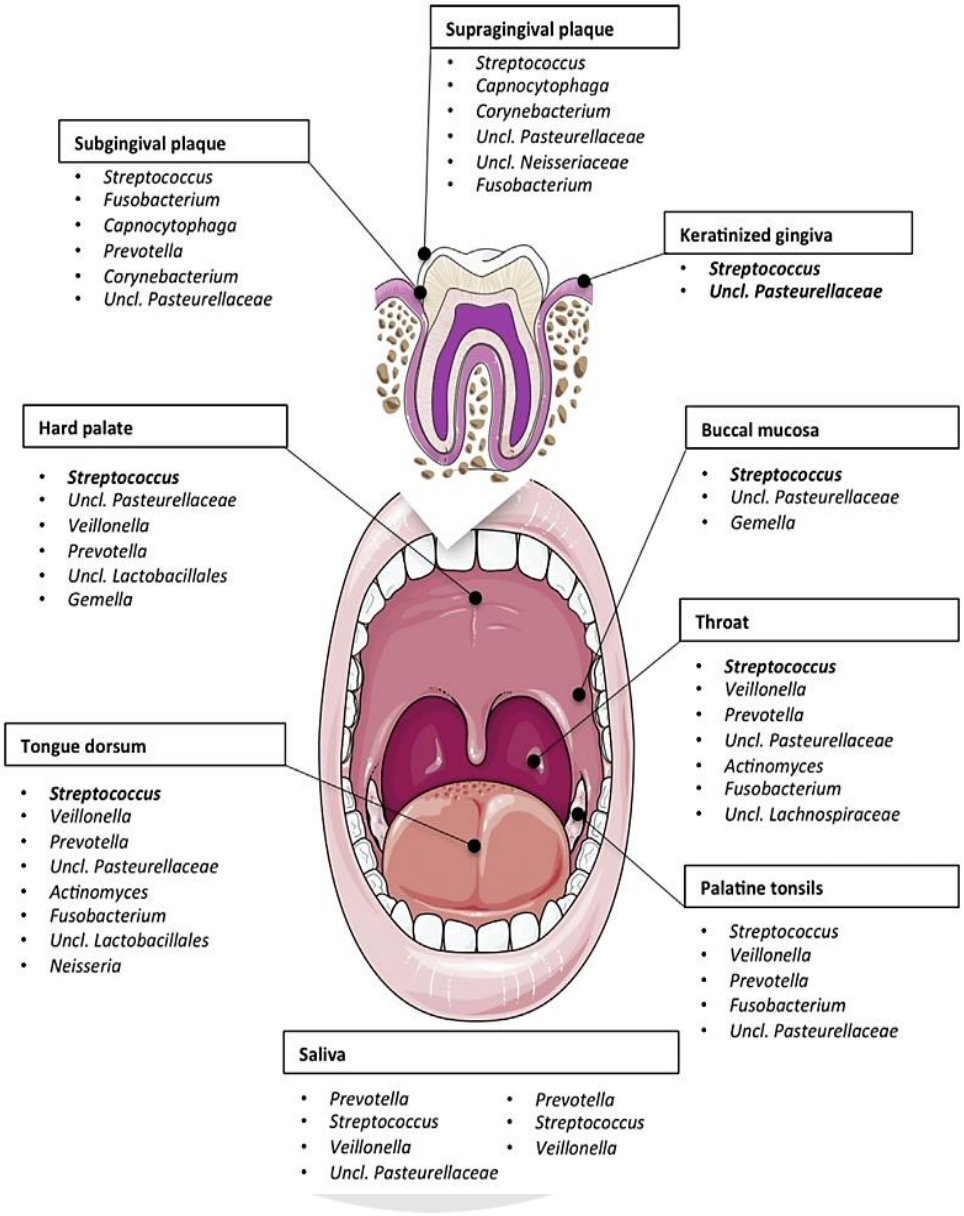

Figure 13 The oral cavity is colonized by a variety of bacterial species (45). The example of bacterial genus and their localization in the different sites in the oral cavity. In the gingival plaque, the frequently identified genus included *Streptococcus*, *Fusobacterium,* and *Capnocytophaga* spp.

2.1 Oral biofilm formation

Biofilms are defined as an organized population of microorganisms adhered to a surface and entwined in an extracellular polymeric matrix. Bacteria are encased in extracellular polymeric substance (EPS), a biopolymer that bacteria secrete (46). Biofilms are composed primarily of water, 5% microbial material, 2% DNA and RNA, and 2% proteins. The composition of a biofilm is determined by the type of microbe and the surrounding environment. When bacteria develop a biofilm, they can

control gene expression to adapt to changes in the environment (47). Oral biofilms are unique from other biofilms in that they are formed by bacteria adhering to host salivary glycoproteins. As illustrated in **Figure 14**, the biofilm generation process is comprised of four phases.

- Pellicle creation; the first phase is the attachment of acquired pellicle components to the clean surface of the teeth, such as proline-rich proteins, amylase, lysozyme, histatin, peroxidase, mucin, and also bacterial components, such as lipoteichoic acid.
- Initial adhesion; some planktonic bacteria may identify binding proteins in the acquired pellicle, such as -amylase and proline-rich glycoproteins/proteins, and attach to the pellicle. Following binding, the pioneer bacteria release EPS, which aids in the bacterium adhesion to the salivary pellicle.
- Maturation; when the pioneer bacteria connect, those early colonizing bacteria provide specialized binding sites for later bacterial colonization, either directly or indirectly via salivary glycoproteins binding to the pioneer organisms, so promoting the growth of biofilm. *Fusobacterium nucleatum*, *Treponema* spp., *Tannerella forsythensis*, *Porphyromonas gingivalis*, and *Aggregatibacter actinomycetemcomitans* are examples of later binding bacteria. Mature biofilms often have numerous porous layers and water channels that provide crucial nutrients to the bacteria.
- Dispersion; cells can be dispersed from the biofilm in single cells or clusters. There are two plausible explanations for biofilm dispersion: 1) due to nutritional scarcity at the original site, which forces bacteria to seek additional resources elsewhere; and 2) due to saliva fluid shear force (48, 49).

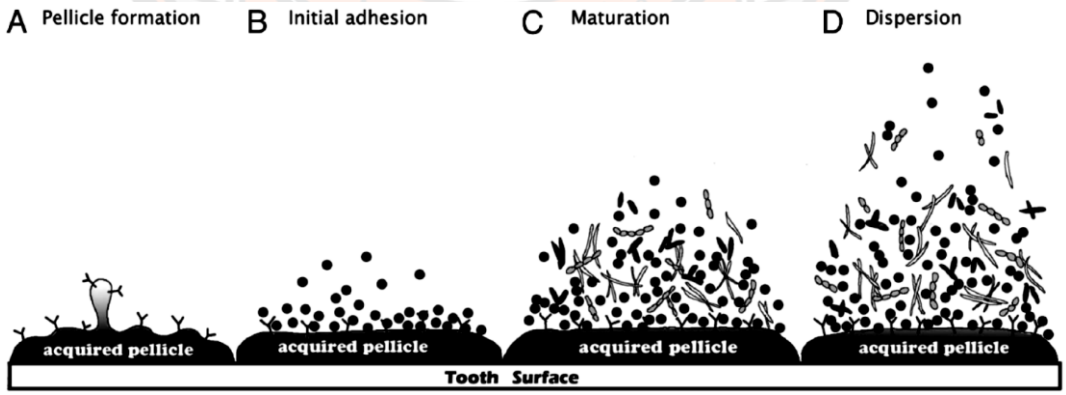

Figure 14 Oral biofilm formation (48).
The pellicle is a thin layer of salivary glycoproteins adhered to a tooth surface (A). Pioneer bacteria in saliva adhere to acquired pellicle by recognizing their binding proteins (B). Various bacterial species congregate and develop into biofilms (C). Bacteria disperse from the biofilm surface and spread to colonize new site (D).

2.2 Immune cells in oral mucosal barrier

Gingiva is one of the locations in the oral cavity that is densely populated with immune cells such as neutrophils, mononuclear phagocytes, granulocytes, and lymphocytes, as demonstrated in **Figure 15**. These cells are critical in bacterial infection, inflammation, wound healing and maintaining oral health balance. In response to bacterial infection, gingival mononuclear phagocytes, including dendritic cells, macrophages, and monocytes, are attracted to the gingiva. Further, given the high level of barrier damage occurring at this site and the potential for rapid healing, all of these cells may engage in continuous wound healing and repair (11).

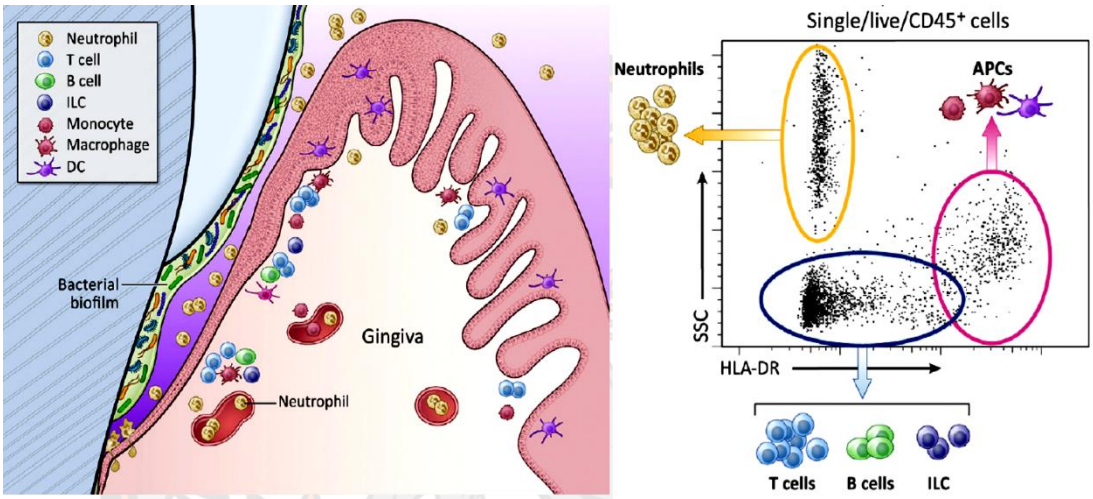

Figure 15 The immunological network of the gingiva (11).
Several types of immune cells located in the gingival tissue respond to the bacterial biofilm, including phagocytic cells (neutrophils, macrophages, monocytes, and dendritic cells (DC)), and lymphocytes (T cells, B-cells, and innate-lymphoid cells (ILC)).

Gingivitis

Gingivitis is the inflammatory condition of the gingival tissue, which strongly affects the soft tissue of the gingival epithelium and connective tissue (15). Among all the periodontal diseases, gingivitis is considered to be the most common. The most frequent variants are a response to bacterial biofilm or are bacterial-induced. Clinical appearances of gingivitis are characterized by swelling, redness, tenderness, a shiny surface, and bleeding upon gentle probing. Gingivitis is a reversible inflammatory condition with good oral hygiene. However, many patients fail to seek medical attention because the symptoms of gingivitis in its early stages are commonly painless. Without proper treatment, the inflammation can progress to periodontitis, the chronic inflammation which can be described by loss of epithelial tissue, alveolar bone, and ligament (1). The clinical appearances of gingivitis and periodontitis are shown in **Figure 16**. The inflamed gingiva can be seen in the central incisor teeth in early gingivitis as shown in **Figure 16b** (black arrow). For periodontitis (**Figure 16c**),

chronic inflammation of the gingival tissue creates periodontal pockets (black arrow) that are a hallmark of the disease (50, 51).

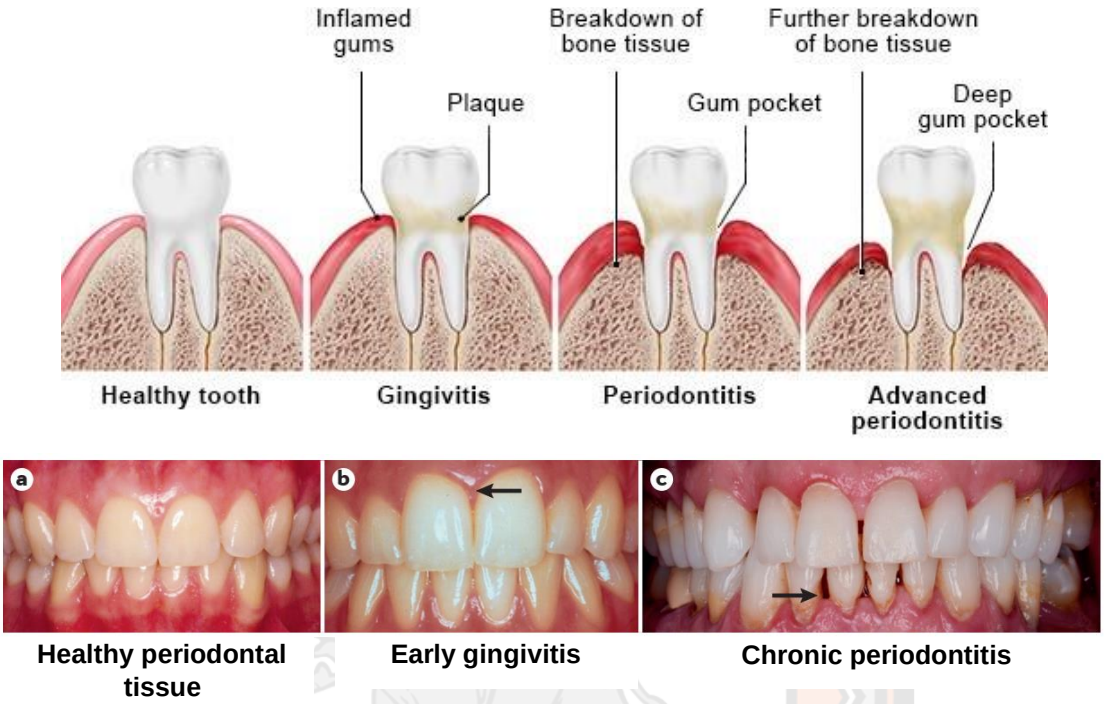

Figure 16 Clinical appearances of the gingiva in different stages (50, 51). Different stages of gingival health from gingivitis to periodontitis. The uncontrolled inflammation of the gingiva from dental plaque results in the alveolar bone destruction, leading to an increase in the depth of the gum pocket and supportive structure, which cause a high risk of tooth loss in severe condition.

3.1 Etiology

The etiology of gingivitis can be classified into four different types.

3.1.1 Plaque-induced gingivitis

This is the most common cause of gingivitis. Plaque is the thin bacterial biofilm that accumulates on the tooth surface. Because the biofilm harbor numerous microorganisms, the inflammatory response from immune cells can occur in the gingival tissue area. Several types of microorganisms have been liked with the etiology including species of *Streptococcus*, *Fusobacterium*, *Actinomyces*, *Veillonella*, and *Treponema*. Some local factors can increase the risk of dental biofilm formation, such as crowded teeth and wearing a dental prosthetic, which can lead to the difficulty of biofilm removal.

3.1.2 Nutritional gingivitis

The imbalance of nutritional intake has been linked to the etiology of gingivitis, such as increased refined carbohydrate intake and the ratio of omega-6 to omega-3 fatty acids. These factors can promote the inflammatory process as well as increase the risk of developing gingivitis (52). Moreover, carbohydrates with a high glycemic index can promote the inflammatory process via the activation of the NF-κB signaling pathway and oxidative stress (53, 54).

3.1.3 Hormonal gingivitis

The alteration of the hormones can contribute to gingivitis. For example, during pregnancy, a high level of estrogen can enhance the inflammatory response of the gingiva even to the minor accumulation of bacterial biofilm. This condition is called pregnancy gingivitis (55, 56). Another type of hormonal gingivitis can be found in adolescence or puberty gingivitis. It has been reported that gingivitis appears earlier in girls than in boys from eleven to fourteen years (57). Because the hormone receptors for both estrogens and testosterone can be found in the cytoplasm of basal and spinous layers of the epithelium, the gingiva is a target for hormonal change (1).

3.1.4 Drug-induced gingivitis

Several drugs for systemic diseases can contribute to the inflammation of the gingiva as a side effect, such as phenytoin (used for epileptic seizures), calcium channel blockers (used for angina, high blood pressure), anticoagulants, and fibrinolytic agents, oral contraceptive agents, protease inhibitors, vitamin A and analogs (1). The mechanism underly this inflammation is thought to increase the proliferation of fibroblasts by drug metabolites. Moreover, these drugs might lead to the imbalance of synthesis and degradation of the protein in the extracellular matrix, resulting in the accumulation of immature proteins. This, in turn, results in gingivitis (58).

3.2 Pathophysiology

Four different stages of gingivitis have been described by Page and Schroeder in 1976 (59) as shown in **Figure 17** (60).

1) Initial lesion: This stage can be seen within four days of initial biofilm accumulation. There is neutrophil migration from the blood vessels to the gingival connective tissue. Collagenase secreted from the neutrophil leads to the destruction of collagen about 5% to 10% of connective tissue (61).

2) Early lesion: After one week of early accumulation of dental plaque, the clinical signs of gingivitis are present, such as redness and bleeding from the gingiva. The inflammatory cells, including lymphocytes and macrophages, are predominant in this stage. The destruction of collagen is affect about 60% to 70% of connective tissue

area. The duration of the early lesion has not been elucidated yet, and it can take more time than previously expected (61).

3) Established lesion: In this stage, a small gingival pocket lined with a pocket epithelium is created. The predominant immune cells are plasma cells and B lymphocytes, along with the increasing of macrophages and T lymphocytes. The outcome of this stage can be either stable for months or years or may progress to a more destructive lesion. However, effective periodontal therapy can reverse the severity of this stage (61).

4) Advanced lesion: At this stage, clinical appearances of periodontitis are presented due to the transition from gingivitis to periodontitis. The inflammation and gingival tissue destruction affect several parts of supporting structures, including gingival, periodontal ligament, and alveolar bone resulting in severe destruction and may eventually result in tooth loss (62, 63).

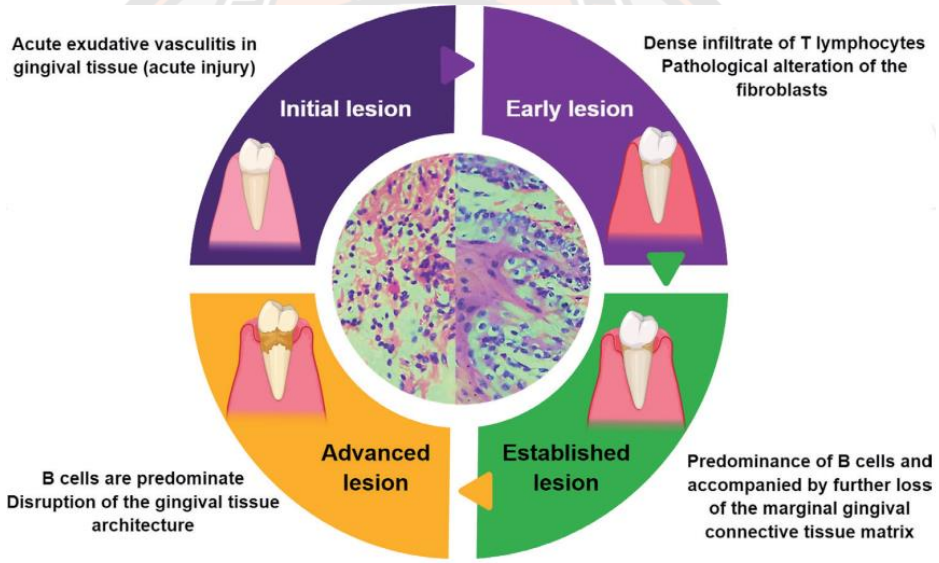

Figure 17 Different stages of gingivitis progression (60).
The histopathological lesion and lymphocyte infiltration in four stages of gingivitis and periodontitis; initial, early, established, and advanced lesions.

3.3 Microbial film associated with the plaque-induced gingivitis

Dental plaque comprises around 150 to 800 species that can be present at any one time in the oral cavity. The debate on which microorganisms drive the onset and progression of gingivitis and periodontitis is not resolved (64, 65). Probably, the causative agent is not a single microorganism but the imbalance of the microbial biofilm (66). Numerous species of bacteria from *Streptococcus*, *Fusobacterium*, *Actinomyces*, *Veillonella*, and *Treponema* are linked to the etiology of gingivitis (1). Another report has identified the taxa associated with early gingivitis including *Fusobacterium nucleatum* subsp. Polymorphum and *Prevotella oulorum* (67). As well, various reports have identified two significant microbes isolated from the oral cavity of gingivitis and periodontitis patients, *S. aureus* (4-6) and *C. albicans* (7-9).

These findings suggested the link between these microorganisms and gingivitis. This prompted one of the objectives of our study which was to investigate the antimicrobial activity that targets both microorganisms.

1) *S. aureus* is a gram-positive cocci-shaped bacteria that typically clusters. The colonies are round, raised, shiny, opaque, β-hemolysis, and smooth with a diameter of 2–3 mm as shown in **Figure 18** (68). *S. aureus* colonization is found in all body areas, including the nares, skin, gastrointestinal system, and oral cavity (69). The study by Smith et al. found the frequency rate of 50% to 52% of *S. aureus* isolated from the dental plaque of gingivitis and periodontitis patients (70). Another study showed that *S. aureus* is the most common causative pathogen in a patient with acute gingivitis who is fitted with orthodontic wires (5). Moreover, *S. aureus* has been identified as the second most prolific microorganisms among *Staphylococci* spp. In the subgingival sample from advanced periodontitis patients (6). These previous findings suggest a link between *S. aureus* and gingivitis pathogenesis.

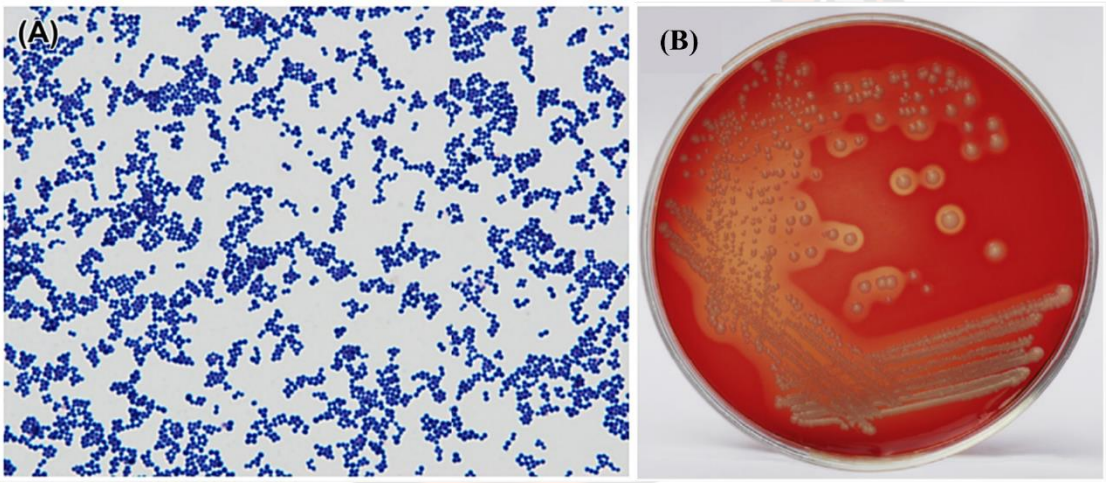

Figure 18 The characteristics of *S. aureus* in gram stain (A) and colony on Blood brain heart infusion (BHI) agar (B) (68).

The characteristic of *S. aureus* in gram stain is cocci-shaped, in clusters formation bacteria with the complete hemolytic ring (β-hemolysis) on blood BHI agar.

S. aureus attaches to the tooth surface via two distinct methods, as shown in **Figure 19**. Since bacterial proteins are not engaged in passive adhesion, it is dependent on electrostatic interactions and hydrophobic or hydrophilic contacts. *S. aureus* utilizes molecules, such as cell wall-anchored microbial surface components recognizing adhesive matrix molecules (MSCRAMMs), which are composed of collagen-binding adhesin (CNA) and fibronectin-binding proteins, for active

attachment (FnBPs). These two molecules, respectively, bind to collagen and fibronectin (71).

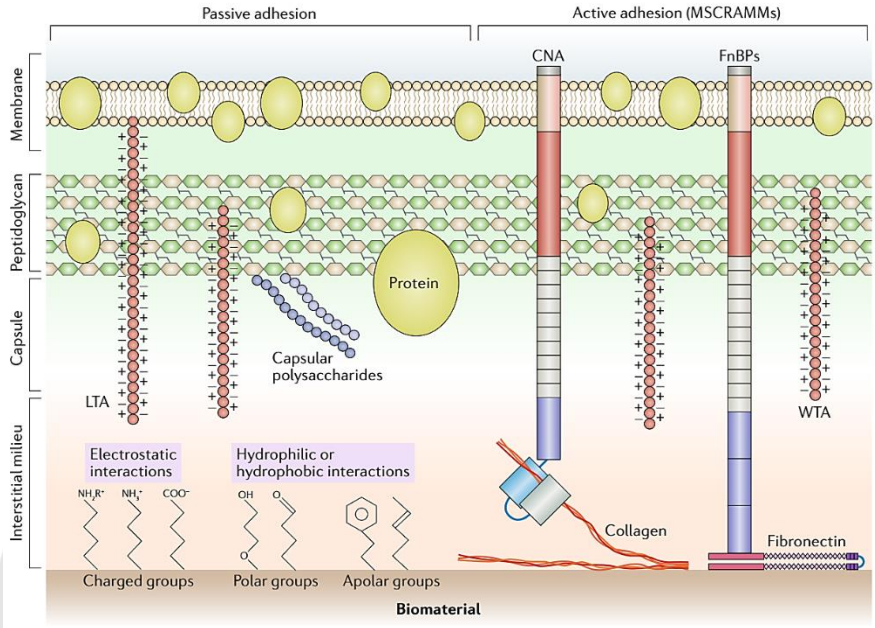

Figure 19 Mechanism of *S. aureus* adhesion (71).
The mechanism of *S. aureus* on adhesion to the different types of surfaces. Passive adhesion occurs through the chemical characteristic of the target surface, including electrostatic, hydrophobic and hydrophilic interactions. The active adhesion relies on the interaction with biomolecules, such as collagen and fibronectin. Following adhesion, *S. aureus* can develop a biofilm involving three factor

1) PIA-dependent biofilm formation: polysaccharide intercellular antigen (PIA) is synthesized from UDP-N-acetylglucosamine (GlcNAc), which is made primarily of 1,6-linked N-acetylglucosamine residues (80–85%) and an anionic fraction including phosphate and ester-linked succinate (15–20%) (72). The PIA is produced by the intercellular adhesion (*ica*) locus, which is composed of the *icaR* (regulatory) and *icaADBC* (biosynthetic) genes. The creation of a PIA-dependent biofilm is depicted in **Figure 21**. The polymerization of N-acetylglucosamine is catalyzed by the N-acetylglucosamine transferase IcaA and requires the accessory protein IcaD to operate. The membrane protein IcaC exports the developing PIA chain. Following export, IcaB de-acetylase eliminates a portion of the N-acetyl group, resulting in the cationic character required for surface attachment (73).

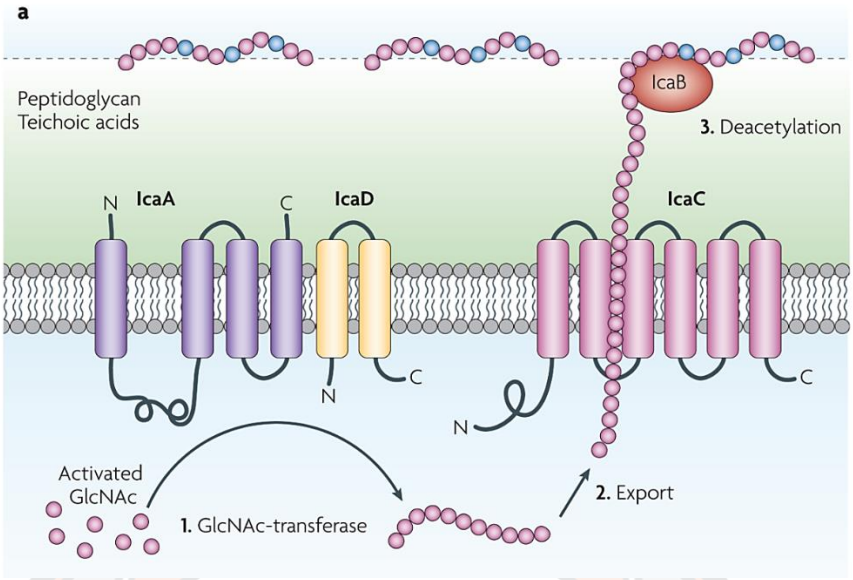

Figure 20 The production of polysaccharide intercellular antigen (PIA) (73). The synthesis of PIA required four accessory proteins to convert GlcNAc to de-acetylated β 1–6 linked N-acetylglucosamine homopolymer that is essential for surface attachment by cationic interaction and immune evasion.

2) PIA-independent biofilm development: the icaADBC locus is not engaged in PIA-dependent biofilm formation. Additionally, cell wall-associated proteins such as the *S. aureus* strain, protein A (*SpA*), accumulation-associated protein (*Aap*), and biofilm-associated protein (*Bap*) all contribute to the production of biofilms in a PIA-independent manner (72).

3) Extracellular DNA (eDNA): DNA produced by bacteria inside the biofilm as a result of altruistic suicide or fratricide killing. The bacterium self-destructed, resulting in the release of eDNA. The purpose of eDNA is to stabilize and strengthen the biofilm matrix, facilitate gene transfer between bacteria, give nutrients, and modulate the immune response (71).

2) *C. albicans* grows as oval, budding yeast cells (3–6 µm in diameter), forming soft, cream-colored colonies with a yeasty odor as shown in **Figure 21** (68). Pseudohyphae are also formed when buds continue to grow but do not detach, resulting in chains of elongated cells that are pinched or constricted at the septations between cells. *C. albicans* is dimorphic due to its ability to generate genuine hyphae on agar media in 24 hr at room temperature or about 37°C (74). *C. albicans* colonizes various human body areas asymptomatically, including the gastrointestinal tract, reproductive tract, mouth cavity, and skin. Various factors contribute to the pathophysiology of *C. albicans* infection, including modification of the host microbiota, immunosuppressive medication, and environmental variation (75). In the gingivitis condition, *C. albicans* was identified as the most common species among *Candida* spp. in the subgingival samples from patients with type 2 diabetes mellitus

(7). Similar to another study, *Candida* spp. was found to have an association with gingivitis in children with nephrotic syndrome or type 1 diabetes (8). In addition, a systematic review showed a positive association between *Candida* species and periodontal diseases (9). All of the findings indicate the relationship of *Candida* spp. in the etiology of gingivitis and periodontitis.

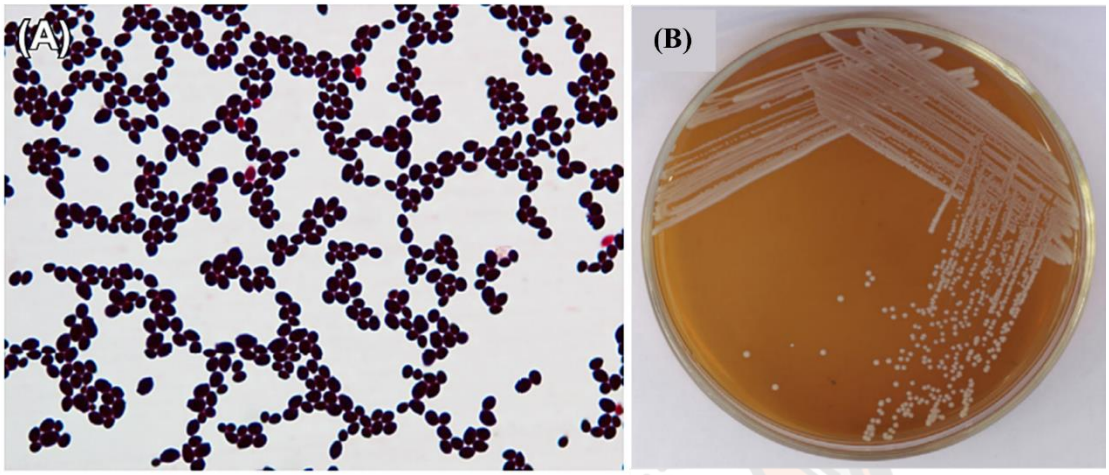

Figure 21 The characteristics of *C. albicans* in gram stain (A) and colony on Sabouraud dextrose agar (SDA) (B) (68).

The characteristic of *C. albicans* in gram stain showed the gram-positive yeast cells with oval-shaped. The colony on SDA showed the cream-colored colonies with a yeasty odor.

As shown in **Figure 22**, four distinct phases in the process that result in the formation of a biofilm. To begin, (a) yeast-form cells attach to the surface, followed by (b) biofilm formation, cell proliferation, and formation of the basal layer of anchoring cells, and (c) extracellular matrix production and hyphae growth. (d) dispersal of a developed biofilm to a new location (75).

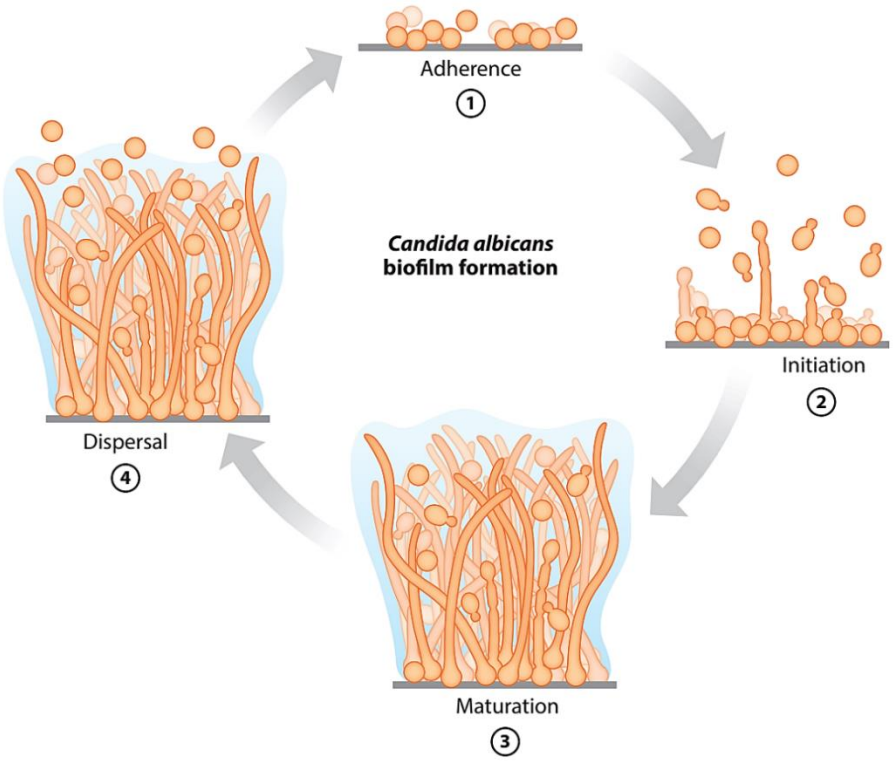

Figure 22 Schematic illustration of *C. albicans* biofilm formation (75).
1) Yeast cells attach to the surface. 2) Cell proliferation results in basal layer anchoring development. 3) Hyphal development with the production of extracellular matrix. 4) Yeast cells in the biofilm disperse to grow in the new location.

In vitro and *in vivo*, the formation of biofilms is regulated by the six master transcriptional regulators Efg1p, Tec1p, Bcr1p, Ndt80p, Brg1p, and Rob1p. These six master regulators interact with operators and influence the expression of approximately 1,000 target genes. Along with the six master regulators, numerous target genes are involved in the formation of biofilms, depending on the stage of biofilm development.

1) Adherence: This is a critical step in the development of biofilms because *C. albicans* must initially adhere to the surface. Bcr1p regulates several cell wall proteins downstream, including Als1, Als3, and Hwp1, which are necessary for adhesion.

2) Hyphae: Hyphae growth is critical for biofilm development. The hyphae contribute to the biofilm architectural integrity by serving as a scaffold for yeast cells and other hyphae. Efg1p, Tec1p, Ndt80p, and Rob1p are transcription factors necessary for hyphae formation.

3) Extracellular matrix: *C. albicans* is enclosed within a complex extracellular matrix. The transcription factors Rlm1p and Zap1p are involved in the regulation of extracellular matrix expression. *RLM1* deletion results in a

decrease in extracellular matrix formation, whereas *ZAP1* deletion lead to an increase in extracellular matrix production.

4) Dispersal: this process contributes to the seeding of the *C. albicans* biofilm in a new location. Nrg1p and Ume6p were identified as transcriptional regulators involved in the dispersion process (75).

Kaffir lime (*Citrus hystrix* DC.)

C. hystrix DC. belongs to the Rutaceae family, Citrus genus, and the Sapindales order. This genus contains approximately 16 species of plants with fragrant flowers and distinctive aromatic fruits. The height of kaffir lime trees is 3–5 meters and a width of 2.5–3 meters. The blooms are small, dark green fruit with warty skins that are around 4 cm in diameter. The characteristics of kaffir lime are shown in **Figure 23**. The leaves are dark green with glossy luster and each leaf is bipartite, resembling a double leaf. The leaf size varies considerably, and the larger leaves are typically deeper in color (76, 77).

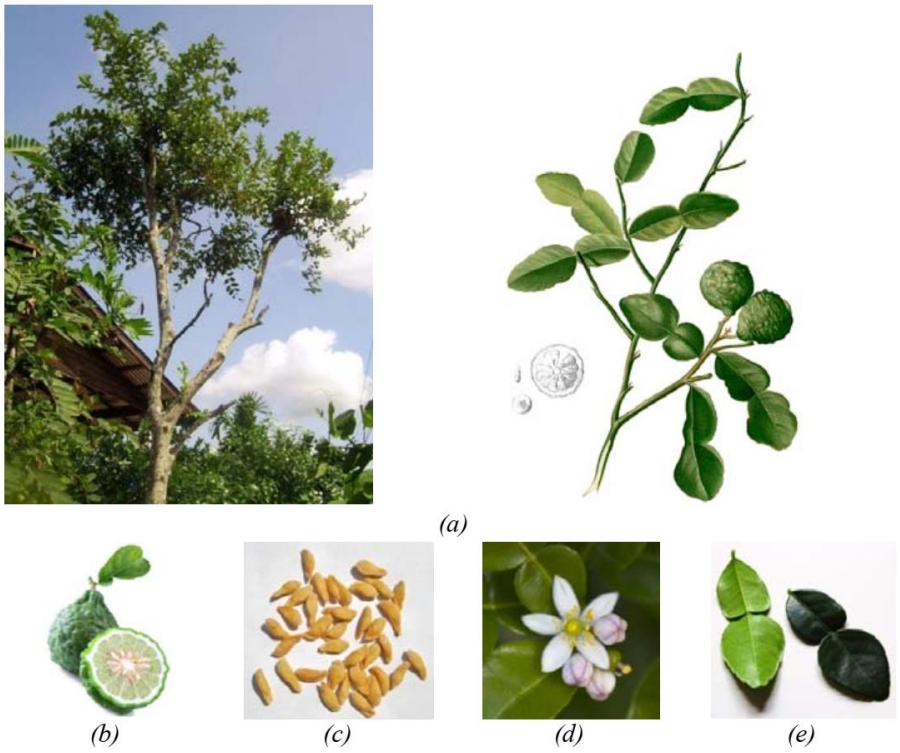

Figure 23 The characteristics of *C. hystrix* DC.; tree (a), fruit (b), seeds (c), flowers (d) and leaf (e) (76).

3.1 Chemical composition

According to Jean Waikedre et al. (78), the distillation extraction of *C. hystrix* DC. leaves followed by chemical ingredient analysis using gas chromatography-mass spectrometry (GC-MS) revealed that monoterpene group chemicals constitute 89% of the essential oils. The other constituents were β-pinene (10.9%), α-terpineol (7.6%), 1,8-cineole (6.4%), and citronellol (6.0%). **Figure 24** indicates the organization of some major constituents (78). Another study published by Wongpornchai et al. (77) extracted the fresh mature *C. hystrix* DC. leaves and peel using the headspace extraction method, followed by GC-MS analysis of the volatile components. The result is summarized in **Table 3**. The most abundant volatiles in fresh kaffir lime leaves are citronellal (48.2%), citronellol (14.3%), and citronellal acetate (7.8%). For the kaffir lime peel, furanoid (10.9%) is the most abundant component, followed by β-fenchyl alcohol (9.6%), erpinene-4-ol (8.4%), citronellal (8.0%), and limonene (7.4%) 32.

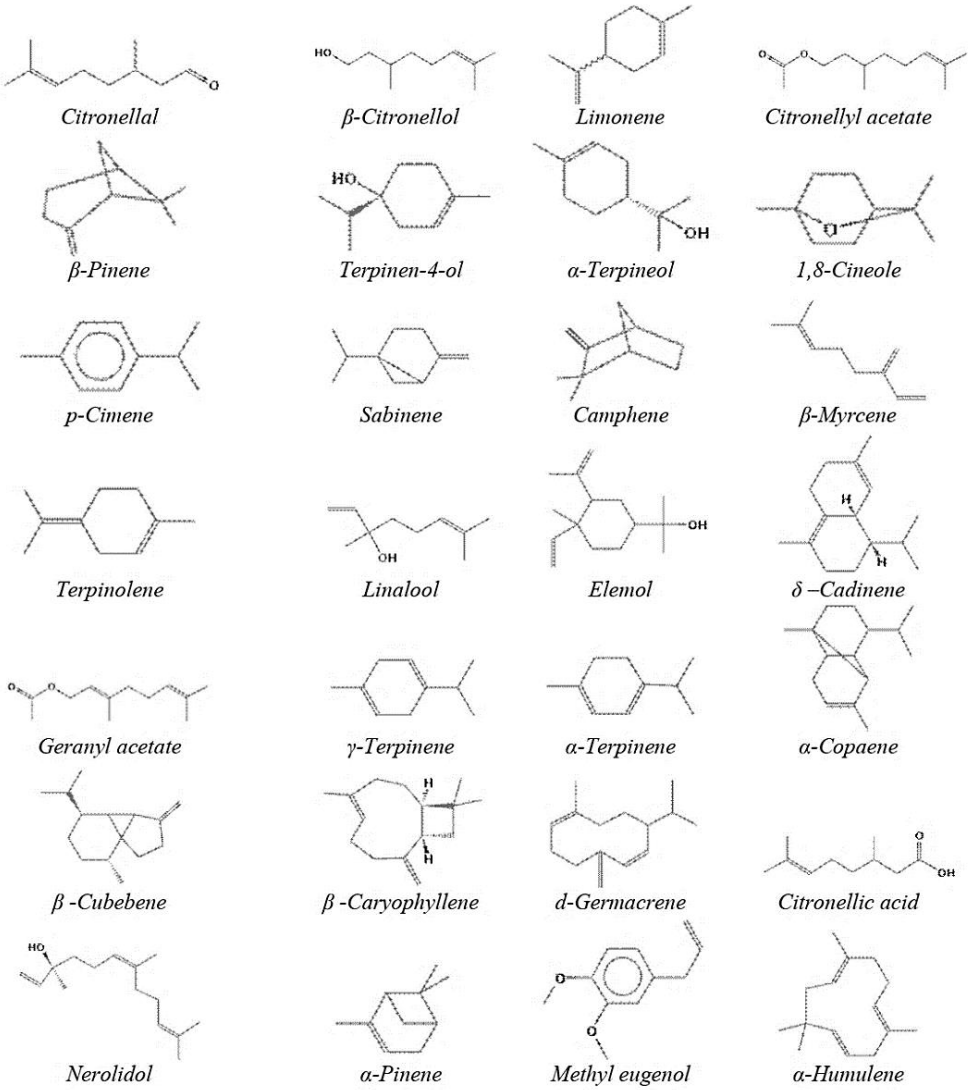

Figure 24 Major chemical constituents from *C. hystrix* DC. leaf (78).

Table 3 List of chemical compounds from the peel and leaves of kaffir lime analyzed by GC-MS (78).

No.	Component	Tr	LTPRI	% Relative content	
				Leaf	Peel
1	2E-hexenal	4.02	867	0.56	0.37
2	3Z-hexenol	4.07	869	2.34	0.29
3	2E-hexenol	4.25	876	0.26	0.37
4	Hexanol	4.31	878	0.36	0.26
5	α-Thujene	5.64	924	0.01	0.15
6	α-Pinene	5.86	932		0.55
7	Camphene	6.33	948	0.05	0.14
8	Benzaldehyde	6.78	964	0.03	0.11
9	Sabinene	7.01	972	0.58	5.38
10	β-Pinene	7.20	979	0.01	5.72
11	Myrcene	7.45	987	0.13	0.72
12	Octanal	7.91	1003		0.26
13	Degydroxy-cis-linalool oxide	7.99	1005		0.14
14	α-Terpinene	8.42	1016		0.17
15	p-Cymene	8.72	1024	0.04	0.81
16	Limonene**	8.96	1031	0.04	7.41
17	β-Phellandrene	9.01	1032	0.12	0.18
18	Satolina alcohol	9.08	1034	0.17	
19	trans-β-Ocimene	9.43	1043	0.10	
20	Benzene acetaldehyde	9.46	1044		0.20
21	Bergamal	9.68	1050	0.34	0.20
22	γ-Terpinene	9.91	1056	0.03	0.49
23	trans-Linalool oxide (furanoid)**	10.60	1074	2.20	10.90
24	cis-Linalool oxide (furanoid)	11.17	1090	1.22	5.96
25	Linalool*	11.72	1104	5.13	3.45
26	trans-Sabinene hydrate	11.79	1105		0.33
27	trans-p-Menth-2-en-1-ol	12.65	1126		0.68
28	cis-p-Menth-2-en-1-ol	13.50	1146		0.55
29	Citronellal*/**	13.84	1154	48.20	8.03
30	Iso-isopulegol	14.12	1161		0.43
31	Pinocarvone	14.21	1163		0.16
32	Neoiso-isopulegol	14.51	1170	0.86	0.21
33	Borneol	14.79	1176		0.86
34	Terpinen-4-ol**	15.19	1186	0.46	8.36
35	β-Fenchyl alcohol**	15.90	1203	0.16	9.58
36	trans-Piperitol	16.30	1212		0.31
37	Citronellol*	17.20	1232	14.25	5.44
38	cis-Citral	17.45	1238	0.43	0.36

No.	Component	Tr	LTPRI	% Relative content	
				Leaf	Peel
39	Geraniol	18.06	1252	0.35	0.86
40	Piperitone	18.16	1254	0.35	0.52
41	Geranial	18.69	1266	0.06	0.27
42	Citronellyl acetate*	22.18	1347	7.78	3.24
43	α-Ylangene	23.23	1371	1.86	1.29
44	β-Maaliene	23.73	1383	0.13	1.58
45	trans-Caryophyllene	25.03	1413	0.61	0.45
46	E-β-Farnesene	26.49	1448	0.20	0.34
47	α-Humulene	26.55	1449		
48	trans-Cadina-1(16),4-diene	27.29	1467		0.17
49	γ-Muurolene	27.55	1473		0.36
50	Bicyclogermacrene	28.10	1486		0.17
51	α-Amorphene	28.27	1490	0.05	0.24
52	β-Selinene	28.37	1493		0.15
53	γ-Cadinene	28.87	1505		
54	δ-Cadinene	29.06	1510	0.29	1.01
55	Elemol	30.32	1541	0.11	0.40
56	E-nerolidol	30.78	1553	0.34	
57	Z-dihydro apofarnesol	31.22	1564		
58	Spathulenol	31.38	1568	0.11	

Tr = retention time (min) in GC–MS chromatograms, LTPRI = linear temperature program retention index.
* Major component in leaves.
** Major component in the peel.

3.2 Biological activities of *C. hystrix* DC.

A broad range of potential bioactivity from the leaves of *C. hystrix* DC. has been assessed both *in vitro* and *in vivo*, including antimicrobial, anti-inflammatory, antioxidant, hepatoprotective, and anti-cancer activities.

1) Antimicrobial and antifungal activities: A study from Kooltheat et al. (2016) showed that the crude water extract of *C. hystrix* DC. leaves inhibited the production of *S. mutans* biofilms with a MIC value of 6,250 mg/mL (21). The essential oil from the leaves inhibited the growth of numerous types of bacteria and fungi *in vitro*. The bacteria included both gram-positive (*S. aureus, S. epidermidis,* and *Bacillus subtilis*) and gram-negative bacteria (*Klebsiella pneumoniae* and *Escherichia coli*). Moreover, five strains of fungi were inactivated, including *Aspergillus fumigates, C. albicans, Cryptococcus neoformans, Saccharomyces cerevisiae*, and *Trichophyton mentagrophytes* (78). The GC-MS analysis of tested essential oil was identified by a high content of terpinen-4-ol (13.0%), α-terpineol (7.6%), 1,8-cineole (6.4%), and citronellol (6.0%).

2) Anti-inflammatory and antioxidant activities: Crude ethanolic extract from *C. hystrix* DC. leaves suppressed the production of nitric oxide (NO) and TNF-α production in LPS-induced RAW267.4 macrophages (79). Another study from

Anuchapreeda et al. (2020) showed the anti-inflammatory activity of crude extract from hexane that significantly inhibited IL-6 secretion. The active compound was identified as agrostophillinol (80). For the antioxidant activity, methanolic extract of the leaves exhibited the potential antioxidant activity based on the DPPH assay with IC_{50} of 24.6 µg/mL (81).

3) Hepatoprotective activity: A study from Abirami et al. (2015) investigated the hepatoprotective activity of methanolic extract from *C. hystrix* DC. leaves in paracetamol-induced toxicity in Swiss albino mice. The mice were given the extract of 200 mg/kg for seven days, and the toxicity was induced by paracetamol (2 mg/kg) on day five. The result showed that the level of liver biomarkers, such as alanine transaminase (ALT), aspartate transaminase (AST), and alkaline phosphatase (ALP) were restored to a level comparable to the normal control (82).

4) Anti-cancer activity: An ethyl acetate extract of *C. hystrix* DC. leaves induced apoptosis in a cervical cancer cell line (HeLa) with the IC_{50} of 57,845 µg/mL and inhibited the proliferation of the cells (83). Another study from Ho et al. (2020) investigated the effect of crude extract from *C. hystrix* DC. leaves and their active compounds on triple-negative breast cancer cell line (MDA-MB-231). Their results showed that crude extract from hexane had the highest cytotoxicity on cancer cells with the IC_{50} of 317.63 µg/mL, as well as the apoptosis cells were increased in the treatment group. The crude extract activated cell cycle arrest and the upregulation of pro-apoptotic protein caspase-3 (84).

Chapter III

Methodology

The experiments were divided into four parts in this study, as shown in **Figure 25**. The first part aimed to extract and identify the active compound in kaffir lime leaf powder. Then, crude extracts and active compound were evaluated for anti-inflammation and anti-NLRP3 inflammasome activities in the second part. The third part was conducted to investigate the antifungal activity of crude extract and active compounds in *the C. albicans* model. The final part aimed to develop a mouthwash containing herbal extracts and evaluated the anti-gingivitis in human subjects.

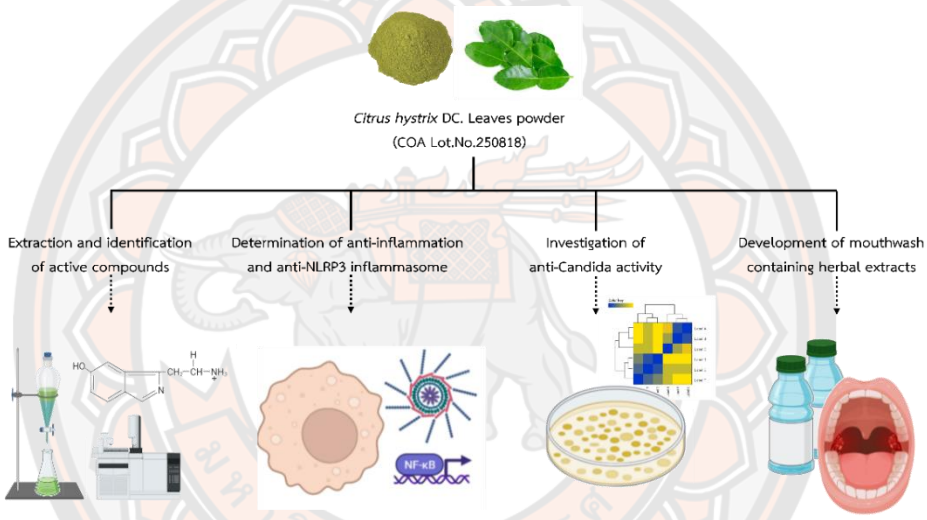

Figure 25 Conceptual framework of the study.
Four parts of the experiments were conducted to investigate the anti-inflammation, anti-NLRP3 inflammasome, and antifungal activities of crude extract and active compound from kaffir lime leaf powder. The anti-gingivitis activity of this plant was evaluated in human volunteers by developing a mouthwash containing leaf extract.

Extraction and identification of active compounds

1.1 Crude extraction of kaffir lime leaf powder

The powdered *C. hystrix* DC. leaves (COA Lot. No.250818) used in this study was acquired from Khaolaor Laboratories Co., Ltd. (Samut Prakan, Thailand). A 1,000 gm sample of the leaf powder was macerated for 3 days in each solvent; in 3,000 mL hexane, followed by 3,000 mL 95% ethyl acetate, and 3,000 mL 95% ethanol at room temperature, and then filtrated. The filtrate from all solvents was collected and evaporated at 35°C using a rotary evaporator. Each solvent was macerated in duplicate as shown in **Figure 26**. All crude extracts were weighed for mass. To evaluate the total phenolic content and antioxidant activity in each crude

extract, the Folin-Ciocalteu assay, and Trolox equivalent antioxidant capacity (TEAC) assay were conducted.

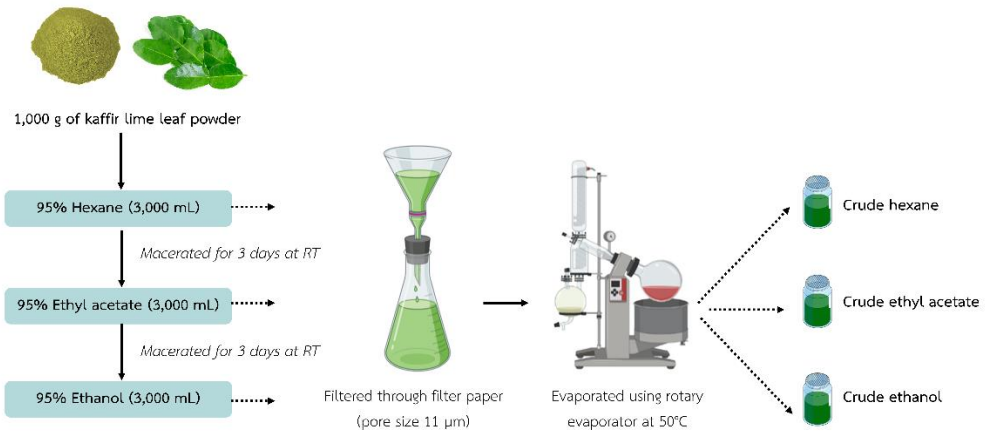

Figure 26 The protocol of the kaffir lime leaf crude extraction.
The kaffir lime leaf powder was sequentially macerated in different solvents (hexane, ethyl acetate, and ethanol). After the filtration and evaporation, three crude extracts were obtained.

1.2 Evaluation of total phenolic content by Folin-Ciocalteu (F-C) assay

The F–C assay is based on the reduction of the Folin–Ciocalteu reagent in the presence of phenolics, which results in the formation of molybdenum–tungsten blue. The intensity of the molybdenum–tungsten blue is measured spectrophotometrically at 760 nm and increases linearly with the concentration of phenolics in the reaction medium (85). In this study, the F-C technique was used with a slight modification (86). In a 96-well plate, 2.5 µL of each of three extracts (100 mg/mL) was added to serially diluted gallic acid. Each well was loaded with 5 µL of F-C reagent (10% v/v), followed by 90 µL of Na_2CO_3 (20% w/v). The plate was incubated at 50°C for 1 hour. The absorbance of the reaction was measured at 760 nm.

1.3 Determination of antioxidants activity by 2,2-diphenyl-1-picrylhydrazyl (DPPH) Assay

The DPPH assay was used to assess the capacity to scavenge free radicals. DPPH (2,2-diphenyl-1-picrylhydrazyl) is a purple-colored chemical that does not dimerize, allowing for crystalline formation. Any molecule capable of donating an electron or hydrogen reacts with DPPH, converting it from purple to yellow

diphenylpicryl hydrazine. The absorbance can be measured at 517 nm (87). The standard substance was Trolox (6-hydroxy-2,5,7,8-tetramethylchroman-2-carboxylic acid), and the results were reported as Trolox equivalents (mg/g). A 5 µL volume of each extract was placed into a 96-well plate, and serially diluted 0.2 mM Trolox was added to each. Then, 50 µL DPPH in methanol (1:5) was added to each sample of extract and incubated at room temperature for 2 hr in the dark. The absorbance of the sample was measured at 517 nm.

1.4 Isolation and identification of active compound

All crude extracts were investigated *in vitro* for anti-inflammatory activity using a primary human monocyte-derived macrophages (MDMs) model stimulated with LPS. Chromatographic methods were then used to fractionate the crude extract with the highest anti-inflammatory activity. Using silica gel column chromatography, ten grams of crude extract were fractionated. As the mobile phase for elution, a gradient of hexane (100%), hexane-dichloromethane (50–50%), dichloromethane (100%), dichloromethane-methanol (90–10%), dichloromethane-methanol (50–50%), and 100% methanol was used. Then, ten milligrams of subfraction no. 4.6 were then fractionated using C-18 column chromatography with deionized water: acetonitrile (5:95 v/v) as the mobile phase. Finally, this protocol resulted in the isolation of the pure chemical. The isolated compound structure was subsequently determined using ^{1}H- and ^{13}C-Nuclear magnetic resonance (NMR) and Fourier-transform infrared spectrophotometer (FT-IR) mass spectroscopy methods. NMR spectra were acquired at 400 MHz for protons and 100 MHz for carbon using a Bruker AV400 (Bruker, Billerica, MA, USA) spectrometer. The FT-IR analysis was performed using PerkinElmer Spectrum GX (PerkinElmer, Waltham, MA, USA). Gas chromatography-mass spectrometry (GC-MS) was used to examine the mass (Agilent, Santa Clara, CA, USA).

Determination of anti-inflammation and anti-NLRP3 inflammasome activities

2.1 Primary human (MDMs) isolation and differentiation

To investigate the anti-inflammatory effect of the kaffir lime leaf extracts, human monocytes were isolated from buffy coats acquired from healthy individuals from the blood bank at Naresuan University Hospital, Phitsanulok, Thailand. This experiment was approved ethically by the Human Ethics Committee of Naresuan University (IRB no. 1065/61). After mixing the buffy coat and pouring it into a 50 mL conical tube, the cells were diluted with Hank's balanced salt solution (HBSS), agitated, and centrifuged at 3000 rpm for 30 min. Plasma was removed, followed by the transfer of buffy coat pellets to a new conical tube.

Human peripheral blood mononuclear cells (PBMCs) were isolated by centrifuging 5 mL of Lymphoprep^{TM} (Axis-Shield PoC AS, Rodelkka, Oslo, Norway) with 10 mL of HBSS-buffy coat mixture at 3000 rpm for 30 min. The supernatant was collected and the PBMC pellet was transferred to a fresh conical tube following centrifugation.

To isolate monocytes, 7 mL of PBMCs were layered over 7 mL of 46% Percoll (GE Healthcare Bio-Sciences AB, Uppsala, Sweden). 23.13 mL Percoll, 27 mL RPMI-1640 supplemented with 10% fetal bovine serum (FBS) and 1% antibiotic-antimycotic (Thermo Fisher Scientific, Inc., Waltham, MA, USA), and 1.87 mL 10X phosphate-buffer saline (PBS) were combined in a conical tube to make 46% Percoll. The overlaying PBMCs were centrifuged at 3000 rpm for 30 min. The monocyte layer was collected and transferred to a fresh tube, which was then diluted with PBS buffer to a final volume of 50 mL. The monocytes were combined and washed five times for 10 min at 2000 rpm, 1700 rpm, 1500 rpm, 1200 rpm, and 900 rpm. After removing the supernatant, the monocytes were resuspended in a completed RPMI-1640 medium.

The monocytes were developed into MDMs by culturing them for 7-14 days at 37°C with 5% CO_2 in a completed RPMI-1640 medium. The phenotypic of MDMs was determined by flow cytometry based on measuring the CD14/16 expressions.

2.2 THP-1 cell differentiation for NLRP3 inflammasome activation

THP-1 cells were obtained from ATCC and cultured at 37°C, 5% CO_2 in completed RPMI-1640. To differentiate the cells into macrophages, they were stimulated for three days with 100 nM phorbol-12-myristate-13-acetate (PMA) (Sigma-Aldrich, St. Louis, MO, USA), followed by four days with a PMA-free complete medium replacement. The expression of macrophage phenotypic markers was investigated by Flow cytometry. To activate the NLRP3 inflammasome, the macrophages were primed with 1 µg/mL LPS from *E. coli* O55:B5 (Sigma-Aldrich, St. Louis, MO, USA) for 3 hr in a completed RPMI-1640 medium. Following priming with LPS, the cell culture media was replaced with RPMI-1640 containing 5 mM adenosine triphosphate (ATP) (Sigma-Aldrich, St. Louis, MO, USA) for 1 hr, as previously described (88).

2.3 Flow cytometry analysis

Cells were harvested and centrifuged before being resuspended in FACS buffer containing PE-conjugated anti-CD14 and FITC-conjugated anti-CD16 (BD Biosciences, San Jose, CA, USA) antibodies for 1 hr at 4°C. After incubation, the cells were washed three times with 1X PBS and examined using a Flow Cytometer FC 500 (Beckman Coulter, Inc., Indianapolis, IN, USA). FITC-conjugated mouse IgG1 isotype control and PE-conjugated mouse IgG1 isotype control (BioLegend, Inc., San Diego, CA, USA) was used as a negative control.

2.4 Evaluation of cytotoxicity by MTT assay

Before evaluating anti-inflammatory activity, it is necessary to determine the safe doses of kaffir lime leaf extracts for MDMs. The MTT assay was used in this study to determine the optimal doses. MTT (3-(4,5-dimethylthiazol-2-yl)-2,5-diphenyltetrazolium bromide) is a yellow compound that can be converted to purple formazan by a specific mitochondrial enzyme found in viable cells. Human MDMs were seeded at a density of 5×10^4 cells/well in a 96-well plate and incubated for 24 hr. Then, cells were treated with various concentrations of kaffir lime leaf extracts for

24 hr. Cell viability was determined using a modified MTT assay as previously described (89). The cells were washed with 100 µL 1X PBS and then incubated with 0.5 mg/mL MTT (Thermo Fisher Scientific, Waltham, MA, USA) in serum-free RPMI-1640 medium for 3 hr at 37°C, 5% CO_2. After discarding the supernatants, 50 µL of 100% dimethyl sulfoxide (DMSO) (VWR International, West Chester, PA, USA) was added for 15 min to solubilize the formazan crystals. The absorbance at 570 nm was used to determine the reaction. The percentage of viable cells was determined, and the concentration of any of the kaffir lime leaf extracts that maintained cell viability greater equal to 90% was chosen for further experimentation.

2.5 Screening for the anti-inflammatory activity of kaffir lime leaf crude extracts and theirs fractions

All the crude kaffir lime leaf extracts were screened for their anti-inflammatory activity based on the ability to suppress TNF-α production in LPS-induced MDMs. In this experiment, MDMs were seeded at a density of 2×10^5 cells per well in a completed RPMI-1640 medium for 24 hr. The cells were pre-treated with the IC_{10} of all the crude kaffir lime leaf extracts for 1 hr, then co-treated with 100 ng/mL LPS and cultured for an additional 12 hr at 37°C, 5% CO_2. The cells were treated with the anti-inflammatory agent dexamethasone (0.1 nM) which was used as a positive control. The supernatants of all conditions were collected and measured for the level of TNF-α using the TNF-alpha enzyme-linked immunosorbent assay (ELISA) kit (Sino Biological, Wayne, PA, USA) according to the manufacturer's protocol. To obtain purer fractions, the extracts with the greatest suppression of TNF-α were chosen for fractionation, and this process was repeated until the fraction was inadequate for further fractionation. The final fraction was used to further investigate the anti-inflammatory and anti-NLRP3 inflammasome activities, as well as the identification of the active compound. The experimental design is shown in **Figure 27**.

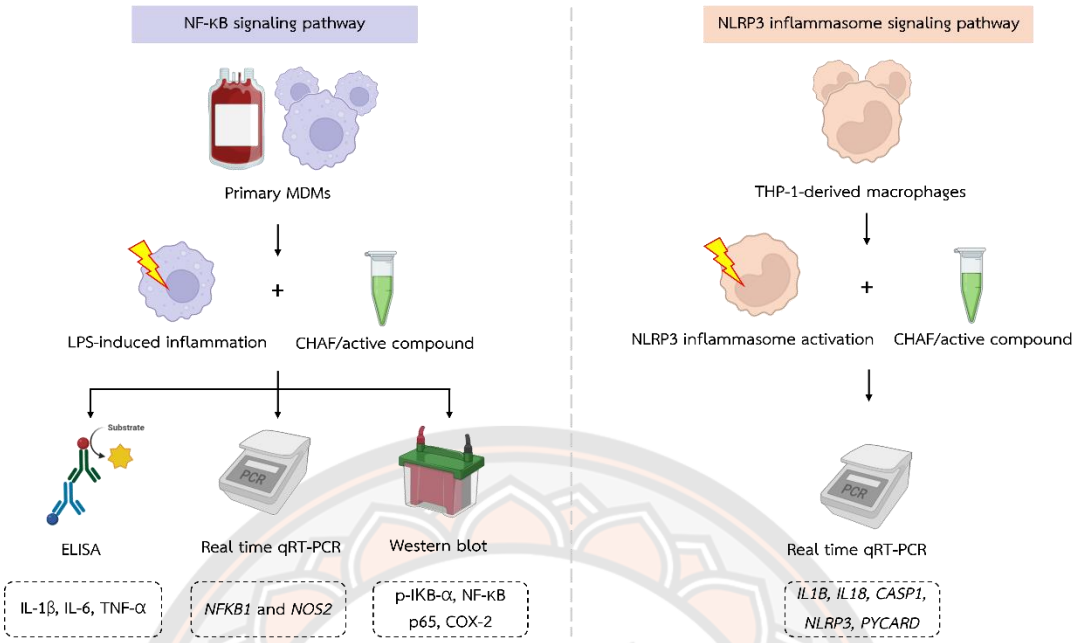

Figure 27 Experimental design to investigate the effect of kaffir lime leaf extract and active compound on NF-κB and NLRP3 inflammasome signaling pathways. The anti-inflammatory and anti-NLRP3 inflammasome activities in both kaffir lime leaf active fractions (CHAF) and active compound were evaluated in LPS-induced human macrophages.

2.6 Determination of the effect on the NF-κB inflammatory signaling pathway

The kaffir lime leaf active fractions (CHAF) and the active compound were tested on the NF-κB inflammatory signaling pathway. To determine the effect on cytokine levels, MDMs at a density of 2×10^5 cells were seeded in each well of a 24-well plate and incubated for 24 hr. The cells were then pre-treated with the IC_{10} of CHAF and active compound for 1 hr, then co-treated with 100 ng/mL LPS and cultured for an additional 24 hr at 37°C, 5% CO_2. Co-treatment of cells with the anti-inflammatory agent dexamethasone (0.1 nM) was used as a positive control. The supernatants were collected to measure the cytokine concentrations. The cell pellets were harvested to determine the transcriptional level and protein expression.

2.7 Determination of the effect on the NLRP3 inflammasome signaling pathway

To determine the effect on the NLRP3 inflammasome signaling pathway, the THP-1-derived macrophages were seeded at a density of 2×10^5 cells per well in a 24-well plate and incubated at cell culture conditions. Then, the cells were primed with 1 µg/mL LPS for 3 hr followed by co-treated with CHAF or an active compound containing 5 mM ATP for a further 1 hr. For positive control, the cells were replaced with 0.1 nM dexamethasone containing 5 mM ATP. The cell pellets were harvested to determine the transcriptional level.

2.8 ELISA

The supernatant from the cell culture was collected and analyzed for the expression of pro-inflammatory cytokines IL-1β, IL-6, and TNF-α using a sandwich ELISA assay according to the manufacturer procedure (Sino Biological, Wayne, PA, USA). Briefly, the primary antibody was coated on a polyvinylchloride (PVC) microtiter plate by adding 50 µL of antibody solution (20 µg/ml in PBS) to each well and incubating overnight at 4°C. After two PBS washes, the wells were blocked with blocking buffer (3% bovine serum albumin/PBS with 0.02% sodium azide) and incubated at room temperature for 1 hr. The plate was washed twice with PBS and then incubated for at least 2 hr at room temperature with 50 µL of cell culture supernatant. The plate was rinsed four times with PBS and then incubated for 2 hr at room temperature with a 50 µL labeled secondary antibody conjugated to horseradish peroxidase (HRP). After washing the plate with PBS, 5,5′-Tetramethylbenzidine (TMB) substrate was added and the absorbance was measured at 450 nm using an EnSpire® Multimode microplate reader (PerkinElmer, Inc., Waltham, MA, USA).

2.9 Evaluation of gene expression by real-time quantitative reverse transcription-polymerase chain reaction (Real-time qRT-PCR)

To determine the effect on the transcriptional level, a RiboZol RNA extraction reagent (VWR International, West Chester, PA, USA) was used to extract RNA from cell pellets from each experimental condition according to the manufacturer's instructions. Total RNA was converted to complementary DNA (cDNA) using a Tetro cDNA synthesis kit (Bioline, London, UK). The qPCR SensiFAST^{TM} SYBR No-ROX kit (Bioline, London, UK) was used to determine the levels of gene expression from two signaling pathways; NF-κB signaling pathways such as nuclear factor kappa B subunit 1 (*NFKB1*) and nitric oxide synthase 2 (*NOS2*). Another group is the NLRP3 inflammasome signaling pathway; interleukin 1 beta (*IL1B*), interleukin 18 (*IL18*), caspase-1 (*CASP1*), NLR family pyrin domain containing 3 (*NLRP3*), and PYD and CARD domain containing (*PYCARD*). The reaction was carried out on a CFX96 Touch Real-Time polymerase chain reaction detection system (Bio-Rad Laboratories, Inc., Hercules, CA, USA). The PCR stage consisted of 1 min of polymerase activation at 95°C, followed by 45 cycles of denaturation at 95°C for 15 sec, followed by 1 min of annealing and extension at 60°C. The housekeeping gene was human actin beta (*ACTB*). All data were analyzed using the $2^{-\Delta\Delta CT}$ approach to normalize gene expression (90). All primer sequences are shown in **Table 4**.

Table 4 Primer sequences used in this study (91).

Gene	Description	Forward (5′ → 3′)	Reverse (5′ → 3′)
IL1B	Interleukin 1 beta	AGCTACGAATCTCCGACCAC	CGTTATCCCATGTGTCGAAGAA
IL18	Interleukin 18	GAAGATGCCAGGGGTAATGA	TACCTGCCCCAAACTGAAAC
CASP1	Caspase-1	CTTGCTTGAAATGTGCTCCA	AGTGGCATCCCTGTTTGTTC
NLRP3	NLR family pyrin domain containing	ACAAACTCATGGTGGCTTCC	GGCCAGAAGAAAAGCAAGTG

Gene	Description	Forward (5′ → 3′)	Reverse (5′ → 3′)
PYCARD	3 PYD and CARD domain containing	TGACGGATGAGCAGTACCAG	AGGATGATTTGGTGGGATTG
NFKB1	Nuclear factor kappa B subunit 1	AACAGAGAGGATTTCGTTT	TTTGACCTGAGGGTAAGAC
NOS2	Nitric oxide synthase 2	TTCAGTATCACAACCTCAGCAAG	TGGACCTGCAAGTTAAAAT
ACTB	Actin beta	AGAAAATCTGGCACCACACC	CCATCTCTTGCTCGAAGTCC

2.10 Determination of protein expression using western blot analysis

For each condition, the cells were lysed for 30 min in ice-cold RIPA buffer containing protease and phosphatase inhibitor cocktails (Thermo Fisher Scientific, Waltham, MA, USA), and then centrifuged at 12,000 rpm for 30 min at 4°C. Bradford reagent was used to measure the protein concentration. Equal amounts of proteins were loaded into a 12% sodium dodecyl sulfate polyacrylamide gel electrophoresis (SDS-PAGE) and then transferred to a 0.2 μm polyvinylidene fluoride membrane (Bio-Rad Laboratories, Inc., Hercules, CA, USA). The membrane was blocked overnight at 4°C with 5% bovine serum albumin (Capricorn Scientific GmbH, Hesse, Germany) in Tris-buffered saline with Tween 20 (TBST) buffer. At room temperature for 1 hr, primary antibodies against phospho-IκBα (Cell Signaling Technology, London, UK), NF-κB p65, and COX-2 (Santa Cruz, CA, USA) were probed into the membrane. The membrane was then rinsed with TBST buffer and incubated at room temperature for 1 hr with a horseradish peroxidase-conjugated goat anti-mouse IgG (H + L) secondary antibody (Thermo Fisher Scientific, Waltham, MA, USA). The protein bands were visualized using a chemiluminescence substrate for 5 min and imaged them using a ChemiDoc XRS+ Imaging System (Bio-Rad Laboratories, Inc., Hercules, CA, USA). The intensity of proteins was determined using the Image Studio Lite software (LI-COR Corporate, Lincoln, NE, USA) as mentioned in **Figure 27**.

Investigation of anti-*Candida* activity

The purpose of this section is to examine the effect of kaffir lime leaf extracts and the active compound β-citronellol, that was identified from crude kaffir lime leaf ethanolic extract (**Table 10**), on *C. albicans* ATCC 90028. Additionally, the experiment will use a proteomic approach to determine the effect of an active compound on whole-cell protein change. **Figure 28** demonstrates the experimental design.

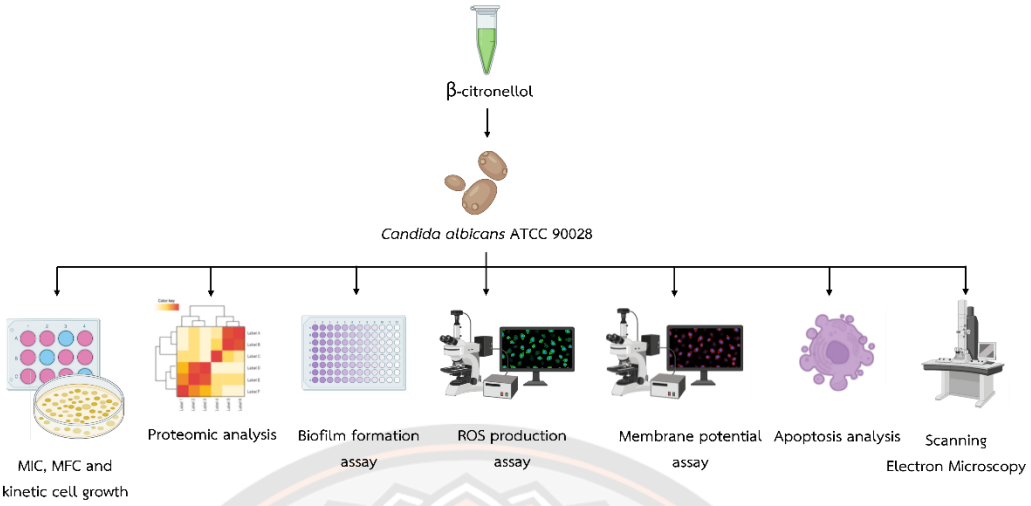

Figure 28 Experimental design for determining the effect of β-citronellol on *C. albicans.*

Seven experiments were conducted to identify the potential target proteins involved in the anti-*Candida* activity mode of action of β-citronellol. The possible mechanism of action of target proteins from proteomic data was confirmed by assays, including ROS production, membrane potential, and apoptosis assays.

3.1 Culture and growth of *C. albicans*

The model organism was *C. albicans* ATCC 90028. Yeast inoculum was prepared using colonies grown for 24 hr on Sabouraud dextrose agar (SDA: HiMedia Laboratories, Mumbai, India). A spectrophotometer (A600 nm) was used to adjust the cell suspension in different broth media to a final concentration of 10^6 cells/mL for cytotoxicity and biofilm formation experiments. For proteome analysis and other experiments, the yeast cells were adjusted to a final concentration of 10^7 cells/mL.

3.2 Determination of minimum inhibitory concentration (MIC) and minimum fungicidal concentration (MFC)

The MIC values for all crude extracts and β-citronellol were determined using a broth microdilution test following the clinical and laboratory standards institute (CLSI) guideline M27-A2 with certain modifications. In brief, 100 µL of a twofold serial dilution of crude extracts (0.20–100 mg/mL) and β-citronellol (2–1,024 µg/mL) in RPMI-1640 medium (Thermo Fisher Scientific, Waltham, MA, USA) were put onto a 96-well plate. At 530 nm, *C. albicans* suspension was adjusted to meet the turbidity of the 0.5 McFarland standard, and then 10 µL of yeast cell suspension was added to each well containing pre-diluted crude extracts and β-citronellol to achieve a final concentration of 0.5-1 × 10^3 cells/mL. The cells were then cultured at 35±2°C for 48 hr. Following incubation, 100 µL of resazurin (0.02 mg/mL) was added and incubated for an additional 3 hr at 35±2°C. Any color changes were observed, and

wells that remained unchanged in color (the blue color of resazurin remained unchanged) were used to determine the MIC value. To determine the MFC values, the spread plate technique was performed by distributing 10 µL of cell suspension on SDA and incubating for 48 hr at 35±2°C. There was no colony growth at the end of the incubation, thus the determined concentration value was used as MFC.

3.3 Kinetic growth inhibition assay

To measure the influence of β-citronellol on yeast growth, cells were cultured in a 96-well plate with 100 µL of Sabouraud dextrose broth (SDB: HiMedia Laboratories, Mumbai, India) combined with different concentrations of β-citronellol. In a multidetector microplate reader, the plate was incubated at 35±2°C for 48 hr. The turbidity was measured at OD_{600} nm for every 2 hr.

3.4 Sample preparation for proteomic analysis

To prepare the sample for proteome analysis, yeast cells were cultured for 24 hr in SDB containing β-citronellol (128 µg/mL). The cells were washed twice with 1X phosphate buffer saline (PBS) pH 7.4 (137 mM NaCl, 2.7 mM KCl, 10 mM Na_2HPO_4, and 1.8 mM KH_2PO_4). The cells were then resuspended in lysis buffer (1% SDS, 5mM dithiothreitol (DTT) in 0.1X PBS pH 7.4 (13.7 mM NaCl, 0.27 mM KCl, 0.43 mM Na_2HPO_4, and 0.147 mM KH_2PO_4) supplemented with 1X protease inhibitor cocktail), sonicated for 30 s, and left on ice, then centrifuged for 20 min at 12,000 RPM, at 4°C. Precipitated proteins were then kept at -20°C for 16 hr. The protein pellet was reconstituted in 0.25% RapidGest SF (Waters, UK) in 10 mM ammonium bicarbonate following precipitation. The protein concentrations were measured using a bicinchoninic acid assay kit (Pierce, New York, NY, USA) with bovine serum albumin serving as the standard. Then, 25 µg of protein were digested without the use of gels. 5 mM DTT was used to reduce sulfhydryl linkages, followed by a 20 min incubation at 80°C. Alkylation of sulfhydryl groups was carried out at room temperature for 30 min in the dark using 25 mM iodoacetamide (IAA). The solution was purified using a molecular weight cut-off of 7 kDa in a volume of 0.5 mL (ZebaTM Spin Desalting Columns, Thermo Fisher Scientific, USA). Proteolytic digestion was performed on the protein solution using 500 ng of sequencing grade trypsin (Promega, Germany) and incubated at 37°C for 3 hr. Before transferring to a TruView LC-MS vial, the peptides were resolubilized in 0.1% formic acid/LC-MS water (Waters, UK).

3.5 Proteomic analysis by liquid chromatography-tandem mass spectrometry (LC-MS/MS)

To examine the protein expression profiles of *C. albicans*, peptide mixtures were evaluated in data-dependent mode on tandem mass spectrometers equipped with an Orbitrap HF hybrid mass spectrometer and an UltiMate 3000 liquid chromatography system. To summarize, the peptides were desalted on a reverse-phase C18 PepMap 100 trapping column and then resolved onto a C18 PepMapTM 100 capillary column using a 150-min gradient of CH_3CN, 0.1% formic acid at the flow

rate of 300 nL/min. The peptides were evaluated using the data-dependent Top15 method, which begins with a comprehensive scan of peptide ions in the Orbitrap analyzer, followed by high-energy collisional dissociation and MS/MS scans of the 15 most abundant precursor ions. From m/z 400 to 1600, full scan mass spectra were obtained with an AGC target set at 3×10^6 ions and a resolution of 60,000. When the ACG target reached 10^5 ions, the MS/MS scan was commenced. A dynamic exclusion window of 12 sec was used to choose ions.

Proteome Discoverer software version 2.4 (Thermo Scientific) was used to analyze raw files using the SEQUEST, Percolator, and Minora algorithms. The LC-MS spectrum was compared to the UniProt reference proteome for *C. albicans* (UP000000559; downloaded 08/08/2021; 6035 items). The following criteria were used for protein identification and quantification: a maximum of two missed trypsin cleavages were permitted with a precursor mass tolerance of 5 ppm and a fragment mass tolerance of 0.01 Da. Static adjustments included carbamidomethylating +57.021 Da (cysteine) and oxidation +15.995 Da (methionine), whereas dynamic modifications included carbamidomethylating +57.021 Da (cysteine) and oxidation +15.995 Da (methionine). In both situations, the false discovery rate (FDR) for peptide and protein identification was set to 0.05. The relative protein abundance ratio was normalized using the total peptide amount for each LC run (across all runs; n = 6) using the Proteome Discoverer software's normalization technique. Multiple consensus procedures inside the Proteome Discoverer program were used to group the PSMs into peptide groups, protein database matches, and lastly non-redundant protein groups utilizing the rigorous parsimony criteria established by the vendor software defaults. Proteomics data from mass spectrometry have been deposited with the ProteomeXchange Consortium via the PRIDE protocol.

3.6 Biofilm formation assay and crystal violet staining

The anti-biofilm formation effect of β-citronellol was determined following the previously described protocol (92). Briefly, 48 hr of *C. albicans* colonies on SDA were adjusted to 10^6 CFU/mL in RPMI-1640 medium. Then, 100 µL yeast was added to a 96-well flat-bottom cell culture plate (Wuxi NEST Biotechnology Co., Ltd., Jiangsu, China). The yeast cells were incubated at 35±2°C for 1.5 hr with constant shaking at 250 rpm. To eliminate non-adherent cells, the plate was washed once with 1X PBS. To ascertain the effects of active substances, 100 µL of citronellol at various doses was applied and incubated at 35±2°C for 24 hr. The cells were treated with 2 µg/mL amphotericin B as a positive control. Following incubation, the *C. albicans* biofilm was rinsed three times with PBS to remove non-adherent cells. The plate was air-dried for 45 min at room temperature. After staining the yeast biofilm with 0.4% crystal violet for 45 min, it was rinsed three times with PBS. To determine the absorbance, 200 µL of 95% ethanol was used to destain crystal violet for 45 min, followed by the transfer of 100 µL of each well to a new plate. The absorbance was determined using a microplate reader at 595 nm.

3.7 Determination of reactive oxygen species (ROS) production

To measure the formation of ROS, cells were treated with β-citronellol, and the ROS level was determined using 2′,7′-dichlorofluorescein diacetate (H_2DCFDA) (Invitrogen, Waltham, MA, USA) according to the manufacturer protocol. *C. albicans* (10^6 cells/mL) was cultured with several doses of β-citronellol in SDB for 4 hr at 35±2°C. As a positive control, yeast cells treated with 2 mM hydrogen peroxide (H_2O_2) in SDB were used in this experiment. Cells were collected after incubation by centrifuging at 12,000 RPM for 5 min and washing once with PBS. The cells were treated with 10 mM H_2DCFDA in PBS at 35±2°C for 30 min in the dark. After a single wash with PBS, the cells were resuspended in the same buffer. We transferred 100 µL of the cell suspension to a 96-well fluorescent plate. The fluorescence intensity was measured at 485/535 nm excitation/emission wavelengths.

3.8 Evaluation of membrane potential disruption

To investigate the influence of β-citronellol on yeast membrane potential, the cell membrane potential was determined using $DiBAC_4(3)$ (Bis-(1,3-dibutylbarbituric acid) trimethine oxonol) (Invitrogen, Waltham, MA, USA) as described previously (88). Yeast cells (10^6 cells/mL) were grown in SDB and then incubated for 4 hr at 35±2°C with diluted β-citronellol. For the positive control group, yeast cells were treated with amphotericin B at a concentration of 2 µg/mL. The cells were harvested by centrifugation at 12,000 RPM for 5 min and then washed once with PBS, and then the yeast cells were incubated in the dark at 35±2°C with 20 µg/mL $DiBAC_4(3)$ in PBS. Centrifuged cells were resuspended in PBS and put on a 96-well fluorescent plate following incubation. The fluorescence intensities were determined using a fluorescence spectrophotometer at 492/518 nm excitation/emission wavelengths.

3.9 Apoptosis analysis in yeast cells

The purpose of this experiment was to investigate the effect of β-citronellol on inducing programmed cell death via apoptosis. Firstly, protoplast preparation was performed (93), and protoplast buffer preparation was conducted, both procedures were performed according to a previously described protocol (94). Cells were exposed to various concentrations of β-citronellol (64, 128, and 256 µg/mL) for 6 hr and then washed twice with protoplast buffer-I (1 M sorbitol, 30 mM DTT, 50 mM Tris base, and 10 mM $MgCl_2$). The cells were then incubated at 25°C for 15 min in the same buffer, followed by centrifugation at 12,000 RPM for 5 min. The pellets were resuspended in protoplast buffer-II (1 M sorbitol, 1 mM DTT, 50 mM Tris base, and 10 mM $MgCl_2$) supplemented with lyticase enzyme (≥ 1.0 µg/mL) (Sigma-Aldrich, MO, USA) and incubated for 1 hour at 25°C. After centrifugation to remove buffer-II, the cells were incubated for 20 min at 25°C in protoplast buffer-III (1 M sorbitol, 50 mM Tris base, and 10 mM $MgCl_2$) and then collected, the supernatants were discarded and the cells were washed once with PBS. The Muse™ Annexin V & Dead Cell Kit (Merck, Darmstadt, Germany) was used to assess the apoptotic phenotype. The protoplasts were resuspended in SDB with 1% fetal bovine serum (FBS), and 100 µL of protoplasts were combined with 100 µL of Muse™ Annexin V & Dead Cell Kit. The mixture was incubated at room temperature in the dark for 20 min and the

yeast cells were then examined according to the manufacturer's protocol using the Muse™ Cell Analyzer.

3.10 Scanning electron microscopy (SEM)

To examine the effect of β-citronellol on the morphology of *C. albicans*, yeast cells were observed using SEM under a previously described protocol (95). The cells were cultured at 35±2°C for 4 hr with various doses of β-citronellol and then centrifuged at 12,000 RPM for 5 min. After resuspending the pellets in PBS, 50 µL of cells were put onto a glass slide and incubated at room temperature for 30 min and then 0.5 mL of primary fixative (4% paraformaldehyde) was applied and the cells were incubated 1 hr at room temperature. The cells were then rinsed 3 times (two min each), then post-fixed with 1% OsO_4 at room temperature for 1 hr. The post-fixed cells were washed once with PBS and dehydrated in ethanol concentrations of 25%, 50%, 75%, 95%, and 100% and then dehydrated for 15 min with a 1:1 solution of hexamethyldisilazane (HMDS) and ethanol, followed by 15 min with 100% HMDS. The excess solution was washed away and the cells were dried for 4 hr at room temperature. The cells were then coated with gold via cathodic spraying, and the morphology of yeast cells was studied at a magnification of 5,000X using the Apreo 2 SEM (Thermo Scientific) in high vacuum mode at 5 kV.

Development of mouthwash containing herbal extracts

First, this section describes the development of a mouthwash containing herbal extracts from the leaves of three plants: *C. hystrix* DC. (KL), *Moringa oleifera* Lam. (MO), and *Azadirachta indica* A. Juss (NE). Three different types of mouthwashes were developed: 1) containing only KL extract, 2) containing both KL and MO extracts (KL+NO), and 3) containing both KL and NE extracts (KL+NE). The section then compares the anti-gingivitis activity of mouthwash to placebo and positive control (0.12% chlorhexidine gluconate mouthwash) (CHX) in gingivitis participants. The protocols for this experiment are represented in **Figure 29**.

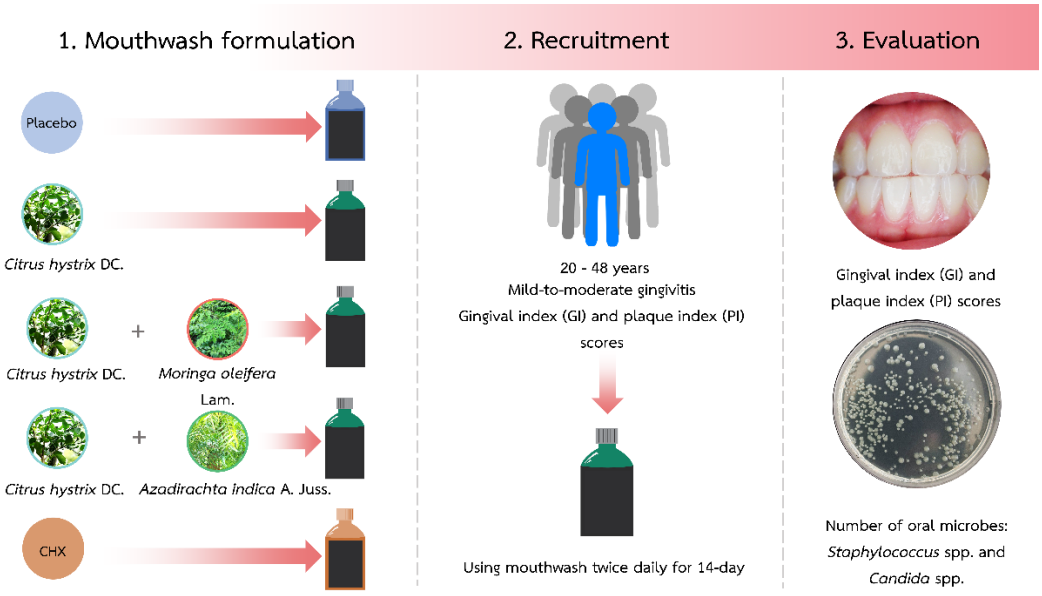

Figure 29 Experimental protocol for evaluating the anti-gingivitis mouthwashes (96). There are three stages to producing an anti-gingivitis mouthwash. All four mouthwash formulations (placebo, KL, KL+MO, and KL+NE) and a commercially available 0.12% chlorhexidine mouthwash (CHX) were utilized. Gingivitis participants were recruited and advised to use mouthwash for 14 days. The parameters, including the GI, PI scores, and the quantity of candidate oral microbials colonies, were examined and assessed at baseline and after 14 days of mouthwash usage.

4.1 Crude extraction protocol for plants

Powdered leaves of KL (COA Lot. No. 250818), MO (COA Lot. No. 5534), and NE (COA Lot. No. 021018) were obtained from Khaolaor Laboratories Co., Ltd. Briefly, three crude extracts were obtained by, first, macerating 1,700 g of KL powder in 5,100 mL of 95% ethanol for three days, then macerating 1,000 g of MO powder in 5,100 mL of 95% ethanol for three days, and, finally, macerating 1,000 g of NE powder in 3,000 mL 95% ethanol for seven days. All three extracts were filtered through 0.45-micron filter paper and evaporated at a temperature of 35°C using a rotary evaporator. The ethanolic extracts yielded 133 g (6.65% yield) of KL, 106.75 g (10.68% yield) of MO, and 89 g (8.9% yield) of NE.

4.2 Evaluation of total phenolic content

The total phenolic content of the ethanolic extracts from KL, MO, and NE was determined according to the Folin-Ciocalcteu technique with minor modifications (86). In a 96-well plate, 2.5 µL of all extracts (100 mg/mL) and serially diluted gallic acid were added. Each well received 5 µL of F-C reagent (10% v/v), followed by 90 µL of Na_2CO_3 (2% w/v). The plate was incubated at 50°C for 1 hr, and then the reaction was determined by measuring the absorbance at 750 nm.

4.3 Investigation of antioxidant activity

The assay for determining Trolox-equivalent antioxidant capacity (TEAC) was applied using the 1,1-diphenyl-2-picrylhydrazyl (DPPH) scavenging reaction, which was modified slightly from a prior publication (97). In a 96-well plate, 5 µL of each extract was added along with serially diluted 0.2 mM Trolox. Then 50 µL of DPPH in methanol (1:5) was added and the reaction was incubated at room temperature for 2 hr in the dark. The absorbance of the sample was measured at 517 nm.

4.4 Chemical constituents analysis by GC-MS

Volatile chemicals were analyzed using a Hewlett Packard Gas Chromatograph model 6890 (Agilent Technologies, Palo Alto, CA, USA) fitted with a mass selective detector. All extracts were separated chemically using a Hewlett Packard HP-5 (5 per cent phenyl methyl siloxane) silica capillary column (30 m × 0.25 mm i.d., 0.25 µm film thickness). The carrier gas was pure helium at a constant flow rate of 13.7 mL/min. With a split ratio of 10:1 and a 1 µL injector capacity, the initial temperature was adjusted to 250°C. The oven was preheated to 70°C for 3 min, then increased to 280°C at a rate of 5°C/min for approximately 20 min. The transfer temperature was set to 280°C, and the mass detection range for the full scan was set at 50 to 700 amu. Volatile chemicals were identified using computer matching of their mass spectral fragmentation patterns stored in the Wiley 7n MS spectral library or with previously published data. The percentages of identified chemicals from the three plants were calculated using the peak regions produced in the chromatogram.

4.5 Mouthwash descriptions

Five different mouthwash formulations were used in this study: (i) a placebo mouthwash, (ii) KL mouthwash, (iii) KL and MO mouthwash, (iv) KL and NE mouthwash, and (v) 0.12% chlorhexidine mouthwash (C-20 Chlorhexidine antiseptic mouthwash, Edwards, Bangkok, Thailand). KL mouthwash contains a 0.03% ethanolic extract of KL leaves. KL and MO mouthwashes included ethanolic extracts of KL and MO leaves at concentrations of 0.015% and 0.015%, respectively. KL and NE mouthwashes included ethanolic extracts of KL and NE leaves at concentrations of 0.015% and 0.015%, respectively. Water, propylene glycol, glycerin, sorbitol, sucralose, flavoring agents, sodium benzoate, and coloring agents were all common constituents in mouthwash in categories (i)–(iv).

4.6 Study design

This clinical trial was conducted in a single-blind, randomized, placebo-controlled fashion. The Human Ethics Committee of Naresuan University (IRB no. 1065/61) accepted the study procedure. The participating volunteers gave written informed consent under the Declaration of Helsinki statement. Each participant was assigned a code and was randomly assigned to one of five experimental groups using computer-based randomization software. Each participant was assigned a three-digit code. The first digit denoted the treatment group assigned between 1 and 5, while the latter two digits denoted the participant number. The examiner and all participants

were unaware of the code explanation. Only the primary researcher has access to identifying data in this study. Each set of subjects was assigned to use a particular type of mouthwash. The study procedure comprised the assessment of GI and PI scores, as well as the quantity of oral microbial colonies, during the initial visit and for 14 days following mouthwash use.

The sample size was estimated using the following formula:

$$n = \frac{2(Z_{\alpha}+Z_{1-\beta})^2\delta^2}{\Delta^2}$$

where n = needed sample size; Z = constants: Z_{α} (1.96) and $Z_{1-\beta}$ (0.84); δ is a standard deviation (0.8); and Δ is the difference in the effects of two interventions (1) (98). This estimate indicates that 50 participants are required for this study.

4.7 Participants

Fifty healthy participants from Naresuan University were recruited for the study. Their ages ranged from 20 to 48 (median 21±6.6). The research team examined all potential participants for appropriateness and 47 participants who met the inclusion criteria were included, as shown in **Table 5**. Eligible participants were informed verbally and in writing about the therapy goods and study objectives, and that they could withdraw from the study at any time. **Figure 30** depicts the flow chart of the study.

Table 5 Recruitment of participants: inclusion and exclusion criteria (96).

Inclusion criteria	Exclusion criteria
• 18 – 60 years of age • Mild to moderate gingivitis (GI and PI score < 2) • Good general health • Able to communicate fluently in Thai	• Use of orthodontic appliances or implants • Periodontitis • Use of antibiotics, anti-inflammatory, anticoagulants, anticonvulsants, immunosuppressants and anticancer drugs within the preceding 6 months • Systemic disease-associated oral health e.g. diabetes, sepsis and oral cancer • Smoking • Xerostomia • Allergic to herbs and mouthwash • Pregnant or breastfeeding

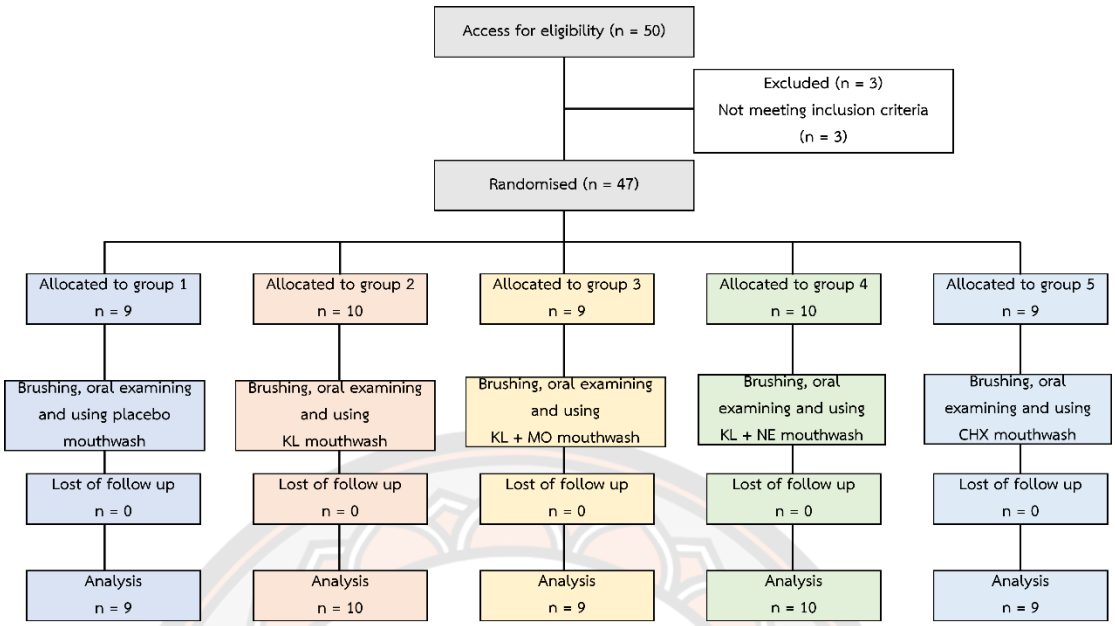

Figure 30 Flow chart of the study (96).

Forty-seven individuals were randomly assigned to one of five groups. There were nine participants in groups (i), (iii), and (v), and ten subjects in groups (ii) and (v) (iv). Participants in all groups were entirely present throughout the trial, and there was no loss of follow-up.

4.8 Interventions

On the first day, all participants were instructed to brush their teeth 5 hr before commencing the activity, and then gargle for 1 minute with normal saline. Oral rinse samples were collected and stored at a temperature of 4°C. The baseline of GI and PI scores were measured by a dentist using a periodontal probe and 6% erythrosine solution staining. Following the assessment, each individual was randomly allocated to one of five groups: Group 1 received a placebo mouthwash, Group 2 received a KL leaf extract mouthwash, Group 3 received a KL leaf extract mouthwash combined with MO leaf extract, Group 4 received a KL leaf extract mouthwash combined with NE leaf extract, and Group 5 received a 0.12% chlorhexidine gluconate mouthwash (CHX). The participants were instructed to gargle with 10–15 mL of the mouthwash twice a day for 30 seconds following tooth brushing, and repeating this daily for 14 days. Subsequent rinsing with water, drinking, and eating was prohibited within 15 min of the gargling process. Commercial mouthwashes were not permitted during the research. The gingival index (GI) and plaque index (PI) scoring systems of Löe-Silness were utilized to assess changes in the gingival conditions of inflammation and plaque development, as shown in **Table 6** (99). Gingival inflammation was evaluated using the GI system, where gum inflammation was assessed on a four-point scale ranging from 0 (normal) to 3 (severe) (severe gingival inflammation). A 6% erythrosine solution was used to assess plaque formation, with scores ranging from 0 to 3

Table 6 The GI and PI scoring criteria (99).

Parameter	Score	Criteria
GI	0	Normal gingival
	1	Mild inflammation – slight color change, a slight change in edema. No bleeding on probing.
	2	Moderate inflammation – redness, edema and glazing. Bleeding on probing.
	3	Severe inflammation – marked redness and edema. Ulceration. Tendency to spontaneous bleeding.
PI	0	No debris or stain present
	1	Soft debris covering not more than one-third of the tooth surface, or the presence of extrinsic stains without other debris regardless of surface area covered
	2	Soft debris covering more than one-third, but not more than two-thirds of the exposed tooth surface
	3	Soft debris covering more than two-thirds of the exposed tooth surface

4.9 Assessment and outcome

The assessment protocol was separated into two sections: one occurring on the baseline Day 0, and again on Day 15. At each visit during the 2 weeks, participants were told to brush their teeth and abstain from food and drink for 5 hr before the assessment, except for water. Gingival index (GI) and plaque index (PI) measurements were taken by a licensed and calibrated dentist.

The GI score was used to determine the severity of the gingivitis by observing the qualitative changes in the gingival tissue, using a mouth mirror. Four regions of the gumline of six selected index teeth were probed with a periodontal probe. After 15 seconds, the amount of bleeding from each region was recorded. The PI score was determined by staining with a solution of 6% erythrosine. After 15 seconds, respondents were informed to rinse their mouths with water, and plaque staining on the four locations of the six selected index teeth was seen using a mouth mirror.

The spread plate method was used to determine the number of microbial colonies. The oral rinse samples were vortexed for 10 seconds, following which 0.1 mL of each sample was deposited on one of two selective mediums: (i) Mannitol salt agar (MSA) and (ii) HiCrome^{TM} *Candida* differential agar. The sample agar plates were incubated at 35±2°C for 20–24 hr. *Staphylococcus* and *Candida* species colonies were detected morphologically and subsequently validated using matrix-assisted laser desorption/ionization time of flight mass spectrometry (MALDI-TOF MS). The colonies were counted using the Image J program and a colony counter plugin. For mean GI and PI, the key efficacy outcome was different. The secondary outcome was a decrease in the number of microbial colonies from baseline Day 0 to Day 15.

Statistical analysis

The data from the anti-inflammatory and anti-NLRP3 inflammasome experiments were analyzed using GraphPad Prism Software version 6 (GraphPad Software Inc., San Diego, CA, USA). In triplicate, three independent experiments were carried out. The mean and standard deviation were used to express all of the data. The means were compared using a one-way ANOVA followed by Tukey's multiple comparison *post hoc* test. A *p*-value of less than 0.05 was deemed statistically significant. * $p < 0.05$, ** $p < 0.01$, *** $p < 0.001$, and **** $p < 0.0001$, respectively.

In the anti-*Candida* experiments, GraphPad Prism version 8.01 was used to perform statistical analyses on all of the data (GraphPad Software, San Diego, CA, USA). The results were subjected to analysis of variance, one-way ANOVA, and Tukey's range test for comparison of means. All of the tests were done in triplicate, and the results were presented as the Mean Standard Error.

For the clinical trials data, SPSS software version 26 (released in 2019) (IBM SPSS Statistics for Windows, Version 26.0., IBM Corp, Armonk, NY, USA) and GraphPad Prism software version 6 (GraphPad Software Inc., San Diego, CA, USA) were used to examine the study parameters. The statistical difference between the means from the *in vitro* experiment was calculated using a one-way ANOVA followed by Tukey's multiple comparison *post hoc* test. The Shapiro-Wilk test was used to determine the data distribution. Both the Wilcoxon signed-rank test and the paired-sample t-test were employed to assess the differences between the baseline Day 0 and the Day 15 data. To compare the mean differences between the five groups, the Kruskal-Wallis test was utilized.

Chapter IV

Results

Extraction and identification of active compounds

1.1 Crude extraction of kaffir lime leaf powder

The extraction yielded three types of kaffir lime leaf crude extracts based on the solvents; crude hexane, crude ethyl acetate, and crude ethanol. The weight and yield percentage of all the crude extracts were 21.03 g (2.10%) from hexane, 39.12 g (3.91%) from ethyl acetate, and 100.56 g (10.056%) from ethanol. The screening tests for the anti-inflammatory activity of all crude extracts were then done *in vitro*. Based on the suppression of TNF-α release in LPS-induced MDMs, the crude ethanolic extract demonstrated the strongest anti-inflammatory activity, followed by crude ethyl acetate and then crude hexane.

1.2 Measurement of the total phenolic content of crude extracts

The phenolic content of all the crude kaffir lime leaf extracts was determined using the Folin-Ciocalteu method, and the data were expressed as mg of gallic acid equivalent (GAE) per gram of dry weight extract. As illustrated in **Figure 31**, the crude ethanol contained the most phenols (430.23±32.11 mg/GAE), followed by the crude ethyl acetate (414.81± 16.34 mg/GAE) and then the crude hexane (203.80 ±12.91 mg/GAE).

1.3 Evaluation of the antioxidants capacity

The three crude extracts of kaffir lime leaves showed a trend of antioxidant activity profiles to their total phenolic contents. As shown in **Figure 31**, the crude ethanol had the highest TEAC (372.57±17.63 µM), followed by the crude ethyl acetate (239.08±4.05 µM) and then the crude hexane (121.76± 5.35 µM).

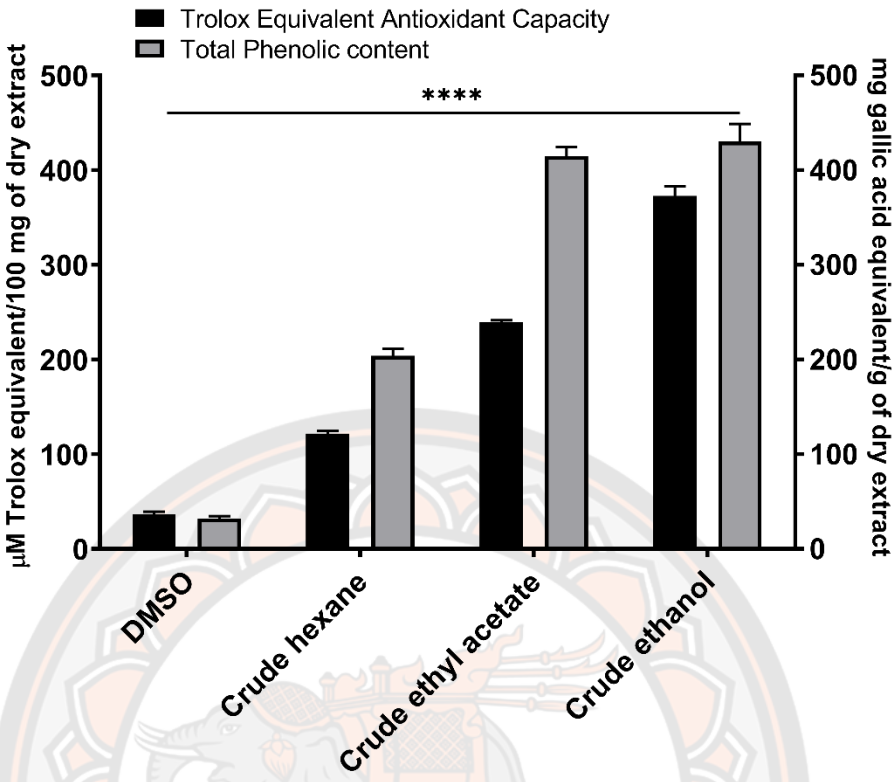

Figure 31 Total phenolic content and TEAC profiles from crude kaffir lime leaf extracts.

Crude ethanolic extract has the highest antioxidant capacity and total phenolic content among the others, followed by crude extracts from ethyl acetate and hexane.

1.4 Active compound isolation and identification

Based on the TNF-α releasing results, the crude ethanol extract was chosen to be further fractionated using Silica-gel column chromatography, as shown in **Figure 32**. Fraction no. 4 has the strongest anti-inflammatory activity, and was selected to be further fractionated. Subfraction no. 4.6 or CHAF was fractionated which yielded 1.2 mg of an unknown white, solid compound. Spectroscopic techniques, including proton nuclear magnetic resonance (^{1}H NMR), electron ionization mass spectroscopy (EI-MS), and Fourier-transform infrared spectroscopy (FT-IR) were used to deduce the structure which was identified by computer matching its recorded mass spectrum to a standard library, Wiley7n, at a 95% match rate. Those spectra were compared to previously published data (100-102), and the structure was identified as lupeol, a well-known pentacyclic triterpenoid (**Figure 33**). Lupeol; $C_{30}H_{50}O$, EI-MS m/z 426 [M]+, FT-IR (ATR) ν_{max} (cm−1): 3315, 2942, 2871, 2853, 1638, 1451, 1188, 1035. 1H NMR (400 MHz, CDCl3, δ ppm): 4.69 (d, J = 2.5 Hz H-29a), 4.56 (dq, J = 2.8, 1.4 Hz H-29b), 3.19 (dd, J = 10.7, 5.0 Hz, H-3), 2.38 (m, H-19), 1.91 (m, H-21), 1.53, 1.68 (overlap, H-2), 1.68 (s, H-30), 1.65 (overlap, H-13), 1.39 (overlap, H-7), 1.37, 1.38 (overlap H-18), 1.36, 1.53 (overlap, H-6), 1.36, 1.45 (overlap, H-16), 1.25 (overlap, H-9), 1.20, 1.40 (overlap, H-11), 1.17, 1.38 (overlap, H-22), 1.08, 1.62

(overlap, H-12), 1.05, 1.60 (overlap, H-15), 1.03 (s, H-26), 0.94, 1.65 (overlap, H-1), 0.96 (s, H-27), 0.94 (s, H-23), 0.83 (s, H-25), 0.79 (s, H-28), 0.76 (s, H-24), 0.67(overlap, H-5). 13C NMR (100 MHz, CDCl3, δ ppm): 151.1 (C-20), 109.5 (C-29), 79.2 (C-3), 55.4 (C-5), 50.6 (C-9), 48.5 (C-18), 48.1 (C-17), 48.1 (C-19), 43.0 (C-14), 41.0 (C-8), 40.2 (C-22), 39.0 (C-1), 38.9 (C-4), 38.2 (C-13), 37.3 (C-10), 35.7 (C-16), 34.4 (C-7), 30.0 (C-21), 28.1 (C-23), 27.6 (C-2), 27.6 (C-15), 25.3 (C-12), 21.1 (C-11), 19.5 (C-30), 18.5 (C-28), 18.2 (C-6), 16.3 (C-25), 16.1 (C-26), 15.5 (C-24), 14.7 (C-27).

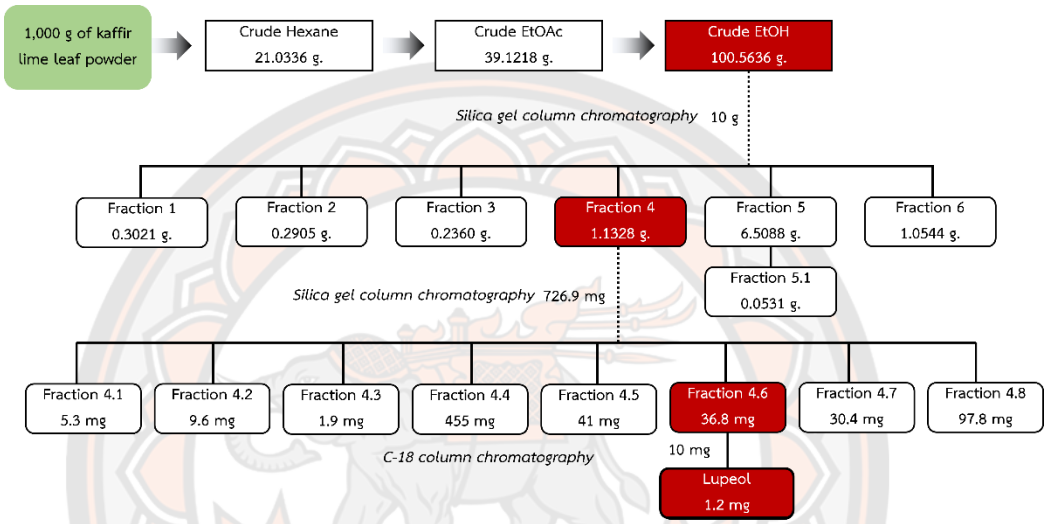

Figure 32 Diagram of kaffir lime leaf extract fractionation to identify an active compound.

To select the candidate crude and fraction for the subsequent experiment on chemical identification, a screening test for anti-inflammatory properties was conducted. The crude or fraction with the highest anti-inflammatory activity was indicated by the red color and was chosen for further fractionation. Finally, one of the active compounds from this fractionation protocol was identified as lupeol.

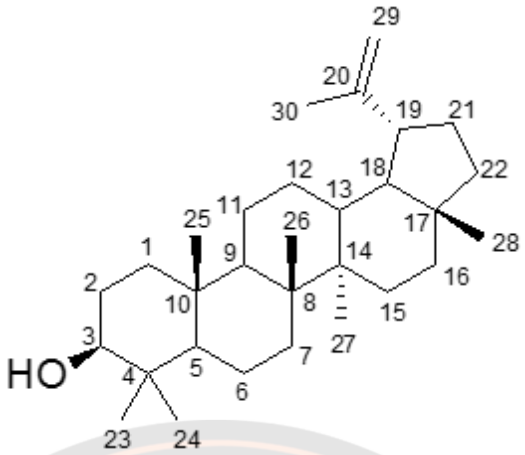

Figure 33 Chemical structure of lupeol ($C_{30}H_{50}O$) (91).

Lupeol is pentacyclic triterpenoid that is lupane in which the hydrogen at the 3β position is substituted by a hydroxy group. Properties computed from the structure of lupeol show that it has a molecular weight of 426.7174 g/mol, and the boiling point is 488.1±14.0 °C at 760 mmHg (103).

Determination of anti-inflammation and anti-NLRP3 inflammasome activities

2.1 Flow cytometry analysis

The expression of CD14/CD16 markers on human MDMs and THP-1-derived macrophages is shown in **Figure 34.** The double-positive staining for both CD14 and CD16 were 85.9% and 23.0% in human monocytes and THP-1 cells, respectively. After seven days of differentiation, the expression of CD14/CD16 was upregulated to 98.2% and 86.7% in the MDMs and THP-1-derived macrophages, respectively. This result indicated that the differentiation protocol for THP-1 was able to induce CD14/CD16 expression and share a similar trend to MDMs.

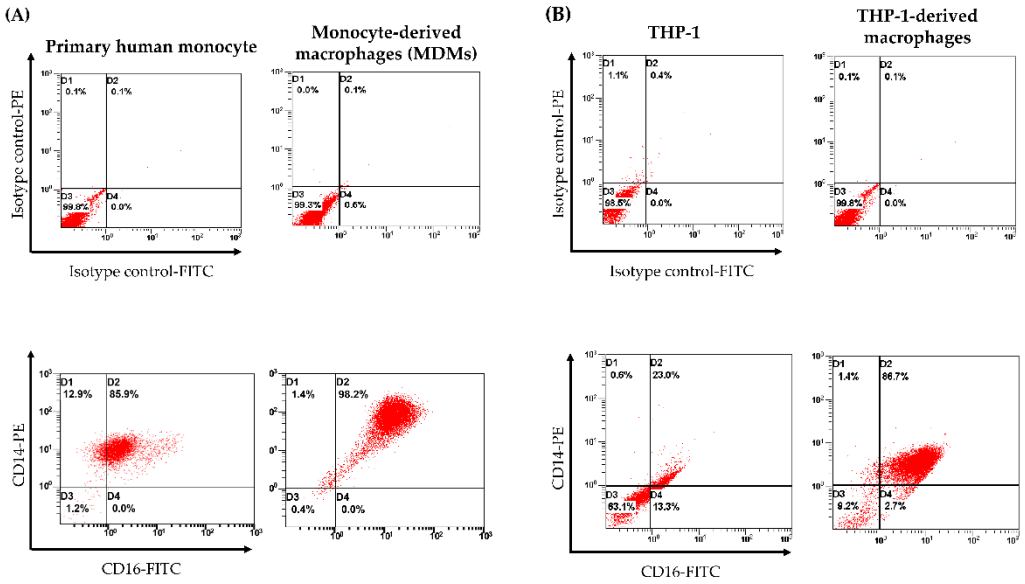

Figure 34 CD14 and CD16 expression profiles of monocytes, MDMs, THP-1, and THP-1-derived macrophages (91).

The study of CD14 and CD16 expression using flow cytometry. (A) The surface marker expression profile of monocytes and MDMs both had positive CD14/CD16 percentages of 85.9% and 98.7%, respectively. (B) The percentage of THP-1 cells expressing the cell surface markers CD14/CD16 was 23.0%. CD14/CD16 expression on cell surface rose to 86.7% after differentiation with PMA.

2.2 Cell viability measurement by MTT assay

The optimal doses for further experiments were determined for all crude kaffir leaf extracts, CHAF, and lupeol as shown in **Figure 35**. MDMs and macrophages derived from THP-1 were used as models. For the MDMs, crude hexane, crude ethyl acetate, and crude ethanol had IC_5 values of 281.74, 52.04, and 247.01 µg/mL, respectively. Due to the low concentrations of CHAF and lupeol, certain concentrations were chosen and tested on MDMs and THP-1-derived macrophages. For subsequent experiments, the optimal doses of CHAF and lupeol were set to be less than or equal to 2.5 and 30 µg/mL, respectively.

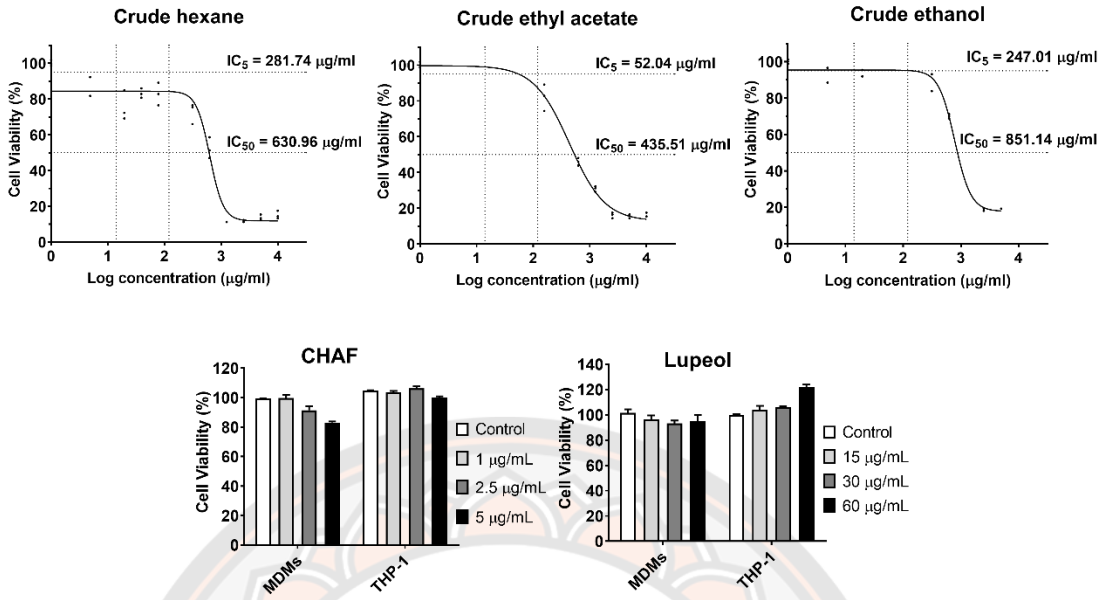

Figure 35 Cellular cytotoxicity of crude kaffir lime leaf extracts, CHAF and lupeol (91).

The effect of crude extracts, CHAF, and lupeol on human MDMs and THP-1-derived macrophages in terms of cell viability percentage. Among all crude extracts, crude ethyl acetate had the greatest cytotoxicity toward MDMs, followed by crude hexane and crude ethanol. MDMs were more CHAF-sensitive than macrophages derived from THP-1. However, even at the highest concentration (60 g/mL), lupeol was less toxic to both cells.

2.3 Screening for the anti-inflammatory activity of kaffir lime leaf crude extracts and their fractions

As shown in **Figure 36**, the fractionation procedure was based on the substance's capacity to reduce TNF-α secretion from LPS-induced MDMs. Crude ethanol, fraction number 4, and sub-fraction number 4.6 (CHAF) had the highest anti-inflammatory activity in each group of crude extract, fraction, and subfraction, respectively.

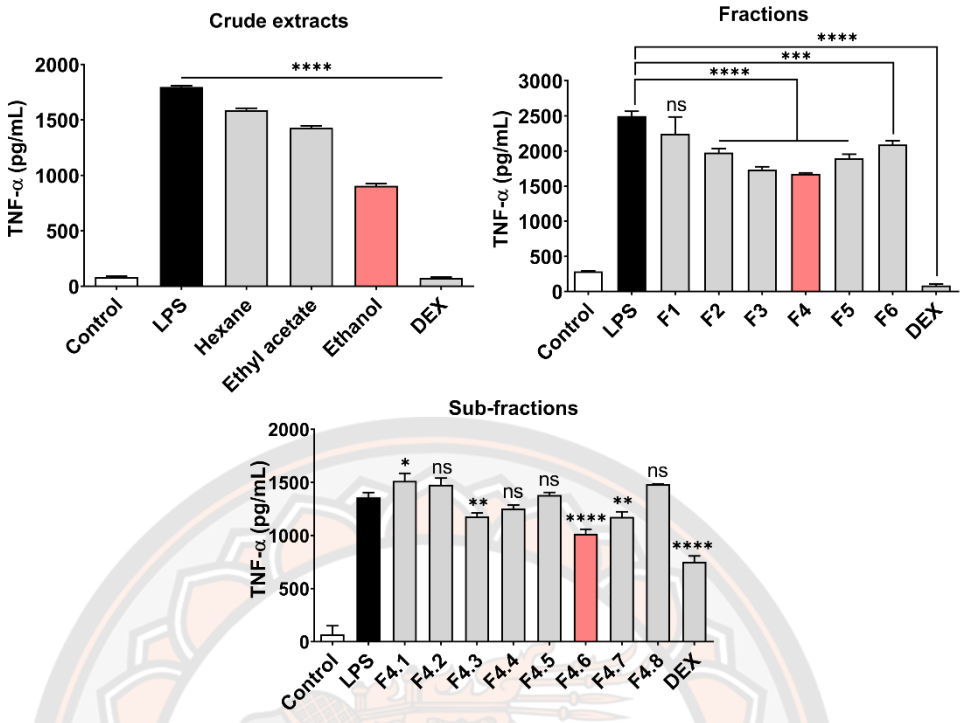

Figure 36 The effect of crude, fractions, and sub-fractions from kaffir lime leaves on TNF-α level (91).

The MDMs were pretreated with crude extracts, fractions, and subfractions for 1 hr, then challenged with LPS for a further 24 hr. The supernatant from all conditions was collected and the amount of TNF-α level was measured using the TNF-α ELISA kit. The data are presented as mean ± standard deviation. * $p < 0.05$; ** $p < 0.01$; *** $p < 0.001$; **** $p < 0.0001$ in comparison to LPS treatment. LPS: macrophages activated with lipopolysaccharide; DEX: dexamethasone.

2.4 Investigation of the effect on NF-κB inflammatory signaling pathway

CHAF and lupeol were found to have anti-inflammatory properties in LPS-stimulated MDMs. In comparison to the LPS-stimulated condition alone, IL-1β, IL-6, and TNF-α levels were significantly decreased in the treatment group, as well as the expression of *NFKB1* and *NOS2* genes, as shown in **Figure 37**. NF-κB-associated protein, IκB-α phosphorylated form, NF-κB p65, and COX-2 were investigated at the protein level. The results indicated that LPS increased the expression of the transcription factors phospho-IκBα, NF-κB p65, and COX-2 proteins (**Figure 38**). Pre-treatment with CHAF and lupeol significantly reduced the expression of all mentioned proteins compared to the LPS-stimulated condition.

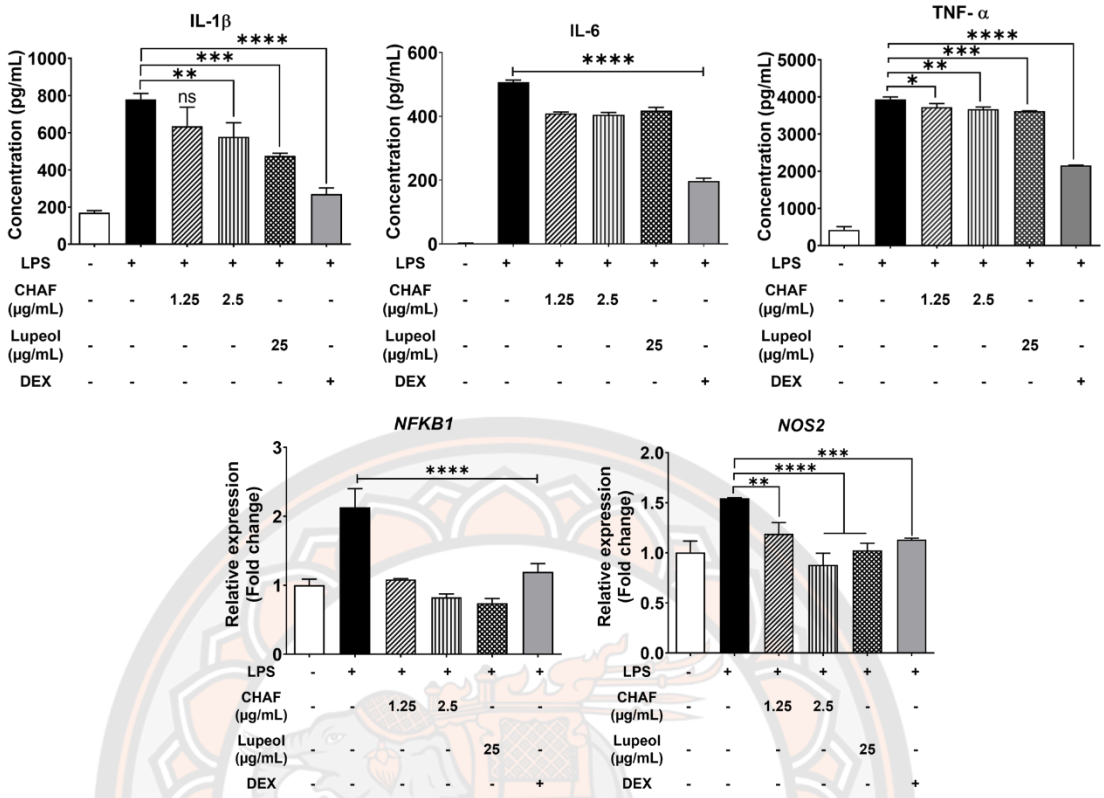

Figure 37 CHAF and lupeol suppressed pro-inflammatory cytokines releasing and inhibiting genes expression in MDMs (91).

In the pre-treatment with CHAF and lupeol, the level of pro-inflammatory cytokines released (IL-1β, IL-6, and TNF-α) and the expression of pro-inflammatory genes (*NFKB1* and *NOS2*) in LPS-induced MDMs were suppressed. The data are presented as mean ± standard deviation. * $p < 0.05$; ** $p < 0.01$; *** $p < 0.001$; **** $p < 0.0001$ in comparison to LPS treatment.

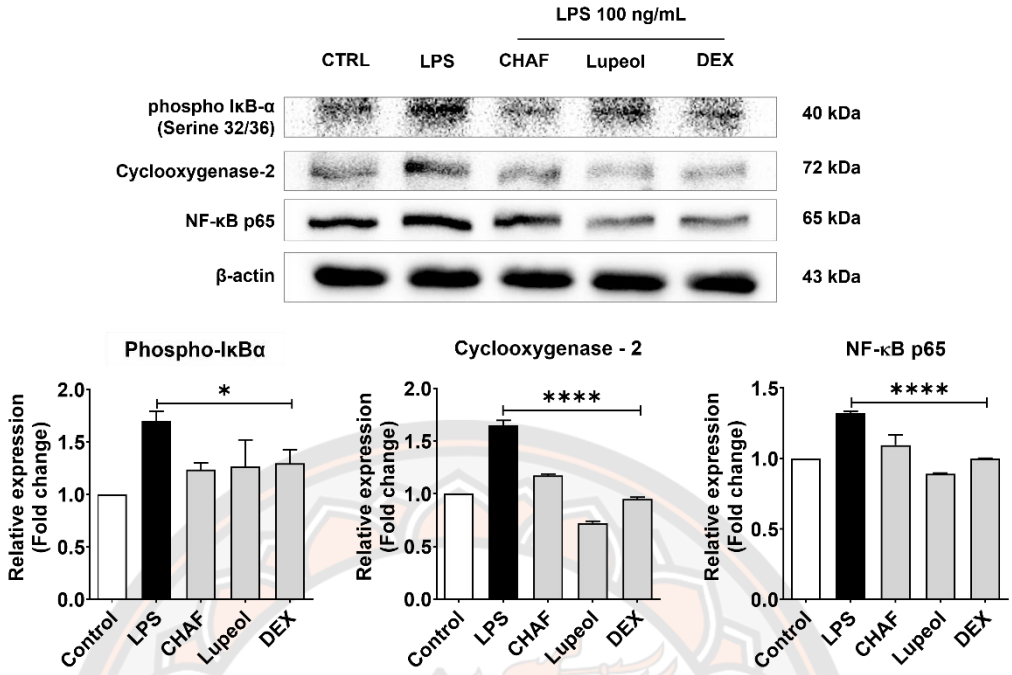

Figure 38 The effect of CHAF and lupeol on COX-2, phospho-IκBα, and NF-κB p65 proteins expression in THP-1-derived macrophages (91).

In pre-treatment conditions with CHAF and lupeol, western blot analysis revealed the decreased expression of pro-inflammatory proteins associated with NF-κB signaling pathway (phospho-IκBα, cyclooxygenase-2, and NF-κB p65). The data are presented as mean ± standard deviation. * $p < 0.05$; ** $p < 0.01$; *** $p < 0.001$; **** $p < 0.0001$ in comparison to LPS treatment.

2.5 The effect on the NLRP3 inflammasome signaling pathway

The anti-NLRP3 inflammasome activity of CHAF and lupeol were investigated in THP-1-derived macrophages. LPS-primed cells showed the upregulation of NLRP3 inflammasome genes (*IL1B*, *CASP1*, *NLRP3*, *IL18*, and *PYCARD*). In contrast, the cells co-treated with CHAF and lupeol both showed a significantly lower expression of inflammasome genes compared to the control (**Figure 39)**.

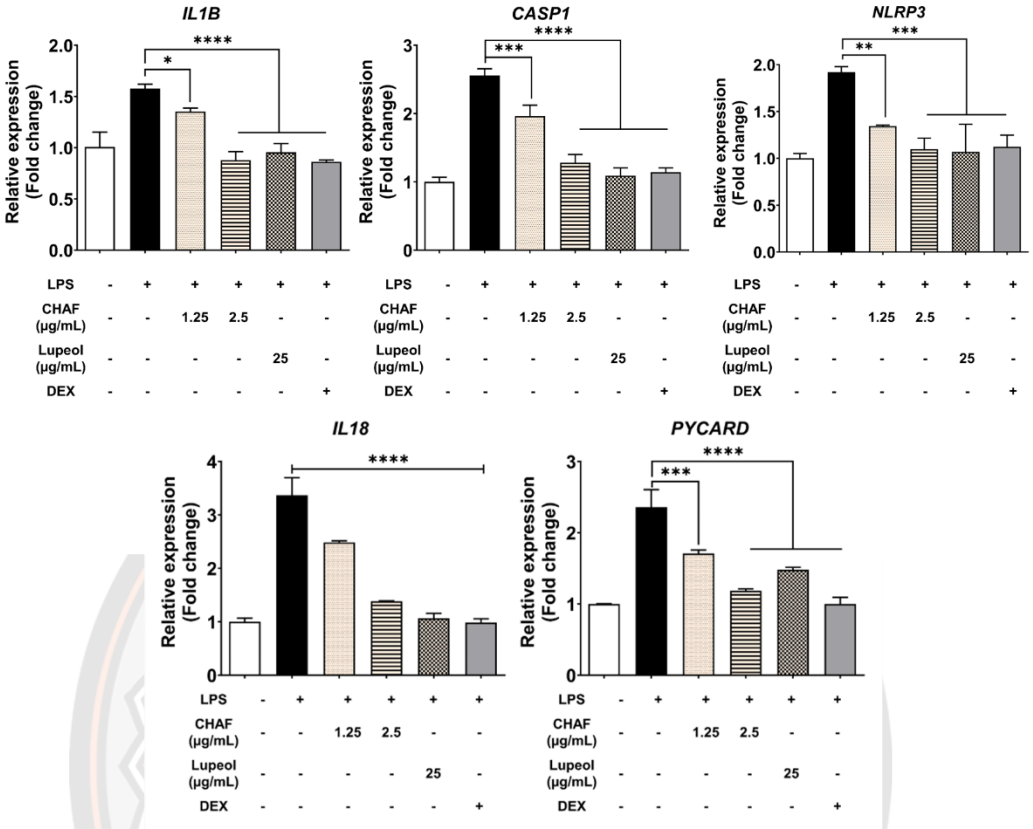

Figure 39 The reduction of NLRP3 inflammasome mRNA expression after CHAF and lupeol treatment in THP-1-derived macrophages (91).

The expression of NLRP3 inflammasome-associated genes was suppressed in the pre-treatment with CHAF and lupeol conditions. The data are presented as mean ± standard deviation. * $p < 0.05$; ** $p < 0.01$; *** $p < 0.001$; **** $p < 0.0001$ in comparison to LPS treatment.

Investigation of anti-*Candida* activity

3.1 Calculation of MIC and MFC values

As shown in **Table 7**, the ethanol extract had the lowest MIC value of 50 mg/mL, whereas hexane and ethyl acetate extracts had MIC values equal to or greater than 100 mg/mL. The MFC of all three crude extracts, on the other hand, was larger than 100 mg/mL. For β-citronellol, the MIC value was 128 µg/mL and the MFC value was 256 µg/mL. Due to it having the lowest MIC and MFC values, β-citronellol was selected for further experiments.

Table 7 The MIC and MFC values of crude extracts and β-citronellol against *C. albicans* (104).

Treatment compound	MIC	MFC
Crude hexane	> 100 mg/mL	> 100 mg/mL
Crude ethyl acetate	> 100 mg/mL	> 100 mg/mL
Crude ethanol	50 mg/mL	> 100 mg/mL
β-citronellol	128 µg/mL	256 µg/mL

3.2 Growth inhibition kinetic assay

Yeast cells treated with β-citronellol showed a delay in cell growth based on the kinetic absorbance at 600 nm for 48 hr, as shown in **Figure 40**. This result indicated the inhibitory effect on yeast cell growth of β-citronellol even at four-fold dilution.

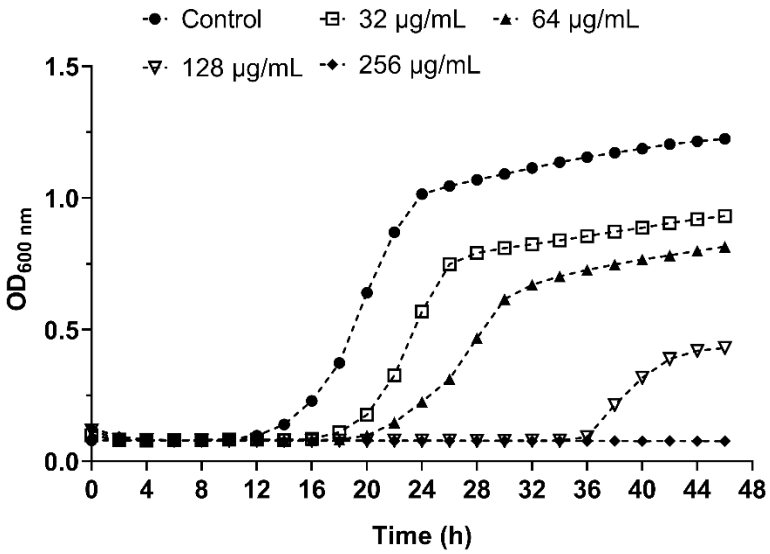

Figure 40 Kinetic growth curve of *C. albicans* (104).
The effect of β-citronellol on the kinetic growth curve of *C. albicans*. Yeast cells were treated with the different concentrations of β-citronellol (32-256 µg/ml) for 48 hr in a microplate reader. The absorbance at 600 nm was measured every 2 hr in each condition. Each dot represented the mean from three replicates. A dose-dependent delayed increasing trend of optical density value at 600 nm was observed.

3.3 Cellular Proteome of *C. albicans*

Post-sample analysis of the LC-MS/MS data was performed to provide protein lists with high certainty and specificity. The mass deviation analysis revealed that ≤ 10 ppm was present in 94.93% of the detected peptide groupings. When it came to digestive specificity, 91.44% of all the discovered peptides lacked miscleavage sites, whereas 8.35% did. The false discovery rate (FDR) was fixed to 0.05 in this study. In

total, 1,326 proteins were identified in the control and treatment groups. As illustrated in **Figure 41A**, proteins common to both groups were assigned a total of 1,199 proteins. The proteins unique to the treatment and control groups were assigned in a total of 59 and 68 proteins. The heatmap depicts the hierarchical clustering of different expression proteins within each category (**Figure 41B**). The columns represent relative protein expression and the rows represent proteins with a maximum distance of 1.0 that are significantly expressed.

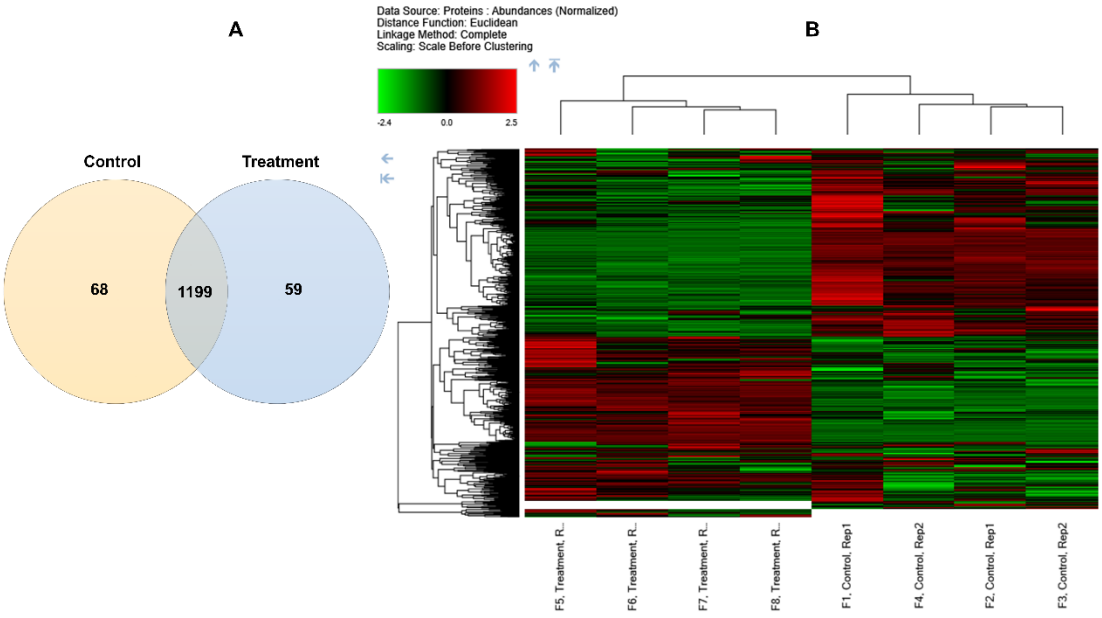

Figure 41 Protein expression profiles in *C. albicans* (104).
Differential protein expression profiles in *C. albicans*. Venn diagram showing the number of unique and common proteins found in the control and treatment groups (A). Heatmap of differentially expressed proteins with hierarchical clustering (B). Green and red are color key expressions that represent lower and higher differential abundance, respectively.

A total of 126 proteins were categorized using the PANTHER-GO Slim Molecular Function analysis tool based on adjusted *p*-value ($p < 0.05$) and 1.5-fold differential expression among the treatment and control groups. The results showed that β-citronellol altered seven groups of proteins based on their molecular function, including catalytic activity (41.8%), binding (39%), molecular function regulator (6.4%), structural molecule activity (5.5%), transporter activity (3.6%), translation regulator activity (2.7%), and molecular adaptor activity (0.9%) (**Figure 42A**). STRING v.11 web-based analysis was performed to visualize the protein-protein interaction network for both up-and down-regulated proteins with a confidence level of 0.4 (**Figure 42B** and **Table 8**).

Numerous pathways are involved in the mode of action of β-citronellol in killing *C. albicans*, as evidenced by the 126 major proteins changed in response to therapy. Among the 46 proteins that are downregulated and 80 proteins that are

increased, β-citronellol-treated yeast cells inhibit ten intriguing proteins, as shown in **Table 9**. The first group was cell wall proteins, including cell wall proteins RTB1 (Rbt1p), agglutinin-like protein 2 (Als2p), and 1,3-beta-glucanosyltransferase PGA4 (Pga4p). The second group was proteins involved in oxidative stress response, including superoxide dismutase [Cu-Zn] (Sod1p), glutathione S-transferase (Gst2p), and stress protein DDR48 (Ddr48p). The last group comprised the proteins involved in ATP synthesis, including ATP synthase subunit gamma (Atp3p), ATP synthase subunit d, mitochondrial (Atp7p), cytochrome c oxidase subunit 1 (Cox1p), and cytochrome b (Cob). In contrast to the downregulated proteins, some protein groups were upregulated under β-citronellol treatment. The first group comprised heat shock proteins, such as SSA2 (Ssa2p), Hsp30p, and Hsp90 cochaperone (Sti1p). Followed by ribosomal proteins, such as 40S ribosomal protein S27 (Rps27Ap), ribosomal protein P1B (Rpp1Bp), 60S ribosomal protein (Rps15p).

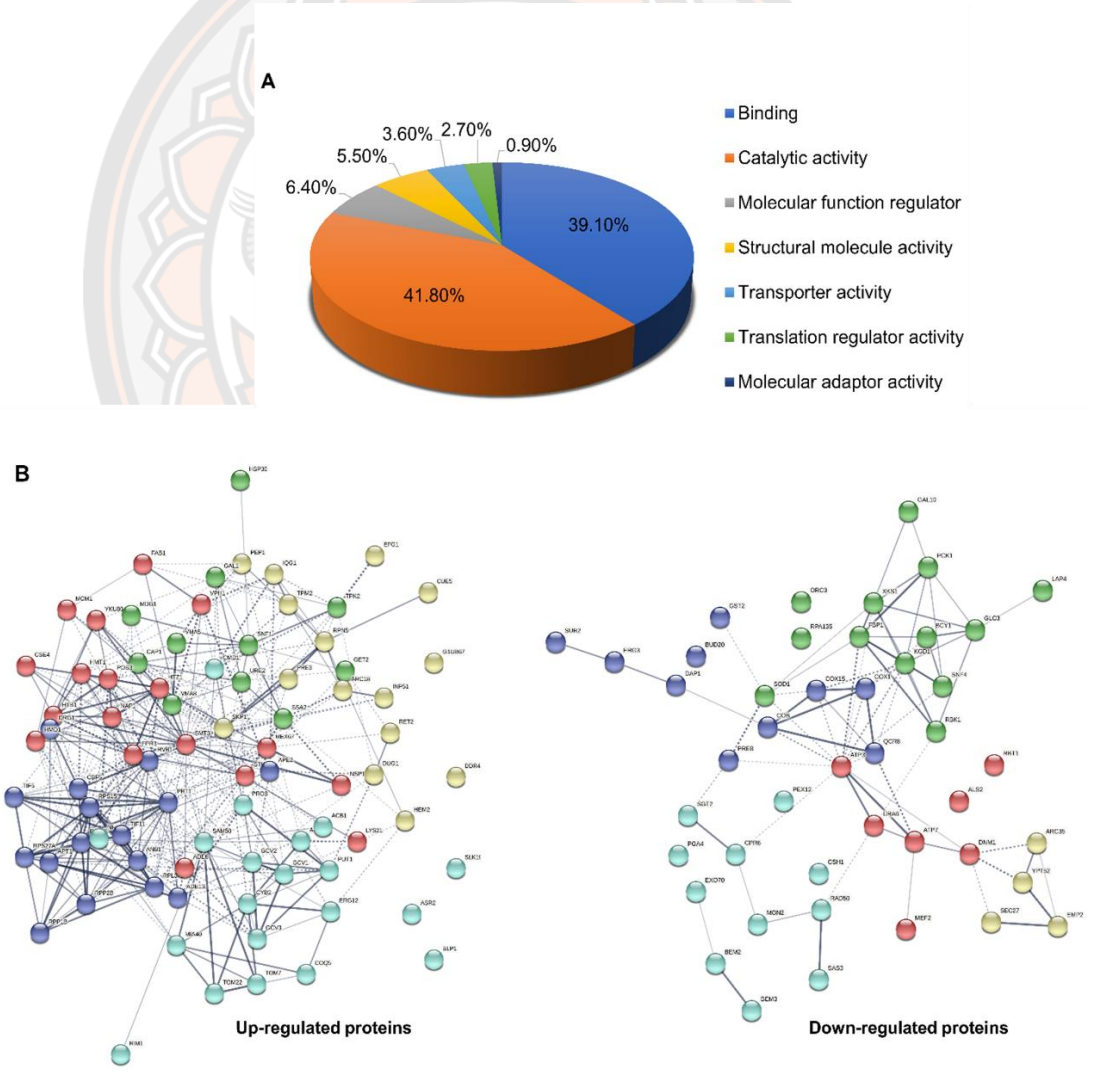

Figure 42 *C. albicans* gene ontology classification and protein-protein interaction network analysis of *C. albicans* influenced by β-citronellol treatment (104).

C. albicans gene ontology classification and protein—protein interaction network analysis influenced by β-citronellol treatment. (A) The PANTHER-GO database was used to classify the molecular function groups of both up- and downregulated proteins. (B) STRING v.11 prediction maps of a protein-protein interaction network. The interaction network nodes represent down- and upregulated proteins discovered in this study, illustrating the potential molecular pathways involved in mode of action of β-citronellol. Each node's color represents a protein cluster as determined by the K-means clustering algorithm.

Table 8 List of differential proteins expression in *C. albicans* under β-citronellol treatment conditions (104).

Protein name	Gene name	Log_2 fold change	Adjusted p-value
MRX complex DNA-binding subunit	*RAD50*	-18.16	3.01217E-15
Bud20p	*BUD20*	-17.69	1.01427E-14
Mon2p	*MON2*	-17.20	5.85441E-13
AMP-activated serine/threonine-protein kinase regulatory subunit	*SNF4*	-17.10	2.35381E-16
Cell wall protein RTB1	*RBT1*	-16.69	2.74374E-16
Agglutinin-like protein 2	*ALS2*	-15.77	5.57978E-13
Rab family GTPase	*YPT52*	-15.42	1.28246E-15
Bem2p	*BEM2*	-15.32	2.14077E-14
Exocyst complex protein EXO70	*EXO70*	-14.32	1.01427E-14
Origin recognition complex subunit 3	*ORC3*	-6.21	1.81551E-10
Histone acetyltransferase	*SAS3*	-4.56	7.62449E-06
Ribosome-releasing factor 2, mitochondrial	*MEF2*	-4.20	0.006295396
Peroxin-12	*PEX12*	-3.79	0.000115408
Coatomer subunit beta'	*SEC27*	-2.89	2.76378E-06
Proteasome subunit beta type-7	*PRE4*	-2.73	7.39922E-08
Sgt2p	*SGT2*	-2.32	2.02162E-07
Uridylate kinase	*URA6*	-2.10	8.06507E-09
Lap4p	*LAP4*	-1.78	5.5872E-05
Gst2p	*GST2*	-1.37	1.68003E-06
Superoxide dismutase [Cu-Zn]	*SOD1*	-1.28	0.037257003
ATP synthase subunit d, mitochondrial	*ATP7*	-1.23	4.45613E-05
Cox15p	*COX15*	-1.14	2.09369E-06
DNA-directed RNA polymerase subunit beta	*RPA135*	-1.07	3.75991E-06
Ribokinase	*RBK1*	-1.02	3.82379E-07
Cytochrome b	*COB*	-0.91	0.000534221
1,3-beta-glucanosyltransferase PGA4	*PGA4*	-0.89	1.78797E-05
Oxoglutarate dehydrogenase (succinyl-transferring)	*KGD1*	-0.88	5.89219E-07
Aldo-ket-red domain-containing protein	*CSH1*	-0.85	2.65849E-06
Fructose-bisphosphatase	*FBP1*	-0.83	7.59687E-06
Arp2/3 complex 34 kDa subunit	*ARC35*	-0.82	0.000664191

Protein name	Gene name	Log_2 fold change	Adjusted p-value
Phosphoenolpyruvate carboxykinase (ATP)	*PCK1*	-0.82	4.55772E-05
Bifunctional UDP-glucose 4-epimerase/aldose 1-epimerase	*GAL10*	-0.81	4.25493E-06
Cytochrome c oxidase subunit 1	*COX1*	-0.79	2.03346E-06
Proteasome core particle subunit alpha 2	*PRE8*	-0.76	1.85623E-05
Bem3p	*BEM3*	-0.76	0.000106366
Dap1p	*DAP1*	-0.76	0.007644593
Sphingosine hydroxylase	*SUR2*	-0.74	5.90462E-05
ATP synthase subunit gamma	*ATP3*	-0.72	3.75468E-06
Ubiquinol-cytochrome-c reductase subunit 8	*QCR8*	-0.70	0.003025807
Delta(7)-sterol 5(6)-desaturase ERG3	*ERG3*	-0.68	0.00074813
Emp24p	*EMP24*	-0.65	2.97306E-05
Xylulokinase	*XKS1*	-0.64	0.000211347
cAMP-dependent protein kinase regulatory subunit	*BCY1*	-0.64	1.16396E-05
Peptidyl-prolyl cis-trans isomerase D	*CPR6*	-0.63	9.96752E-06
Dynamin-related GTPase	*DNM1*	-0.60	4.19258E-05
1,4-alpha-glucan-branching enzyme	*GLC3*	-0.60	0.00016763
Phosphoinositide 5-phosphatase	*INP51*	18.96	3.80205E-17
Enhanced filamentous growth protein 1	*EFG1*	17.01	4.09147E-13
Protein-arginine omega-N methyltransferase	*HMT1*	16.53	1.28902E-07
mRNA export factor MEX67	*MEX67*	16.20	1.64181E-15
AP-1-like transcription factor CAP1	*CAP1*	15.62	1.48422E-14
Golgi to ER traffic protein 2	*GET2*	15.30	1.28246E-15
Delta-aminolevulinic acid dehydratase	*HEM2*	14.85	1.28246E-15
FG-nucleoporin	*NSP1*	14.49	4.88599E-16
Tom7p	*TOM7*	4.11	2.51163E-08
V-type proton ATPase subunit D	*VMA8*	3.65	9.90528E-08
Long-chain fatty acid transporter	*ACB1*	3.00	8.15303E-09
Eukaryotic translation initiation factor 4C	*TIF11*	2.94	2.5387E-09
Calmodulin	*CMD1*	2.89	8.15303E-09
Actin-related protein 2/3 complex subunit 3	*ARC18*	2.64	2.63026E-10
Tropomyosin	*TPM2*	2.56	2.0898E-06
GTP-binding protein	*DRG1*	2.51	6.15809E-07
Tom22p	*TOM22*	2.27	3.76269E-08
Blood-induced peptide 1	*BLP1*	2.17	2.51013E-08
Stress protein DDR48	*DDR48*	2.15	4.11631E-06
Mevalonate kinase	*ERG12*	1.81	7.99628E-08
Glycine cleavage system P protein	*GCV2*	1.77	8.81781E-06
Ubiquitin-binding protein	*CUE5*	1.77	6.72245E-07
Proline dehydrogenase	*PUT1*	1.62	7.40773E-06

Protein name	Gene name	Log_2 fold change	Adjusted p-value
Mdg1p	*MDG1*	1.58	2.22984E-06
Asr2p	*ASR2*	1.51	7.925E-08
E3 ubiquitin ligase complex SCF subunit	*SKP1*	1.51	1.62635E-05
Coatomer subunit delta	*RET2*	1.49	4.98621E-07
Ribosomal protein P1B	*RPP1B*	1.47	9.63755E-07
1-phosphatidylinositol-3-phosphate 5-kinase	*FAB1*	1.47	2.84155E-07
Non-histone chromosomal protein 6	*NHP6*	1.44	4.4867E-08
Hsp30p	*HSP30*	1.40	2.70703E-05
Histone H3-like centromeric protein CSE4	*CSE4*	1.29	6.90335E-08
Non-specific serine/threonine protein kinase	*SNF1*	1.28	2.23391E-05
Eukaryotic translation initiation factor 5A	*ANB1*	1.27	1.64279E-05
Adenylosuccinate lyase	*ADE13*	1.22	7.23007E-07
Histone H2A.Z	*HTZ1*	1.16	7.40773E-06
Aminomethyltransferase	*GCV1*	1.15	1.74722E-05
Ribosomal protein P2B	*RPP2B*	1.12	7.1798E-07
Glycine cleavage system H protein	*GCV3*	1.10	1.99403E-07
V-type proton ATPase subunit a	*VPH1*	1.05	8.81781E-06
Proteasome endopeptidase complex	*PRE3*	1.01	6.97507E-06
Histone H2B.1	*HTB1*	0.99	8.95516E-07
Transcriptional regulator HMO1	*HMO1*	0.99	3.5035E-06
Ribosomal 40S subunit protein S15	*RPS15*	0.97	4.21377E-05
Mitochondrial intermembrane space import and assembly protein 40	*MIA40*	0.97	1.15022E-05
Homocitrate synthase	*LYS21*	0.97	0.007104253
Heat shock protein SSA2	*SSA2*	0.96	2.03949E-07
Acetyl-coenzyme A synthetase	*ACS1*	0.95	0.012978934
Translation initiation factor eIF5	*TIF5*	0.93	0.029095105
Single-stranded DNA-binding protein	*RIM1*	0.92	2.30606E-07
H/ACA ribonucleoprotein complex subunit CBF5	*CBF5*	0.92	3.18021E-05
Eukaryotic translation initiation factor 3 subunit B	*PRT1*	0.91	1.29315E-05
Protein URE2	*URE2*	0.87	1.6667E-05
Formylglycinamide ribonucleotide amidotransferase	*ADE6*	0.85	9.28313E-05
Slk19p	*SLK19*	0.84	2.96101E-06
SAM complex subunit	*SAM50*	0.84	0.006068136
ATP-dependent DNA helicase II subunit 2	*YKU80*	0.82	0.000547408
40S ribosomal protein S27	*RPS27A*	0.81	0.016012806
RNA polymerase II degradation factor 1	*DEF1*	0.77	3.52533E-06
Transcription factor of morphogenesis MCM1	*MCM1*	0.76	1.27252E-05
Proteasome regulatory particle lid subunit	*RPN5*	0.75	0.038865914

Protein name	Gene name	Log_2 fold change	Adjusted p-value
Hsp90 cochaperone	*STI1*	0.75	3.45556E-05
Adenine phosphoribosyltransferase	*APT1*	0.74	0.006011399
Ras GTPase-activating-like protein IQG1	*IQG1*	0.74	0.00184567
Cys-Gly metallodipeptidase DUG1	*DUG1*	0.72	2.76378E-06
FK506-binding protein 3	*FPR3*	0.72	0.001494096
Nucleosome assembly protein 1	*NAP1*	0.71	5.43861E-05
RuvB-like helicase 1	*RVB1*	0.69	0.000441487
Pyrroline-5-carboxylate reductase	*PRO3*	0.69	0.02525234
SUMO family protein	*SMT3*	0.68	4.52665E-05
Galactokinase	*GAL1*	0.66	0.007244711
Ribosomal protein L37	*RPL37B*	0.66	2.54103E-05
V-type proton ATPase subunit C	*VMA5*	0.64	0.001168801
cAMP-dependent protein kinase catalytic subunit	*TPK2*	0.63	2.65332E-05
2-methoxy-6-polyprenyl-1,4-benzoquinol methylase, mitochondrial	*COQ5*	0.62	0.204793578
60S ribosomal protein L13	*RPL13*	0.62	0.001505826
FACT complex subunit POB3	*POB3*	0.62	0.000331606
Aminopeptidase 2	*APE2*	0.62	7.42869E-05
Cyb2p	*CYB2*	0.61	0.008525198
Type I sorting receptor	*PEP1*	0.61	9.73125E-05

Table 9 A list of intriguing proteins that have been altered by treatment with β-citronellol (104).

Protein name	Log_2 fold change	Description/function	References
Cellular response to oxidative stress/ stress response			
Superoxide dismutase [Cu-Zn]	-1.28	Cytosolic copper- and zinc-containing superoxide dismutase. Destroys radicals by converting them into less damaging hydrogen peroxide.	(105)
Gst2p	-1.37	Glutathione S transferase. Cellular response to oxidative stress.	(106)
Stress protein DDR48	2.15	A cell surface protein that senses and responds to changes in the host environment. It is required for stress response and confers partial antifungal drug resistance. Contributes to the DNA damage response.	(107)
Cell wall and cell adhesion molecules			
Cell wall protein RTB1	-16.69	GPI-anchored cell wall protein is required for virulence, mating efficiency, and biofilm formation.	(108-111)

Protein name	Log_2 fold change	Description/function	References
		Normal disseminated infection, but not intestinal colonization.	
Agglutinin-like protein 2	-15.77	Cell surface adhesion protein that promotes yeast-to-host tissue adherence as well as yeast aggregation. Play a critical role in the pathogenesis of *C. albicans* infections.	(112-114)
1,3-beta-glucanosyltransferase PGA4	-0.89	Involved in the elongation of 1,3-beta-glucan chains in the cell wall by internally splitting a 1,3-beta-glucan molecule and transferring the newly generated reducing end (the donor) to the non-reducing end of another 1,3-beta-glucan molecule (the acceptor). Involved in cell wall biosynthesis and morphogenesis.	(115, 116)
ATP synthesis			
ATP synthase subunit gamma	-0.72	Mitochondrial proton-transporting ATP synthase complex, catalytic sector F(1). Play an important role in proton motive force-driven ATP synthesis.	(117)
ATP synthase subunit d, mitochondrial	-1.23	Mitochondrial membrane ATP synthase (F_1F_0 ATP synthase or Complex V) produces ATP from ADP in the presence of a proton gradient across the membrane which is generated by electron transport complexes of the respiratory chain.	(117)
Cytochrome c oxidase subunit 1	-0.79	Component of cytochrome c oxidase, the final enzyme in the mitochondrial electron transport chain responsible for oxidative phosphorylation.	(118)
Cytochrome b	-0.91	Component of the ubiquinol-cytochrome c reductase complex in the mitochondrial respiratory chain (cytochrome b-c1 complex). Involved in the transfer of electrons from ubiquinol to cytochrome c.	(119, 120)

3.4 Biofilm formation of *C. albicans*

As presented in **Figure 43**, β-citronellol treatment affected *C. albicans* biofilm formation. The lowest concentration of β-citronellol (32 µg/mL) significantly inhibited the biofilm formation compared to the control and the inhibition was in a dose-dependent manner.

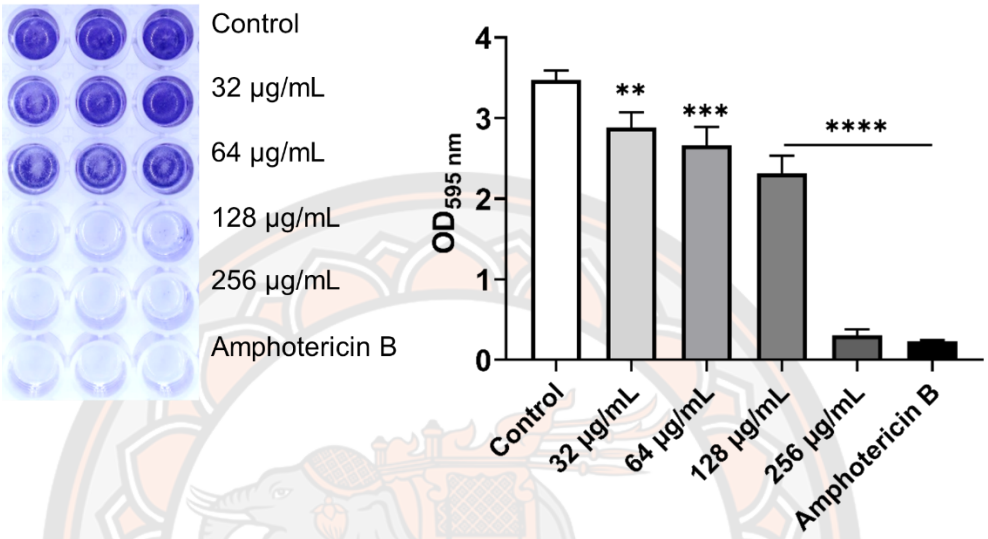

Figure 43 Biofilm formation assay of *C. albicans* (104).
C. albicans biofilm formation assay. Crystal violet staining of *C. albicans* biofilm after treated for 24 hr with different concentrations of β-citronellol and amphotericin B (2 µg/ml) (Left). The absorbance at 595 nm of destaining solution from all treatment conditions (Right). The data are presented as mean ± standard deviation. ** $p < 0.01$; *** $p < 0.001$; **** $p < 0.0001$ in comparison to control.

3.5 The effect of β-citronellol on the production of reactive oxygen species (ROS)

An H_2DCFDA probe was used to investigate the effect of β-citronellol on ROS production. *C. albicans* treated with β-citronellol for 4 hr increased ROS production by upregulating the intensity of the green fluorescence compared to the control group (**Figure 45)**. The generation of ROS increased dose-dependently.

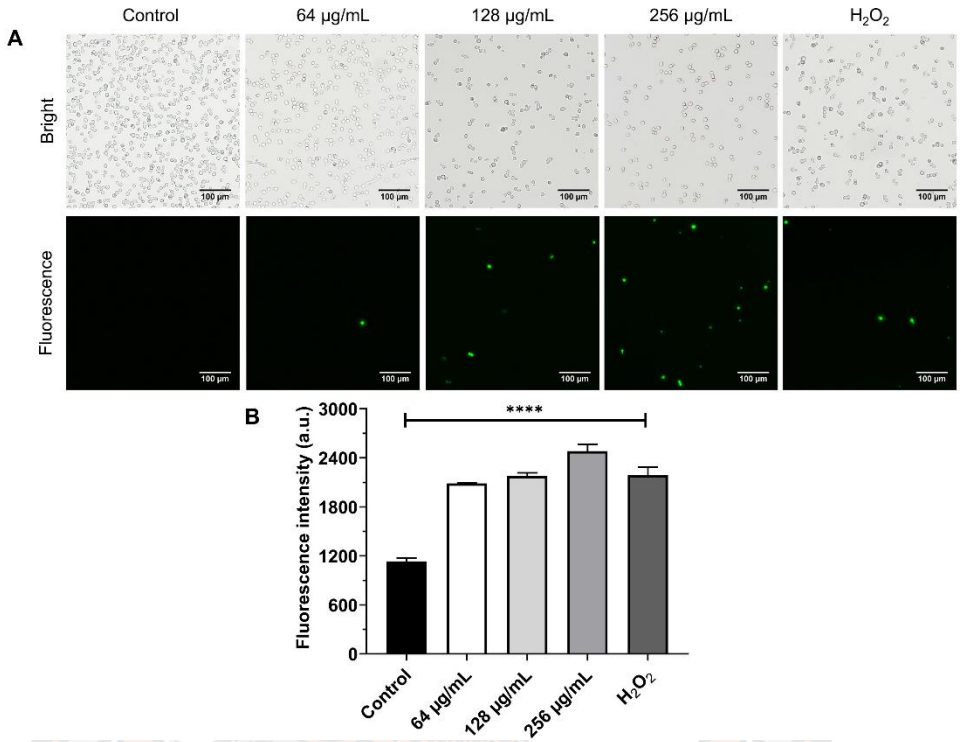

Figure 44 β-citronellol increased ROS production in *C. albicans* (104). The influence of β-citronellol on ROS production. For 4 hours, Yeast was treated with β-citronellol and H_2O_2 (0.2 mM) for 4 hr, followed by incubated with H_2DCFDA probe. The morphology of yeast as seen through a bright field and fluorescence microscope (A). Fluorescence intensity of the H_2DCFDA probe at 485/535 nm excitation/emission wavelength (B). The data is represented as mean ± SD. **** $p <$ 0.0001 in comparison to control.

3.6 Cell membrane potential

The $DiBAC_4(3)$ penetrates yeast cells via a depolarized membrane, where it binds to intracellular proteins or membranes, generating a fluorescence signal. As seen in **Figure 46**, red fluorescence increased dramatically in the β-citronellol treated groups, demonstrating that β-citronellol affected the cell membrane by induced the depolarization state of the cell membrane.

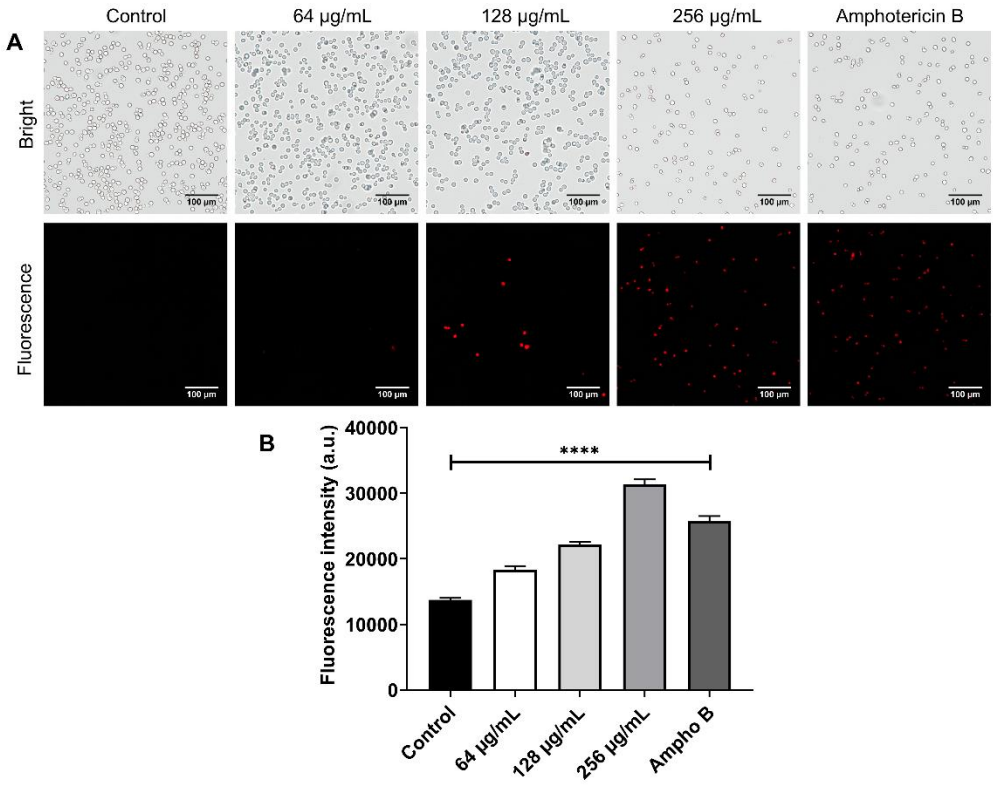

Figure 45 *C. albicans* cell membrane potential changed upon β-citronellol treatment (104).

The depolarization of *C. albicans* cells after β-citronellol treatment for 4 hr. Yeast cell morphology observed under bright field and fluorescence microscope (A). The red fluorescence intensity of $DiBAC_4(3)$ probe at excitation/emission wavelengths 492/518 nm. The data are presented as mean ± SD. **** $p < 0.0001$.

3.7 Apoptosis analysis

The apoptosis profile of the yeast cells exposed to β-citronellol was investigated. After 6 hr of treatment with β-citronellol at 64, 128, or 256 µg/mL, the rate of early apoptosis increased to 20.75%, 47.20%, and 26.60%, respectively (**Figure 46)**. The rate of late apoptosis/dead positive cells was dose-dependent and reached a maximum of 16.35% in the presence of β-citronellol at 256 µg/mL. Dead or necrotic cells were positive for 0.20% and 0.05% in conditions treated with β-citronellol at 256 µg/mL and amphotericin B, respectively. The results indicated that β-citronellol treatment for 6 hr resulted in induced programmed cell death in *C. albicans*, largely triggering the early to late apoptotic stages.

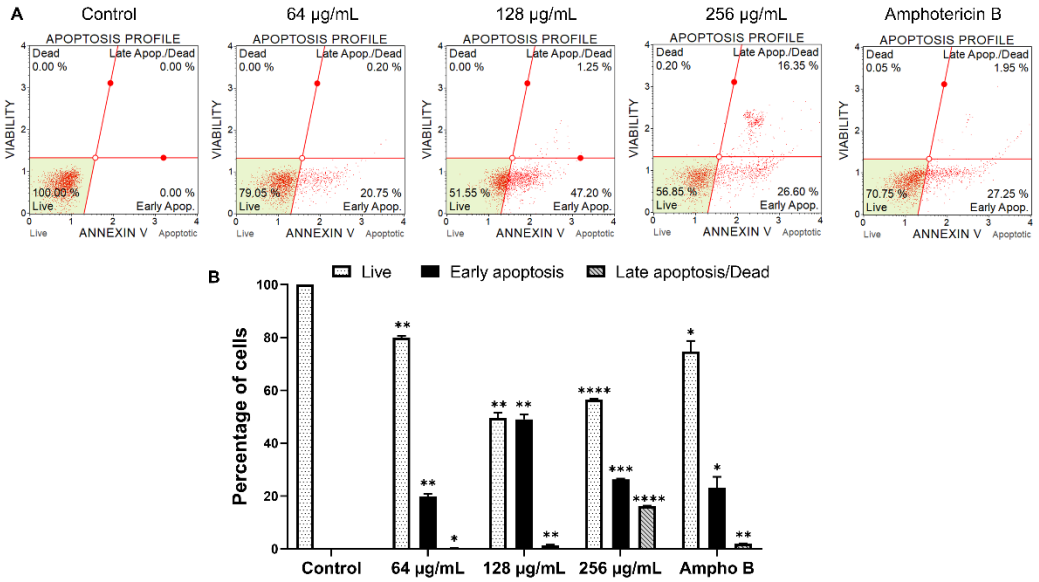

Figure 46 *C. albicans* apoptosis profile influenced by β-citronellol (104).

Yeast cells were incubated with β-citronellol (64–256 µg/ml) and amphotericin B (2 µg/ml) for 6 h. Chromatogram of the apoptosis profile of *C. albicans* in different conditions. The proportion of positive cells in each phase, including live, early- and late-stage apoptosis, is shown (B). All data are presented as mean ± SD. * $p < 0.05$, ** $p < 0.01$, *** $p < 0.001$, **** $p < 0.0001$.

3.8 Observation of *C. albicans* morphological changes under SEM

The morphological and structural changes in *C. albicans* treated with β-citronellol were observed under SEM, as illustrated in **Figure 48**. In normal conditions, the cell morphology was round with smooth surfaces (A). After 24 hr of β-citronellol treatment, wrinkled surfaces with irregular shapes of cells had developed (B-D). This finding suggested that the cell wall and/or membrane of yeast cells had been damaged by the β-citronellol treatment.

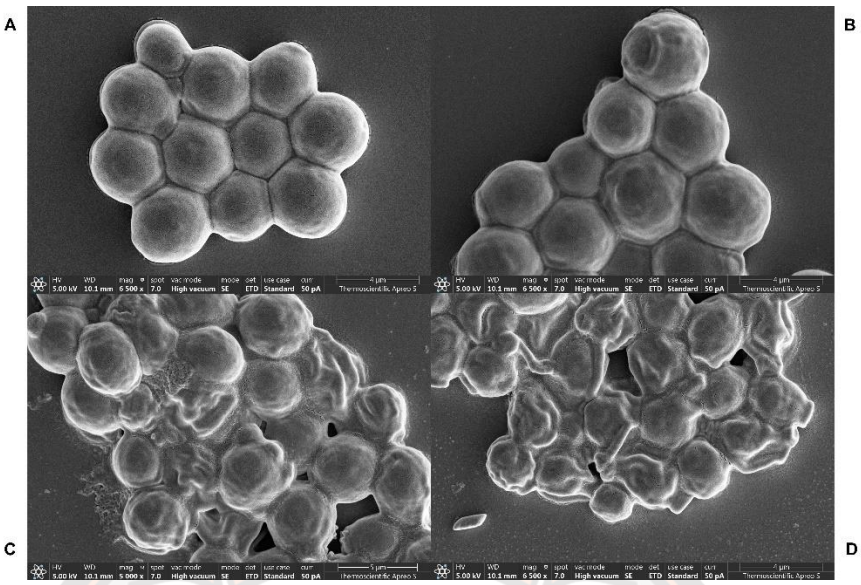

Figure 47 The morphology of *C. albicans* treated with β-citronellol was observed under SEM (104).
The typical structure of yeast cells in cell culture medium-only environment (A). After incubation with 64 g/ml (B), 128 g/ml (C), and 256 g/ml (D) of β-citronellol, structural alteration was detected.

Development of mouthwash containing herbal extracts

4.1 Total phenolic content

The total phenolic content of the leaves of the three plants is illustrated in **Figure 48**. The crude extract from the KL had the highest phenolic content (237.97±8.10 mg/GAE), followed by the crude extract from the MO (127.710±2.29 mg/GAE) and then the crude extract from the NE (104.62±8.47 mg/GAE).

4.2 Antioxidant activity

The TEAC profiles of the ethanolic extracts from the three plants were comparable in their overall phenolic contents. As demonstrated in **Figure 49**, the KL had the highest TEAC (245.99±17.01 µM) with the MO (189.93±5.24 µM) and then the NE (149.04±7.99 µM) of Trolox equivalent.

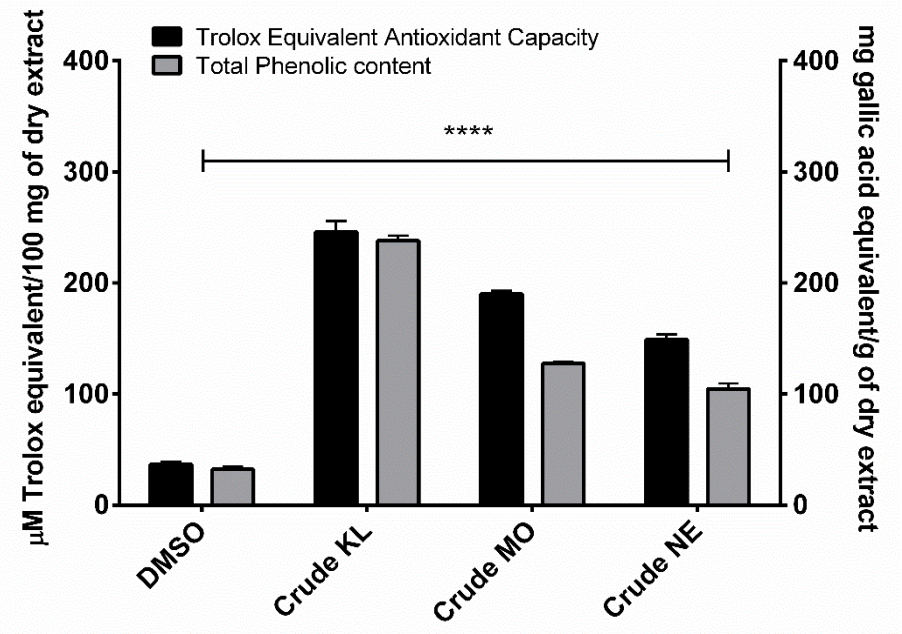

Figure 48 TEAC and total phenolic content of crude extracts from three different plants (96).

Crude ethanolic extract from KL has the highest antioxidant capacity and total phenolic content, followed by crude MO and crude NE extracts. All data are presented as mean ± SD. **** $p < 0.0001$ compared to DMSO.

4.3 GC-MS analysis of chemical constituents from crude extracts

The bioactive chemicals identified as terpenoid components from the KL, the MO, and the NE are listed in **Table 10**. The major identified substances in the KL leaf extract were terpenoids (86.89%), which included monoterpenes (13.50%), sesquiterpenes (6.39%), diterpenes (57.34%), and triterpenes (11.59%). Three primary terpenoids, including tetraprenol, phytol, and citronellol. In the MO leaf extract, the terpenoids (16.42%) were classified as diterpenes (9.81%) and triterpenes (6.61%). Phytol, β-sitosterol, and β-amyrin were the three major terpenoids in the MO. In the NE leaf extract, the terpenoids were comprised of 23.32%, including sesquiterpenes (0.15%), diterpenes (9.13%), triterpenes (5.48%), and tetraterpenes (8.56%). Among the terpenes, astaxanthin, phytol, and stigmasterol were found to be the major terpenes in the NE leaf extract. GC-MS chromatogram of all plant extracts was shown in **Figure 49**.

Table 10 Chemical constituents identified by GC-MS from crude extracts of three plants (96).

RT (min)	Identified compounds	Classification	Relative area (%)		
			C. hystrix	*M. oleifera*	*A. indica*
9.29	*trans*-Linalool oxide	Monoterpene	0.26	-	-
10.00	β-Linalool	Monoterpene	1.61	-	-
11.36	Isopulegol	Monoterpene	1.06	-	-

RT (min)	Identified compounds	Classification	Relative area (%)		
			C. hystrix	*M. oleifera*	*A. indica*
11.51	Citronellal	Monoterpene	3.16	-	-
11.68	Isopregol	Monoterpene	0.71	-	-
13.63	β-Citronellol	Monoterpene	4.28	-	-
14.37	*cis*-Geraniol	Monoterpene	0.17	-	-
16.01	Citronellic acid	Monoterpene	0.31	-	-
16.56	2-(2-Hydroxy-2-propanyl)-5-methylcyclohexanol	Monoterpene	0.59	-	-
17.02	Citronellol acetate	Monoterpene	1.94	-	-
17.15	Menthoglycol	Monoterpene	0.25	-	-
17.75	Copaene	Sesquiterpene	0.50	-	0.15
17.97	Ethoxycitronellal	Monoterpene	0.18	-	-
18.51	(2*E*)-1-Ethoxy-3,7-dimethyl-2,6-octadiene	Monoterpene	1.88	-	-
18.91	β-Caryophyllene	Sesquiterpene	2.64	-	-
19.33	Sucrose	Disaccharide	0.75	24.20	4.66
19.77	α-Caryophyllene	Sesquiterpene	0.40	-	-
20.1	1-Dodecanol	Fatty alcohol	-	0.91	0.58
21.43	δ-Cadinene	Sesquiterpene	0.78	-	-
22.05	Elemol	Sesquiterpene	0.20	-	-
22.31	*trans*-Nerolidol	Sesquiterpene	1.08	-	-
22.77	(-)-Spathulenol	Sesquiterpene	0.38	-	-
22.92	Caryophyllene oxide	Sesquiterpene	0.41	-	-
23.70	Ethyl α-d-glucopyranoside	Glycoside	-	1.59	1.31
25.20	Dodecyl acrylate	Fatty ester	0.95	4.24	1.70
28.30	Phytol acetate	Diterpene	-	1.42	1.26
29.17	3,7,11,15-Tetramethyl-2-hexadecen-1-ol	Diterpene	-	-	0.31
30.47	Isophytol	Diterpene	0.13	-	-
31.35	Ethyl palmitate	Fatty acid ethyl ester	1.21	6.09	2.45
31.72	Lauryl 3-mercaptopropionate	Fatty acid ester	-	0.59	0.21
31.75	Tetraprenol	Diterpene	47.42	-	-
32.00	*trans*-Geranylgeraniol	Diterpene	3.22	-	-
33.57	Phytol	Diterpene	6.57	8.39	7.56
34.44	Ethyl-9,12-octadecadienoate	Fatty acid ethyl ester	0.32	2.33	0.30
34.56	Ethyl linolenate	Fatty acid ethyl ester	1.05	18.89	3.85
34.99	Ethyl stearate	Fatty acid ethyl ester	0.22	0.88	0.23
40.15	Glycerol β-palmitate	Fatty acid ester	-	-	0.46
42.97	α-Glyceryl linolenate	Fatty acid ester	-	1.82	1.01
43.5	4-(2,3-Dihydroxy-3-methylbutoxy)furo(3,2-	Furanocoumarin	0.52	-	-

RT (min)	Identified compounds	Classification	Relative area (%)		
			C. hystrix	*M. oleifera*	*A. indica*
	g)chromen-7-one				
44.84	Squalene	Triterpene	4.12	-	0.21
50.14	α-Tocopherol	Triterpene	3.26	14.80	5.87
51.52	Astaxanthin	Tetraterpene	-	-	8.56
53.2	Stigmasterol	Sterol	0.54	-	3.97
54.83	β-Sitosterol	Sterol	1.57	3.79	1.29
55.36	24-*n*-propylidenecholesterol	Sterol	-	3.11	0.66
55.44	Dihydrolanosterol	Triterpene	0.93	-	-
55.82	β-Amyrin	Triterpene	-	2.82	-
56.05	Phorbol	Diterpene	-	-	16.81
57.31	Lupeol	Triterpene	2.10	-	-
58.91	Olean-12-ene-3,15,16,21,22,28-hexol	Triterpene	-	-	5.37
58.92	Cycloeucalenol acetate	Triterpene	2.32	-	-
60.03	14,15β-epoxy-3β,5-dihydroxy-5β-Bufa-20,22-dienolide	Diterpene	-	-	12.28
64.25	Olean-12-ene-3,16,21,22,23,28-hexol	Triterpene	-	-	18.94

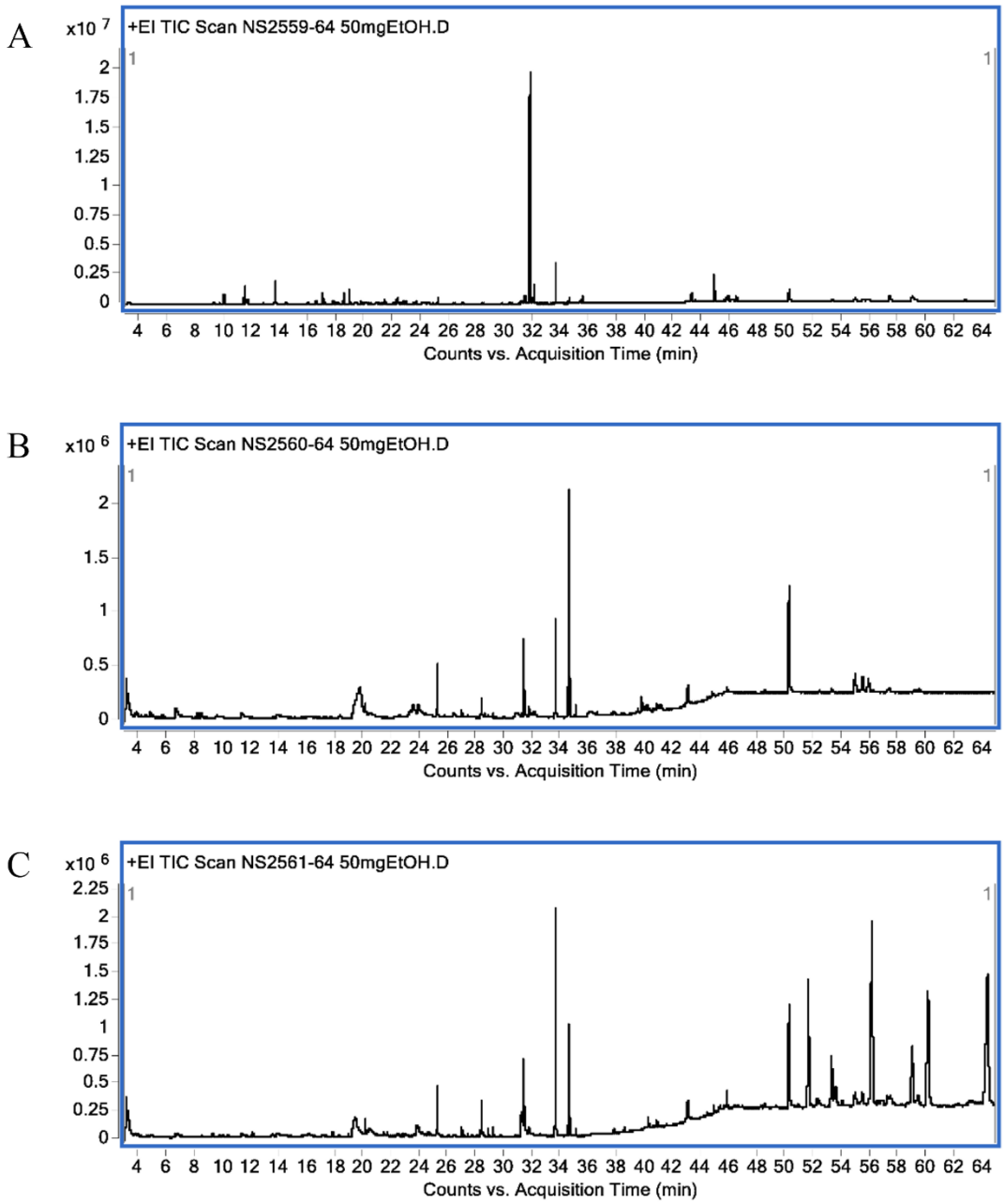

Figure 49 Chromatogram from GC-MS analysis. *C. hystrix* DC. (A), *Moringa oleifera* Lam. (B) and *Azadirachta indica* A. Juss. (C) (96).

From the list of chemical constituents in **Table 10**, β-citronellol was chosen as a candidate for evaluating the protein involved in the anti-*Candida* activity due to its potential antimicrobial activity (121-125). β-citronellol ($C_{10}H_{20}O$) is an alcoholic monoterpene found in essential oils in several plants, including the genus *Cymbopogon* (126). In plants, β-citronellol is a secondary metabolite whose primary function is plant defense (126). The chemical structure of β-citronellol is shown in **Figure 50.**

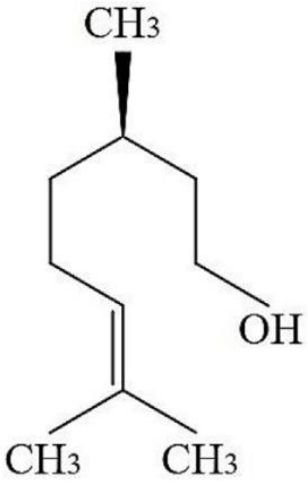

Figure 50 Chemical structure of β-citronellol ($C_{10}H_{20}O$) (126).

β-citronellol is a monoterpenoid that is oct-6-ene substituted by a hydroxy group at position 1 and methyl groups at positions 3 and 7. It has a molecular weight of 156.26 g/mol, and the boiling point is 224.25 °C (127).

4.4 Assessment for quality control of formulated mouthwashes

For quality control, three formulated types of mouthwash containing plant extracts (KL, KL+MO, and KL+NE) were evaluated for appearance, pH, heavy metal concentration, and microbes, according to the Food and Drug Administration (FDA) of Thailand's mouthwash formulation standard. As demonstrated in **Table 11**, the tested parameters were within the permissible specification range.

Table 11 The results of quality control testing of formulated mouthwashes (96).

Test parameters	**Test procedure**	**Specification**	**Mouthwash**		
			KL	**KL + MO**	**KL + NE**
Turbidity	Organoleptic	Transparent	Transparent	Transparent	Transparent
Color	Organoleptic	Green	Green	Green	Green
pH	pH Meter	5.5 - 8.5	6.6	6.7	6.8
Lead (Pb)	Based on AOAC (2016) method	< 10.0 ppm	Not detected	Not detected	Not detected
Arsenic (As)	Based on AOAC (2016) method	< 4.0 ppm	< 0.5 ppm	Not detected	< 0.5 ppm
Mercury (Hg)	Based on AOAC	< 0.5 ppm	Not detected	Not detected	Not detected

	(2016) method				
Clostridium spp.	USP 41 <62>	Absent / 1 g.	Absent / 1 g.	Absent / 1 g.	Absent / 1 g.
Staphylococcus aureus	USP 41 <62>	Absent / 1 g.	Absent / 1 g.	Absent / 1 g.	Absent / 1 g.
Pseudomonas aeruginosa	USP 41 <62>	Absent / 1 g.	Absent / 1 g.	Absent / 1 g.	Absent / 1 g.
Candida albicans	USP 41 <62>	Absent / 1 g.	Absent / 1 g.	Absent / 1 g.	Absent / 1 g.

AOAC: The association of official agricultural chemists
USP: The United States Pharmacopeia

4.5 Baseline information of participants

Fifty participants were recruited for the study. Three individuals were excluded due to antibiotic usage. Demographic information, such as age, gender, and mean GI and PI scores of the 47 participants were recorded, as shown in **Table 12**. The ages of the 47 participants; 31 females and 16 males, ranging from 20 to 48 years with a mean age of 23.51±6.60. At baseline, the mean ± SD of PI and GI scores were 1.12±0.55 and 1.42±0.65, respectively. Among the five groups, there were no statistical differences in age, PI, and GI scores.

Table 12 The clinical parameters at baseline (mean ± SD) (96).

Parameters	Placebo (n = 9)	KL (n = 10)	KL + MO (n = 9)	KL + NE (n = 10)	CHX (n = 9)	*p*-value
Age (years)	23.11 ± 4.43	21.40 ± 1.71	22.89 ± 5.33	23.90 ± 8.14	26.44 ± 10.42	0.6749[a]
GI score	1.21 ± 0.50	0.88 ± 0.58	1.18 ± 0.54	1.03 ± 0.63	1.35 ± 0.48	0.228[a]
PI score	1.63 ± 0.77	1.08 ± 0.51	1.63 ± 0.65	1.33 ± 0.52	1.45 ± 0.74	0.371[a]
Sex, Female / Male	8/1	6/4	6/3	6/4	5/4	

4.6 The change in GI and PI scores

The GI and PI scores were changed from baseline Day 0 to Day 15 in all groups, as depicted in **Figure 51**. Significant reductions in GI and PI scores were found in the KL, KL + MO, KL+NE, and CHX groups.

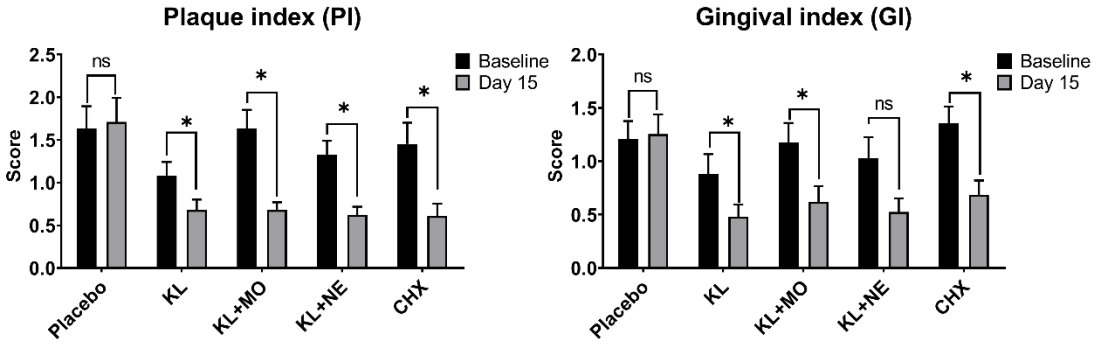

Figure 51 GI and PI scores profiles in all groups (96).
Intragroup comparison of gingival index (left) and plaque index (right) scores between baseline and day 15 after mouthwash usage by the Wilcoxon signed-rank test. Data are presented as mean ± SD. * $p < 0.05$ in comparison to placebo group.

4.7 Changes in the number of microbial colonies in the oral cavity

The colonies of *Staphylococcus* spp. and *Candida* spp. from all groups were evaluated. The colony count and accumulative reduction percentage for each period are shown in **Table 13**. The CHX group showed the highest accumulative reduction percentage of *Staphylococcus* spp. colony count, followed by the KL + MO, KL + NE, KL, and placebo groups. In contrast, the highest reduction percentage of *Candida* spp. colony count was found in KL + NE group, followed by the KL + MO and CHX groups.

Table 13 The number of microbial counts ($\times 10^8$) in mean ± SD and accumulative reduction percentage compared to the baseline (96).

Microorganisms	**Intervals**	**Placebo**	**KL**	**KL + MO**	**KL + NE**	**CHX**
Staphylococcus spp.	Baseline	21 ± 38	91 ± 188	62 ± 69	132 ± 148	28 ± 39
	Day 15	78 ± 114	109 ± 176	46 ± 87	83 ± 161	27 ± 48
Accumulative reduction percentage		12.66	30.14	45.53	33.23	54.11
Candida spp.	Baseline	1 ± 0	0 ± 1	1 ± 2	1 ± 1	8 ± 23
	Day 15	1 ± 0	1 ± 3	0 ± 0	1 ± 1	2 ± 5
Accumulative reduction percentage		0	0	20	35.83	17.63

Chapter V

Conclusion and discussion

Anti-inflammatory and anti-NLRP3 inflammasome activities

Several studies have demonstrated that certain parts of *C. hystrix* DC., such as the peel and essential oil, have anti-inflammatory properties (19, 20, 128). Nonetheless, the data on the leaves and proof of the effect on the NLRP3 inflammasome is lacking. In this study, we identified lupeol, a pentacyclic triterpenoid, from an ethanolic extract of *C. hystrix* DC. leaves. This triterpenoid can be found in a variety of vegetables and plants, such as *Aloe vera* (Aloe), *Cucumis sativus* (Cucumber), *Phoenix dactylifera* (Date Palm), and *Helianthus annuus* (Sunflower) (103). The roles of lupeol and triterpenoid in plants are to serve as plant metabolites, as well as to maintain the integrity of the phospholipid bilayers of plant cells (129). Lupeol contains a wide range of pharmacological activities, such as anti-inflammation, anti-adipogenicity, and anti-cancer (103, 130-132). The anti-inflammatory activity of lupeol from the leaves of *C. hystrix* DC. on human macrophages was found in this study by targeting the NF-κB signaling pathway. The theory was that the NF-κB signaling proteins, such as NF-κB p65 and p-IκBα, might be the targets for lupeol. Another possible mechanism of action of lupeol is that it inhibits inflammatory activation at the receptor level. Some studies have shown that lupeol can inhibit TLR4 expression in mice with coxsackievirus B3-induced viral myocarditis (133). However, intensive investigation into target protein interaction and protein binding to lupeol is required. Apart from the NF-κB pathway, this study established the first report on the anti-NLRP3 inflammasome signaling in human macrophages. The expression of all candidate NLRP3 inflammasome genes was decreased with lupeol treatment. The study by Markley et al. (134) reported a similar influence of lupeol on *NLRP3* gene expression in astrocytes. The suppression of NF-κB signaling may affect the transcription of NLRP3 inflammasome-associated genes. Thus, a protein level study is needed to elucidate the effect on the NLRP3 inflammasome signaling pathway.

Anti-*Candida* activity

The potential anti-*Candida* activity of β-citronellol, in term of proteomics analysis, was reported in this study. β-citronellol is a monoterpenoid that is mainly found in essential oil and play an important role as a metabolite in various type of plants, including plants of the genus *Cymbopogon* (126) and *C. hystrix* DC. (84). Several reports demonstrated the anti-*Candida* activity of β-citronellol (121, 122), yet the data on possible target proteins remains scarce. Proteomic analysis in this study identified three unique classes in *C. albicans* that might be targeted for β-citronellol. First, the cell wall-associated proteins, including Als2p, Rbt1p, and Pga4p. The cell wall of *C. albicans* has a two-layered composition, and the exterior layer is composed of glycosylphosphatidylinositol (GPI) proteins. The inner layer consists of polysaccharides, such as chitin, β-1,3-, and β-1,6-glucans (135). Another two GPI protein members, agglutinin-like sequence (ALS) and Rbt1p, have been studied for their roles in *C. albicans*, including assisting the adhesion to host epithelial cells,

involved in the biofilm formation, the effectiveness of mating, and pathogenicity. (108, 136-138). Additionally, the treatment with β-citronellol can suppress Pga4p expression, which is an enzyme playing a role in the elongation of 1,3-beta-glucan chains (115, 116). Not only cell wall localization, but some studies have also reported the presence of Als2p and Pga4p proteins in the cell membrane (139-141). As a consequence, we believe that β-citronellol may affect both the cell wall integrity and the cell membrane integrity, which eventually leads to cell death. Thus, decreasing these proteins may be responsible for the reduction of biofilm formation **(Figure 43)**, alteration of cell membrane potential **(Figure 45)**, and the irregular shape of cells **(Figure 47)**. From these results, it can be suggested that the cell wall and cell membrane are the target sites of β-citronellol.

Exposure to β-citronellol altered the cellular oxidative stress response system. The treatment with β-citronellol enhanced intracellular ROS accumulation compared to the control group **(Figure 44)**. Moreover, we found the reduction of superoxide dismutase (SOD) protein, Sod1p, from the proteomic analysis **(Table 8)**. In *C. albicans*, six SODs genes are encoded: *SOD1*, a cytosolic copper- and zinc-containing superoxide dismutase; *SOD2*, a manganese-dependent superoxide dismutase; *SOD3*, a manganese-dependent superoxide dismutase; and *SOD4*, *SOD5*, and *SOD6*, which are GPI-anchored cell wall-associated copper-zinc-containing superoxide dismutases (142, 143). The reduction of Sod1p expression by β-citronellol treatment may lead to an imbalance redox reaction to fight against ROS accumulation from β-citronellol. In addition, ROS accumulation has been reported to link with apoptosis (144), which coincides with dose-dependent increases in cell apoptosis (**Figure 46)**, and the upregulation of heat shock proteins. The treatment suppressed the expression of Gst2p, which is required for filamentous development in the presence of nitrogen deficit (106). These data show that treating *C. albicans* with β-citronellol may inhibit stress adaption and increase sensitivity to stress-induced environments, such as malnutrition.

The other potential target protein group is ATP synthesis-related proteins. In fungi, ATP is mostly synthesized by oxidative phosphorylation via the enzyme F_1F_o-ATP synthase (145). The complex is composed of two domains: a globular F_1 catalytic domain (α3β3 domain) and a membrane-bound F_o proton-translocating domain (ab_2c_{8-12} domain). The F_1F_o domains are connected to the stalk that contains the γ, ε, and δ subunits (146, 147). The converting of ADP to ATP is occurring via the process of proton transport in the mitochondria by the function of F_1F_o-ATP synthase. From proteomic data, β-citronellol treatment downregulates the expression of two F_1F_o-ATP synthase subunits, γ (Atp3p) and δ (Atp7p). Moreover, the treatment can reduce the expression of two proteins, Cox1p and Cobp, which play a role in the mitochondrial respiratory chain. Therefore, ATP synthesis in *C. albicans* may be impaired, and eventually, affect the viability of yeast cells. Notably, increased ROS levels are linked with the reduction in ATP/ADP carrier activity (144). As a consequence, more research on the interaction between β-citronellol and F_1F_o-ATP synthase proteins in *C. albicans* is required to elucidate the exact mechanism of action.

As seen in **Figure 46**, treatment with β-citronellol results in numerous forms of cell death, including apoptosis. The AP-1-like transcription factor CAP1 (Cap1p), one of the well-studied proteins associated with apoptosis in this study, was shown to

exhibit an unexpected pattern. Cap1p is a transcription factor that has been involved in a variety of *C. albicans* pathways, including multidrug resistance (148), oxidative stress response (149), and apoptosis (150). According to a previous study, overexpression of Cap1p inhibits Baicalein-induced apoptosis in *C. albicans* (151). Additionally, Cap1p can regulate the expression of the glutathione reductase gene, as well as the level of glutathione (150). The expression of Cap1p was upregulated in the treatment of β-citronellol, similar to the percentage of apoptosis yeast. We suggest that yeast cells may upregulate Cap1p expression to maintain redox equilibrium. Due to the multifunctional activity of Cap1p in the oxidative stress response. A similar pattern of Cap1p expression in *C. albicans* has been reported in the stress-induced environment, including caspofungin treatment (152).

Mouthwash development and anti-gingivitis activities

Dental plaque accumulation is a major contributor to the development of gingivitis. Plaque buildup at the gingival edge results in inflammation known as plaque-induced gingivitis, which is prevalent in dentate populations of all ages (153). Depending on the degree of plaque-induced gingivitis, common symptoms include redness, bleeding, and pain. Gingivitis that is left untreated raises the chance of periodontitis advancement, which finally results in tooth loss. Chlorhexidine (CHX) mouthwash is an efficient method of preventing the production of dental plaque. Long-term negative effects, on the other hand, may restrict its usage in dental care regimens. As such, developing a safe supplementary oral care product may prevent the risk of developing a severe form of gingivitis. Numerous plants have been demonstrated to be useful in treating gingivitis (154). This research concentrated on formulated anti-gingivitis mouthwash-containing extracts from the leaves of KL, MO, and NE. A significant decrease in PI and GI scores was found after 14 days of usage in formulated mouthwashes groups compared to the placebo **(Figure 51)**. These findings indicate the potential anti-inflammatory activity of the formulated mouthwashes.

GC-MS analysis identified major terpenoid substances in the crude extracts which may contribute to the anti-inflammatory activity of the mouthwashes due to factors previously reported (155) (156). Phytol, acyclic diterpene alcohol, and a component of chlorophyll, were detected in all three ethanolic extracts of the plant leaves. This diterpene may possess a variety of biological properties, including antioxidant (157), anti-inflammation (158), and antimicrobial activity (159). Previous work purposed the anti-inflammatory activity of phytol by downregulating mitogen-activated protein kinase (MAPK) and NF-κB signaling molecules (160). Additionally, citronellal, citronellol, and lupeol were found as key active terpenoid components in *C. hystrix* DC. leaf extract.

The spread plate technique was used to investigate the growth of oral bacteria to determine the antimicrobial activity of the prepared mouthwashes. According to certain findings, *Staphylococcus* spp. colonization may be related to the occurrence of gingivitis (6, 161). *Staphylococcus* spp. was detected in the oral rinse samples in this study. As indicated in **Table 13**, an increase in accumulative reduction percentage was found in all groups, as well as the placebo. One potential explanation for this decrease is the Hawthorne effect (162), which can be described as people changing

their oral hygiene behavior when included in a clinical trial. Another oral microbial colony, *Candida* spp., was reduced by the formulated mouthwashes. However, smaller colonies of *Candida* spp. than *Staphylococcus* spp. were found in all groups. The possible reason is that, due to the prevalence of *Candida* spp., colonization is primarily found in some conditions, such as in immunocompromised patients (163), rather than in healthy individuals.

The primary limitation of this study was the insufficient number of subjects. The minimum number of subjects in each group should be 10, whereas the number of participants in the placebo, KL+MO, and CHX groups was 9. Three subjects were excluded from the research due to their use of antibiotics, which is one of the exclusion criteria in this study.

In conclusion, mouthwash containing kaffir lime leaf extracts can alleviate mild to moderate gingivitis by suppressing the inflammation of gingival tissue, reducing the dental biofilm formation, and lowering the number of oral microbes (*Staphylococcus* and *Candida* spp.). One of the compounds found in kaffir lime leaves known as lupeol has anti-inflammatory properties. It works by reducing the expression of NF-κB genes (*NFKB1* and *NOS2*) and proteins (phospho-IκBα, NF-κB p65, and COX-2) and inhibiting the synthesis of pro-inflammatory cytokines (IL-1β, IL-6, and TNF-α). The expression of NLRP3 inflammasome-associated genes (*IL1B*, *IL18*, *CASP1*, *NLRP3*, *PYCARD*) was also down-regulated in lupeol treatment. For the antimicrobial activity, β-citronellol, another active compound from kaffir lime leaf exhibit anti-*Candida* activity by influencing three categories of essential proteins: those involved in cellular oxidative stress response (Sod1p, Gst2p, and Ddr48p), those involved in the cell wall and cell adhesion molecules (Als2p, Rbt1p, and Pga4p), and those involved in ATP synthesis (Atp3p, Atp7p, Cox1p, and Cobp). The results from this study implemented the potential biological activity of kaffir lime leaf extract as the active ingredient in developing an adjunctive anti-gingivitis oral care product.

Abbreviation list

ACTB	Actin beta (gene)
AIM2	Absent in melanoma 2
ALP	Alkaline phosphatase
Als	Agglutinin-like sequence
ALT	Alanine transaminase
ANOVA	Analysis of variance
ASC	Apoptosis-associated speck-like protein containing a CARD
AST	Aspartate transaminase
ATP	Adenosine triphosphate
Bcr1p	Biofilm and cell wall regulator 1 protein
BHI	Brain heart infusion
Brg1p	Biofilm regulator 1 protein
CARD	Caspase recruitment domains
CASP1	Caspase 1 (gene)
CCR2	C-C motif chemokine receptor 2
CD	Cluster of differentiation
cDNA	Complementary DNA
CDP	Dendritic cell precursors
CFU-GM	Colony-forming unit for granulocytes and macrophages
CFU-M	Colony-forming units of macrophage progenitor
CHAF	*Citrus hystrix* DC. Active fraction
CHX	Chlorhexidine
cIAP	Cellular inhibitor of apoptosis protein 1
CLSI	Clinical and laboratory standards institute
cMoPs	Common monocyte progenitors
COA	Certificate of analysis
Cobp	Cytochrome B protein
Cox1p	Cytochrome oxidase 1 protein
COX-2	Cyclooxygenase-2
CSF-1	Colony-stimulating factor 1
DAMPs	Damage-associated molecular patterns
DD	Death domain
Ddr48p	Stress protein DDR48
DEX	Dexamethasone
DMSO	Dimethyl sulfoxide
DPPH	2,2-diphenyl-1-picrylhydrazyl
DTT	Dithiothreitol
EI-MS	Electron ionization mass spectroscopy
ELISA	Enzyme-linked immunosorbent assay
EPS	Extracellular polymeric substances
F-C	Folin-Ciocalteu
FITC	Fluorescein isothiocyanate
FT-IR	Fourier-transform infrared spectrophotometer
GAE	Gallic acid equivalent

GC-MS	Gas chromatography-mass spectrometry
GI	Gingival index
GlcNAc	N-acetylglucosamine
GM-CSF	Granulocyte-macrophage colony-stimulating factor
GMP	Granulocyte/macrophage precursor
GSDMD	Gasdermin D
Gst2p	Glutathione S transferase protein
H_2DCFDA	2′,7′-dichlorofluorescein diacetate
H_2O_2	Hydrogen peroxide
HBSS	Hank balanced salt solution
HK	Hexokinase
HMDS	Hexamethyldisilazane
HPP-CFC	Colony-forming cells with high proliferative potential
HRP	Horseradish peroxidase
Hwp1	Hyphal wall protein 1
IC_{10}	Inhibitory concentration at 5%
IC_5	Inhibitory concentration at 10%
IC_{50}	The half-maximal inhibitory concentration
IFN-γ	Interferon gamma
IgE	Immunoglobulin E
IκBα	Nuclear factor of kappa-light-chain-enhancer in B-cells inhibitor, alpha
IKK	IκB kinase
IL18	Interleukin 18 (gene)
IL1B	Interleukin 1 beta (gene)
IL-1β	Interleukin 1 beta
IL-3	Interleukin 3
IL-6	Interleukin 6
iNOS	Inducible nitric oxide synthase
IRAK	Interleukin-1 receptor-associated kinase
IRB	Institutional review board
IRF	Interferon regulatory factors
kDA	Kilodaltons
KL	Kaffir lime
LC-MS/MS	Liquid chromatography-tandem mass spectrometry
LPS	Lipopolysaccharide
LRR	Leucine-rich repeat
Ly6c	Lymphocyte antigen 6 complex
MALDI-TOF MS	Matrix-assisted laser desorption/ionization time of flight mass spectrometry
MAPK	Mitogen-activated protein kinase
MAVS	Mitochondrial antiviral signaling protein
MD-2	Myeloid differentiation factor 2
MDMs	Monocyte-derived macrophages
MDP	Monocyte/dendritic cell precursor
MFC	Minimum fungicidal concentration
MHC	Major histocompatibility complex

MIC	Minimum inhibitory concentration
MO	Moringa
mtROS	Mitochondrial reactive oxygen species
MTT	3-(4,5-dimethylthiazol-2-yl)-2,5-diphenyltetrazolium bromide
MyD88	Myeloid differentiation primary response 88
NALP3	Nacht Domain-, Leucine-Rich Repeat-, and PYD-Containing Protein 3
Ndt80p	Meiosis-specific transcription factor protein
NE	Neem
NFKB1	Nuclear factor kappa B subunit 1
NF-κB	Nuclear factor kappa-light-chain-enhancer of activated B cells
NF-κB p65	NF-κb p65 subunit
NK cells	Natural killer cells
NLR	NOD-like receptor
NLRP3	NLR family pyrin domain containing 3
NMR	Nuclear magnetic resonance
NOD	Nucleotide-binding oligomerization domain
NOS2	Nitric oxide synthase 2
OD	Optical density
Ox-mtDNA	Oxidized mitochondrial DNA
P2X7	P2X purinoceptor 7
PAMPs	Pathogen-associated molecular patterns
PBMCs	Peripheral blood mononuclear cells
PBS	Phosphate-buffered saline
PE	Phycoerythrin
Peli	Pellino E3 ubiquitin protein ligase
Pga4p	1,3-beta-glucanosyltransferase PGA4 protein
PGE2	Prostaglandin E2
PGH2	Prostaglandin H2
IκBα	Nuclear factor of kappa-light-chain-enhancer in B-cells inhibitor, alpha
PI	Plaque index
PIA	Polysaccharide intercellular antigen
PRRs	Pattern recognition receptors
PVC	Polyvinylchloride
PYCARD	PYD and CARD domain containing (gene)
PYD	Pyrin domain
qRT-PCR	Quantitative reverse transcription PCR
Rbt1p	Cell wall proteins RTB1
RIP	Receptor-interacting serine/threonine protein kinase
Rob1p	Regulator of biofilm protein
ROS	Reactive oxygen species
RPM	Revolutions per minute
RPMI-1640	Roswell park memorial institute-1640
SDA	Sabouraud dextrose agar

SDB	Sabouraud dextrose broth
SDS-PAGE	Sodium dodecyl-sulfate polyacrylamide gel electrophoresis
SEM	Scanning electron microscopy
Sod1p	Cytosolic copper- and zinc-containing superoxide dismutase
TAK	Transforming growth factor beta-activated kinase
TAMs	Tumor-associated macrophages
TANK	TRAF family member-associated NF-kappa-B activator
TEAC	Trolox equivalent antioxidant capacity
Tec1p	TEA/ATTS transcription factor
TGF-β	Transforming growth factor-beta
TIR	Toll/interleukin 1 receptor
TLRs	Toll-like receptors
TMB	5,5′-tetramethylbenzidine
TNFR	Tumor necrosis factor receptor
TNF-α	Tumor necrosis factor alpha
TRAM	TRIF-related adaptor molecule
TRIF	TIR-domain-containing adapter-inducing interferon-β
Ume6p	Zn(II)2Cys6 transcription factor
Zap1p	Candida suppressor of ROK1

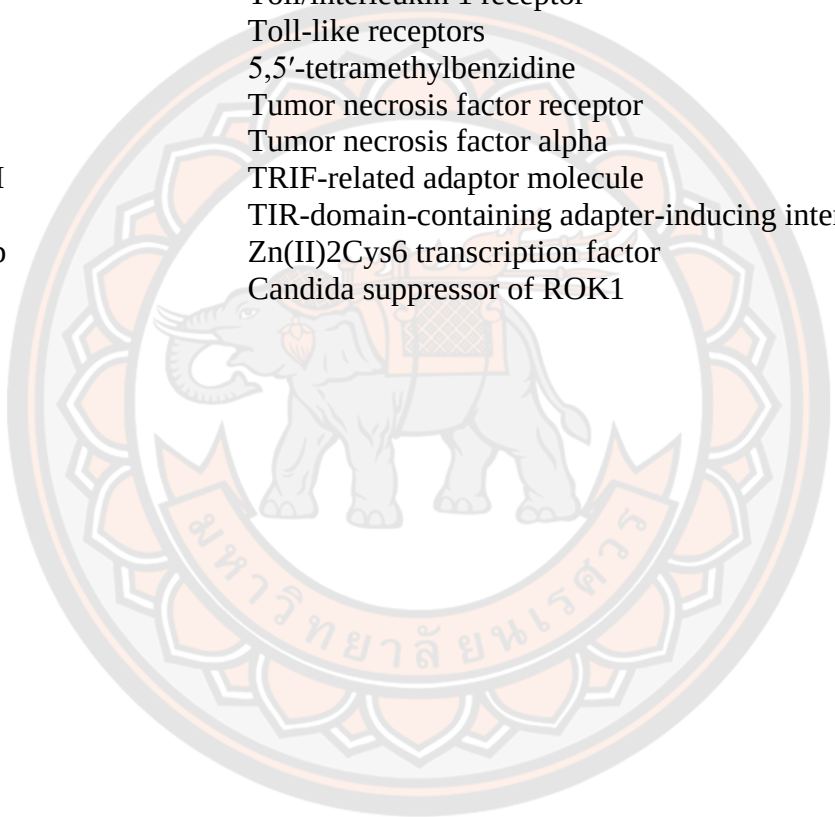

REFERENCES

1. Rathee M JP. Gingivitis. Treasure Island (FL): StatPearls Publishing; 2022 [updated March 26, 2022]. Available from: https://www.ncbi.nlm.nih.gov/books/NBK557422/.
2. สำนักทันตสาธาณสุข. ผลการสำรวจสภาวะสุขภาพช่องปากแห่งชาติ ครั้งที่ 8 พ.ศ.2560. นนทบุรี: กรมอนามัย กระทรวงสาธารณสุข; 2017 [updated January 1, 2017]. Available from: https://dental.anamai.moph.go.th/th/national-survey-of-dental-health.
3. Arigbede AO, Babatope BO, Bamidele MK. Periodontitis and systemic diseases: a literature review. Journal of Indian Society of Periodontology. 2012;16(4):487-491.
4. Cuesta A, Jewtuchowicz V, Brusca M, Mujica MT, Rosa A. Antibiotic susceptibility of *Staphylococcus aureus* isolates in oral mucosa and pockets of patients with gingivitis-periodontitis. Acta Odontológica Latinoamericana. 2011;24:35-40.
5. Hussein M, Al-Yaseen A, Alhamadi W. Prevalence of *Staphylococcus aureus* among gingivitis in patient with orthodontic wires in Kufa city/Iraq. Pakistan Journal of Biotechnology. 2017;14:91-96.
6. Rams TE, Feik D, Slots J. Staphylococci in human periodontal diseases. Oral Microbiology and Immunology. 1990;5(1):29-32.
7. Al Mubarak S, Robert AA, Baskaradoss JK, Al-Zoman K, Al Sohail A, Alsuwyed A, et al. The prevalence of oral *Candida* infections in periodontitis patients with type 2 diabetes mellitus. Journal of Infection and Public Health. 2013;6(4):296-301.
8. Olczak-Kowalczyk D, Pyrżak B, Dąbkowska M, Pańczyk-Tomaszewska M, Miszkurka G, Rogozińska I, et al. *Candida* spp. and gingivitis in children with nephrotic syndrome or type 1 diabetes. BMC Oral Health. 2015;15(1):57.
9. Suresh Unniachan A, Krishnavilasom Jayakumari N, Sethuraman S. Association between *Candida* species and periodontal disease: A systematic review. Current Medical Mycology. 2020;6(2):63-68.
10. Müller H-DHD, Cvikl BB, Lussi AA, Gruber RR. Salivary pellets induce a pro-inflammatory response involving the TLR4–NF-κB pathway in gingival fibroblasts. BMC oral health. 2017;17(1):1-10.
11. Moutsopoulos NM, Konkel JE. Tissue-specific immunity at the oral mucosal barrier. Trends in Immunology. 2018;39(4):276-287.
12. Roh JS, Sohn DH. Damage-associated molecular patterns in inflammatory diseases. Immune network. 2018;18(4):27.
13. Arabaci T, Cicek Y, Canakci V, Canakci CF, Ozgoz M, Albayrak M, et al. Immunohistochemical and stereologic analysis of NF-κB activation in chronic periodontitis. European Journal of Dentistry. 2010;4(4):454-461.
14. Ambili R, Janam P. A critique on nuclear factor-kappa B and signal transducer and activator of transcription 3: the key transcription factors in periodontal pathogenesis. Journal of Indian Society of Periodontology. 2017;21(5):350-356.
15. Marchesan JT, Girnary MS, Moss K, Monaghan ET, Egnatz GJ, Jiao Y, et al. Role of inflammasomes in the pathogenesis of periodontal disease and therapeutics. Periodontology 2000. 2020;82(1):93-114.
16. Surlin P, Lazar L, Sincar C, Gheorghe DN, Popescu DM, Boldeanu VM, et al. NLRP3 inflammasome expression in gingival crevicular fluid of patients with

periodontitis and chronic hepatitis C. Mediators of Inflammation. 2021;2021:1-8.
17. James P, Worthington HV, Parnell C, Harding M, Lamont T, Cheung A, et al. Chlorhexidine mouthrinse as an adjunctive treatment for gingival health. The Cochrane Database of Systematic Reviews. 2017;3(3):8676.
18. Brookes ZLS, Bescos R, Belfield LA, Ali K, Roberts A. Current uses of chlorhexidine for management of oral disease: A narrative review. Journal of Dentistry. 2020;103:103497-103497.
19. Lertsatitthanakorn P, Taweechaisupapong S, Aromdee C, Khunkitti W. *In vitro* bioactivities of essential oils used for acne control. International Journal of Aromatherapy. 2006;16(1):43-49.
20. Kidarn S, Saenjum C, Hongwiset D, Phrutivorapongkul A. Furanocoumarins from kaffir lime and their inhibitory effects on inflammatory mediator production. Cogent Chemistry. 2018;4(1):1-10.
21. Kooltheat N, Kamuthachad L, Anthapanya M, Samakchan N, Sranujit RP, Potup P, et al. Kaffir lime leaves extract inhibits biofilm formation by *Streptococcus mutans*. Nutrition. 2016;32(4):486-490.
22. Nendissa SJ, Nendissa DM. Test for the antibacterial inhibition of kaffir lime leaf (*Citrus hysteric* DC.) extract against pathogen bacteria in improving food safety. Earth and Environmental Science. 2021;883(1):12056.
23. Srifuengfung S, Bunyapraphatsara N, Satitpatipan V, Tribuddharat C, Junyaprasert VB, Tungrugsasut W, et al. Antibacterial oral sprays from kaffir lime (*Citrus hystrix* DC.) fruit peel oil and leaf oil and their activities against respiratory tract pathogens. Journal of Traditional and Complementary Medicine. 2020;10(6):594-598.
24. Pumival P, Tadtong S, Athikomkulchai S, Chittasupho C. Antifungal activity and the chemical and physical stability of microemulsions containing *Citrus hystrix* DC. Leaf oil. Natural Product Communications. 2020;15(9):1934578.
25. Hovijitra RS, Choonharuangdej S, Srithavaj T. Effect of essential oils prepared from Thai culinary herbs on sessile *Candida albicans* cultures. Journal of Oral Science. 2016;58(3):365-371.
26. Medzhitov R. Origin and physiological roles of inflammation. Nature. 2008;454(7203):428-435.
27. Provan D, Gribben J. Molecular hematology: Wiley; 2019.
28. Kapellos TS, Bonaguro L, Gemünd I, Reusch N, Saglam A, Hinkley ER, et al. Human monocyte subsets and phenotypes in major chronic inflammatory diseases. Frontiers in Immunology. 2019;10:2035.
29. Cormican S, Griffin MD. Human monocyte subset distinctions and function: insights from gene expression analysis. Frontiers in Immunology. 2020;11:1070.
30. Varol C, Mildner A, Jung S. Macrophages: Development and tissue specialization. Annual Review of Immunology. 2015;33(1):643-675.
31. Patel U, Rajasingh S, Samanta S, Cao T, Dawn B, Rajasingh J. Macrophage polarization in response to epigenetic modifiers during infection and inflammation. Drug Discovery Today. 2017;22(1):186-193.
32. Newton K, Dixit VM. Signaling in innate immunity and inflammation. Cold Spring Harbor Perspectives in Biology. 2012;4(3):6049.
33. Kang JY, Lee J-O. Structural biology of the Toll-like receptor family. Annual Review of Biochemistry. 2011;80(1):917-941.
34. Zhang J-M, An J. Cytokines, inflammation, and pain. International

Anesthesiology Clinics. 2007;45(2):27-37.
35. Kaneko N, Kurata M, Yamamoto T, Morikawa S, Masumoto J. The role of interleukin-1 in general pathology. Inflammation and Regeneration. 2019;39(1):12.
36. Yasuda K, Nakanishi K, Tsutsui H. Interleukin-18 in health and disease. International Journal of Molecular Sciences. 2019;20(3):649.
37. Turner MD, Nedjai B, Hurst T, Pennington DJ. Cytokines and chemokines: at the crossroads of cell signalling and inflammatory disease. Biochimica et Biophysica Acta (BBA) - Molecular Cell Research. 2014;1843(11):2563-2582.
38. Walter MR. The molecular basis of IL-10 function: from receptor structure to the onset of signaling. Current Topics in Microbiology and Immunology. 2014;380:191-212.
39. Huang F, Chen Y-G. Regulation of TGF-β receptor activity. Cell & Bioscience. 2012;2:9.
40. Rouzer CA, Marnett LJ. Cyclooxygenases: structural and functional insights. Journal of lipid research. 2009;50 29-34.
41. Broz P, Dixit VM. Inflammasomes: mechanism of assembly, regulation and signalling. Nature Reviews Immunology. 2016;16(7):407-420.
42. Davis BK, Wen H, Ting JPY. The inflammasome NLRs in immunity, inflammation, and associated diseases. Annual Review of Immunology. 2011;29:707-735.
43. Swanson KV, Deng M, Ting JPY. The NLRP3 inflammasome: molecular activation and regulation to therapeutics. Nature reviews Immunology. 2019;19(8):477-489.
44. Brown L, Wolf JM, Prados-Rosales R, Casadevall A. Through the wall: extracellular vesicles in gram-positive bacteria, mycobacteria and fungi. Nature reviews Microbiology. 2015;13(10):620-630.
45. Sampaio-Maia B, Caldas IM, Pereira ML, Pérez-Mongiovi D, Araujo R. The oral microbiome in health and its implication in oral and systemic diseases: Academic Press; 2016 2016/01/01/. 171-210 p.
46. Bowen WH, Burne RA, Wu H, Koo H. Oral biofilms: Pathogens, matrix, and polymicrobial interactions in microenvironments. Trends in Microbiology. 2018;26(3):229-242.
47. Berger D, Rakhamimova A, Pollack A, Loewy Z. Oral biofilms: Development, control, and analysis. High-Throughput. 2018;7(3):24.
48. Huang R, Li M, Gregory RL. Bacterial interactions in dental biofilm. Virulence. 2011;2(5):435-444.
49. Krzyściak W, Jurczak A, Kościelniak D, Bystrowska B, Skalniak A. The virulence of *Streptococcus mutans* and the ability to form biofilms. European Journal of Clinical Microbiology & Infectious Diseases. 2014;33(4):499-515.
50. InformedHealth.org. Gingivitis and periodontitis: overview. Cologne, Germany: Institute for Quality and Efficiency in Health Care (IQWiG); 2020 [updated February 27, 2020]. Available from: https://www.ncbi.nlm.nih.gov/books/NBK279593/.
51. Kinane DF, Stathopoulou PG, Papapanou PN. Periodontal diseases. Nature Reviews Disease Primers. 2017;3:17038.
52. Bosma-den Boer MM, van Wetten M-L, Pruimboom L. Chronic inflammatory diseases are stimulated by current lifestyle: how diet, stress levels and medication prevent our body from recovering. Nutrition & Metabolism. 2012;9(1):32-32.

53. Dickinson S, Hancock DP, Petocz P, Ceriello A, Brand-Miller J. High–glycemic index carbohydrate increases nuclear factor-κB activation in mononuclear cells of young, lean healthy subjects. The American Journal of Clinical Nutrition. 2008;87(5):1188-1193.
54. Hu Y, Block G, Norkus EP, Morrow JD, Dietrich M, Hudes M. Relations of glycemic index and glycemic load with plasma oxidative stress markers. The American Journal of Clinical Nutrition. 2006;84(1):70-76.
55. Gürsoy M, Gürsoy UK, Sorsa T, Pajukanta R, Könönen E. High salivary estrogen and risk of developing pregnancy gingivitis. Journal of Periodontology. 2013;84(9):1281-1289.
56. Bilińska M, Sokalski J. Pregnancy gingivitis and tumor gravidarum. Ginekologia Polska. 2016;87(4):310-313.
57. Nakagawa S, Fujii H, Machida Y, Okuda K. A longitudinal study from prepuberty to puberty of gingivitis. Journal of Clinical Periodontology. 1994;21(10):658-665.
58. Tungare S PA. Drug induced gingival overgrowth. Treasure Island (FL): StatPearls Publishing; 2021 [updated September 25, 2021]. Available from: https://www.ncbi.nlm.nih.gov/books/NBK538518/.
59. Page RC, & Schroeder, H. E. Pathogenesis of inflammatory periodontal disease. A summary of current work. Laboratory Investigation; A Journal of Technical Methods and Pathology. 1976;34(3):235–249.
60. Muñoz-Carrillo JL. Pathogenesis of periodontal disease: Intech Open; 2019. 1-14 p.
61. Page RC. Gingivitis. Journal of Clinical Periodontology. 1986;13(5):345-355.
62. Bosshardt DD, Selvig KA. Dental cementum: the dynamic tissue covering of the root. Periodontology 2000. 1997;13(1):41-75.
63. Syndergaard B, Al-Sabbagh M, Kryscio RJ, Xi J, Ding X, Ebersole JL, et al. Salivary biomarkers associated with gingivitis and response to therapy. Journal of Periodontology. 2014;85(8):295-303.
64. Perez-Chaparro PJ, Gonçalves C, Figueiredo LC, Faveri M, Lobão E, Tamashiro N, et al. Newly identified pathogens associated with periodontitis: a systematic review. Journal of Dental Research. 2014;93(9):846-858.
65. Pérez-Chaparro PJ, Duarte PM, Shibli JA, Montenegro S, Lacerda Heluy S, Figueiredo LC, et al. The current weight of evidence of the microbiologic profile associated with peri-implantitis: a systematic review. Journal of Periodontology. 2016;87(11):1295-1304.
66. Feres M, Teles F, Teles R, Figueiredo LC, Faveri M. The subgingival periodontal microbiota of the aging mouth. Periodontology 2000. 2016;72(1):30-53.
67. Kistler JO, Booth V, Bradshaw DJ, Wade WG. Bacterial community development in experimental gingivitis. PloS One. 2013;8(8):71227.
68. Zhou X, Li Y. Atlas of oral microbiology: from healthy microflora to disease: Elsevier Science; 2015.
69. Thomer L, Schneewind O, Missiakas D. Pathogenesis of *Staphylococcus aureus* bloodstream infections. Annual Review of Pathology: Mechanisms of Disease. 2016;11(1):343-364.
70. Smith AJ, Jackson MS, Bagg J. The ecology of *Staphylococcus* species in the oral cavity. Journal of Medical Microbiology. 2001;50(11):940-946.

71. Arciola CR, Campoccia D, Montanaro L. Implant infections: adhesion, biofilm formation and immune evasion. Nature Reviews Microbiology. 2018;16(7):397-409.
72. Archer NK, Mazaitis MJ, Costerton JW, Leid JG, Powers ME, Shirtliff ME. *Staphylococcus aureus* biofilms: Properties, regulation, and roles in human disease. Virulence. 2011;2(5):445-459.
73. Otto M. *Staphylococcus epidermidis*—The "accidental" pathogen. Nature Reviews Microbiology. 2009;7(8):555-567.
74. Carroll KC, Butel JS, Morse SA. Jawetz Melnick&Adelbergs Medical Microbiology 27/E: McGraw-Hill Education; 2015.
75. Nobile CJ, Johnson AD. *Candida albicans* biofilms and human disease. Annual Review of Microbiology. 2015;69:71-92.
76. Agouillal F, Taher Z, Moghrani H, Nasrallah N, El Enshasy H. A review of genetic taxonomy, biomolecules chemistry and bioactivities of *Citrus hystrix* DC. Biosciences Biotechnology Research Asia. 2017;14:285-305.
77. Peter KV. Handbook of Herbs and Spices: Second Edition: Woodhead Publishing; 2012 01/01. 1-607 p.
78. Waikedre J, Dugay A, Barrachina I, Herrenknecht C, Cabalion P, Fournet A. Chemical composition and antimicrobial activity of the essential oils from new caledonian *Citrus macroptera* and *Citrus hystrix* Chemistry & Biodiversity. 2010;7(4):871-877.
79. Muangnoi C, Failla M. Anti-inflammatory activities of extracts of Thai spices and herbs with lipopolysaccharide-activated RAW 264.7 murine macrophages. Journal of Medicinal Food. 2009;12(6):1213-1220.
80. Anuchapreeda S, Anzawa R, Viriyaadhammaa N, Neimkhum W, Chaiyana W, Okonogi S, et al. Isolation and biological activity of agrostophillinol from kaffir lime (*Citrus hystrix*) leaves. Bioorganic & Medicinal Chemistry Letters. 2020;30(14):127256.
81. Wungsintaweekul J, Sitthithaworn W, Putalun W, Pfeifhoffer H, Brantner A. Antimicrobial, antioxidant activities and chemical composition of selected Thai spices. Songklanakarin Journal of Science and Technology. 2010;32:589-598.
82. Arumugam A, Nagarani G, Siddhuraju P. Hepatoprotective effect of leaf extracts from *Citrus hystrix* and *C. maxima* against paracetamol induced liver injury in rats. Food Science and Human Wellness. 2015;4(1):35-41.
83. Wijayanti N, Tunjung W, Setyawati Y. Cytotoxicity and apoptosis induction by kaffir lime leaves extract (*Citrus hystrix* DC.) in HeLa cells culture (human cervical cancer cell line). KnE Life Sciences. 2015;2(1):631.
84. Ho Y, Suphrom N, Daowtak K, Potup P, Thongsri Y, Usuwanthim K. Anticancer effect of *Citrus hystrix* DC. leaf extract and its bioactive constituents citronellol and, citronellal on the triple negative breast cancer MDA-MB-231 cell line. Pharmaceuticals. 2020;13(12):476.
85. Malta LG, Liu RH. Analyses of total phenolics, total flavonoids, and total antioxidant activities in foods and dietary supplements. Oxford: Academic Press; 2014 2014/01/01/. 305-314 p.
86. Ainsworth EA, Gillespie KM. Estimation of total phenolic content and other oxidation substrates in plant tissues using Folin–Ciocalteu reagent. Nature Protocols. 2007;2(4):875-877.
87. Ebada SS, Edrada RA, Lin W, Proksch P. Methods for isolation, purification and

structural elucidation of bioactive secondary metabolites from marine invertebrates. Nature Protocols. 2008;3(12):1820-1831.
88. Kim J, Ahn H, Han B-C, Shin H, Kim J-C, Jung E-M, et al. Obovatol inhibits NLRP3, AIM2, and non-canonical inflammasome activation. Phytomedicine. 2019;63:153019.
89. Präbst K, Engelhardt H, Ringgeler S, Hübner H. Basic colorimetric proliferation assays: MTT, WST, and resazurin. Methods in Molecular Biology 2017;1601:1-17.
90. Rao X, Huang X, Zhou Z, Lin X. An improvement of the 2ˆ (–delta delta CT) method for quantitative real-time polymerase chain reaction data analysis. Biostatistics, Bioinformatics and Biomathematics. 2013;3(3):71-85.
91. Buakaew W, Pankla Sranujit R, Noysang C, Thongsri Y, Potup P, Nuengchamnong N, et al. Phytochemical constituents of *Citrus hystrix* DC. leaves attenuate inflammation via NF-κB signaling and NLRP3 inflammasome activity in macrophages. Biomolecules. 2021;11(1):105.
92. Gulati M, Lohse MB, Ennis CL, Gonzalez RE, Perry AM, Bapat P, et al. *In vitro* culturing and screening of *Candida albicans* biofilms. Current Protocols in Microbiology. 2018;50(1):60.
93. Lone SA, Wani MY, Fru P, Ahmad A. Cellular apoptosis and necrosis as therapeutic targets for novel Eugenol Tosylate Congeners against *Candida albicans.* Scientific Reports. 2020;10(1):1191.
94. Khan A, Ahmad A, Khan LA, Manzoor N. *Ocimum sanctum* (L.) essential oil and its lead molecules induce apoptosis in *Candida albicans*. Research in Microbiology. 2014;165(6):411-419.
95. Fischer ER, Hansen BT, Nair V, Hoyt FH, Dorward DW. Scanning Electron Microscopy. Current Protocols in Microbiology. 2012;25(1):1-47.
96. Buakaew W, Sranujit RP, Noysang C, Sangouam S, Suphrom N, Thongsri Y, et al. Evaluation of mouthwash containing *Citrus hystrix* DC., *Moringa oleifera* Lam. and *Azadirachta indica* A. Juss. leaf extracts on dental plaque and gingivitis. Plants. 2021;10(6):1153.
97. Rahman MM, Islam MB, Biswas M, Alam AHMK. *In vitro* antioxidant and free radical scavenging activity of different parts of *Tabebuia pallida* growing in Bangladesh. BMC Research Notes. 2015;8(1):1-9.
98. Kadam P, Bhalerao S. Sample size calculation. International Journal of Ayurveda Research. 2010;1(1):55-57.
99. Löe H. The gingival index, the plaque index and the retention index systems. The Journal of Periodontology. 1967;38(6):610-616.
100. Jain PS, Bari SB. Isolation of lupeol, stigmasterol and campesterol from petroleum ether extract of woody stem of *Wrightia tinctoria*. Asian Journal of Plant Sciences. 2010;9(3):163.
101. Shwe HH, Win KK, Moe TT, Myint AA, Win T. Isolation and structural characterization of lupeol from the stem bark of *Diospyros ehretioides* Wall. IEEE-SEM. 2019;7:140-144.
102. Ragasa CY, Tan MCS, Fortin DR, Shen C-C. Chemical constituents of *Ixora philippinensis* Merr. Journal of Applied Pharmaceutical Science. 1930;5(9):62-67.
103. Saleem M. Lupeol, a novel anti-inflammatory and anti-cancer dietary triterpene. Cancer Letters. 2009;285(2):109-115.
104. Buakaew W, Pankla Sranujit R, Noysang C, Krobthong S, Yingchutrakul Y,

Thongsri Y, et al. Proteomic analysis reveals proteins involved in the mode of action of β-citronellol identified from *Citrus hystrix* DC. leaf against *Candida albicans*. Frontiers in Microbiology. 2022;13:894637.
105. Hwang C-S, Rhie G-e, Kim S-T, Kim Y-R, Huh W-K, Baek Y-U, et al. Copper- and zinc-containing superoxide dismutase and its gene from *Candida albicans*. Biochimica et Biophysica Acta (BBA) - General Subjects. 1999;1427(2):245-255.
106. So-Hyoung L, Soon-Chun C, Jongheon S. *GST2* is required for nitrogen starvation-induced filamentous growth in *Candida albicans*. Journal of Microbiology and Biotechnology. 2014;24(9):1207-1215.
107. Cleary IA, MacGregor NB, Saville SP, Thomas DP. Investigating the function of Ddr48p in *Candida albicans*. Eukaryotic cell. 2012;11(6):718-724.
108. Ene IV, Bennett RJ. *HWP1* and related adhesins contribute to both mating and biofilm formation in *Candida albicans*. Eukaryotic Cell. 2009;8(12):1909-1913.
109. Braun BR, Head WS, Wang MX, Johnson AD. Identification and characterization of *TUP1*-regulated genes in *Candida albicans*. Genetics. 2000;156(1):31-44.
110. Bennett RJ, Uhl MA, Miller MG, Johnson AD. Identification and characterization of a *Candida albicans* mating pheromone. Molecular and Cellular Biology. 2003;23(22):8189-8201.
111. White SJ, Rosenbach A, Lephart P, Nguyen D, Benjamin A, Tzipori S, et al. Self-regulation of *Candida albicans* population size during GI colonization. PLoS Pathogens. 2007;3(12):184.
112. Aoki W, Kitahara N, Miura N, Morisaka H, Kuroda K, Ueda M. Profiling of adhesive properties of the agglutinin-like sequence (ALS) protein family, a virulent attribute of *Candida albicans*. FEMS Immunology & Medical Microbiology. 2012;65(1):121-124.
113. Fanning S, Xu W, Beaurepaire C, Suhan JP, Nantel A, Mitchell AP. Functional control of the *Candida albicans* cell wall by catalytic protein kinase A subunit Tpk1. Molecular Microbiology. 2012;86(2):284-302.
114. Monroy-Pérez E, Sáinz-Espuñes T, Paniagua-Contreras G, Negrete-Abascal E, Rodríguez-Moctezuma JR, Vaca S. Frequency and expression of *ALS* and *HWP1* genotypes in *Candida albicans* strains isolated from Mexican patients suffering from vaginal candidosis. Mycoses. 2012;55(3):151-157.
115. Plaine A, Walker L, Da Costa G, Mora-Montes HM, McKinnon A, Gow NAR, et al. Functional analysis of *Candida albicans* GPI-anchored proteins: roles in cell wall integrity and caspofungin sensitivity. Fungal genetics and biology : FG & B. 2008;45(10):1404-1414.
116. Ene IV, Heilmann CJ, Sorgo AG, Walker LA, de Koster CG, Munro CA, et al. Carbon source-induced reprogramming of the cell wall proteome and secretome modulates the adherence and drug resistance of the fungal pathogen *Candida albicans*. Proteomics. 2012;12(21):3164-3179.
117. Gaudet P, Livstone MS, Lewis SE, Thomas PD. Phylogenetic-based propagation of functional annotations within the Gene Ontology consortium. Briefings in Bioinformatics. 2011;12(5):449-462.
118. Hartley AM, Lukoyanova N, Zhang Y, Cabrera-Orefice A, Arnold S, Meunier B, et al. Structure of yeast cytochrome c oxidase in a supercomplex with cytochrome bc(1). Nature Structural & Molecular Biology. 2019;26(1):78-83.

119. Brivet-Chevillotte P, di Rago J-P. Electron-transfer restoration by vitamin K3 in a complex III-deficient mutant of *S. cerevisiae* and sequence of the corresponding cytochrome b mutation. FEBS Letters. 1989;255(1):5-9.
120. Beattie DS, Jenkins HC, Howton MM. Biochemical evidence for the orientation of cytochrome b in the yeast mitochondrial membrane in the eight-helix model. Archives of Biochemistry and Biophysics. 1994;312(1):292-300.
121. Sharma Y, Rastogi SK, Perwez A, Rizvi MA, Manzoor N. β-citronellol alters cell surface properties of *Candida albicans* to influence pathogenicity related traits. Medical Mycology. 2020;58(1):93-106.
122. Silva D, Diniz-Neto H, Cordeiro L, Silva-Neta M, Silva S, Andrade-Júnior F, et al. (R)-(+)-β-citronellol and (S)-(-)-β-citronellol in combination with amphotericin B against *Candida* Spp. International Journal of Molecular Sciences. 2020;21(5):1785.
123. Ngan LTM, Moon J-K, Kim J-H, Shibamoto T, Ahn Y-J. Growth-inhibiting effects of *Paeonia lactiflora* root steam distillate constituents and structurally related compounds on human intestinal bacteria. World Journal of Microbiology and Biotechnology. 2012;28(4):1575-1583.
124. Nostro A, Scaffaro R, D'Arrigo M, Botta L, Filocamo A, Marino A, et al. Development and characterization of essential oil component-based polymer films: a potential approach to reduce bacterial biofilm. Applied Microbiology and Biotechnology. 2013;97(21):9515-9523.
125. Zore GB, Thakre AD, Rathod V, Karuppayil SM. Evaluation of anti-*Candida* potential of geranium oil constituents against clinical isolates of *Candida albicans* differentially sensitive to fluconazole: inhibition of growth, dimorphism and sensitization. Mycoses. 2011;54(4):99-109.
126. Santos PL, Matos JPSCF, Picot L, Almeida JRGS, Quintans JSS, Quintans-Júnior LJ. Citronellol, a monoterpene alcohol with promising pharmacological activities - A systematic review. Food and Chemical Toxicology. 2019;123:459-469.
127. (ChEBI) CEoBI. CHEBI:50462 - citronellol. 2015 [updated August 17, 2015]. Available from: https://www.ebi.ac.uk/chebi/searchId.do?chebiId=CHEBI:50462.
128. Murakami A, Gao G, Kim OK, Omura M, Yano M, Ito C, et al. Identification of coumarins from the fruit of *Citrus hystrix* DC as inhibitors of nitric oxide generation in mouse macrophage RAW 264.7 cells. Journal of Agricultural and Food Chemistry. 1999;47(1):333-339.
129. Wal P, Awani R, Wal A, Sharma G. Biological activities of lupeol. Systematic Reviews in Pharmacy. 2011;2(1):44-66.
130. Liu K, Zhang X, Xie L, Deng M, Chen H, Song J, et al. Lupeol and its derivatives as anticancer and anti-inflammatory agents: molecular mechanisms and therapeutic efficacy. Pharmacological Research. 2021;164:105373.
131. Lucetti DL, Lucetti ECP, Bandeira MAM, Veras HNH, Silva AH, Leal LKAM, et al. Anti-inflammatory effects and possible mechanism of action of lupeol acetate isolated from *Himatanthus drasticus* (Mart.) Plumel. Journal of Inflammation. 2010;7(1):60.
132. Vasanth K, Minakshi GC, Velu K, Priya T, Kumar RM, Kaliappan I, et al. Anti-adipogenic β-sitosterol and lupeol from *Moringa oleifera* suppress adipocyte differentiation through regulation of cell cycle progression. Journal of Food Biochemistry. 2022;10:1111.
133. Xu M, Li X, Song L, Tao C, Fang J, Tao L. Lupeol alleviates coxsackievirus B3-

induced viral myocarditis in mice via downregulating toll-like receptor 4. Journal of International Medical Research. 2020;48(4):1-11.
134. Oliveira-Junior MS, Pereira EP, de Amorim VCM, Reis LTC, do Nascimento RP, da Silva VDA, et al. Lupeol inhibits LPS-induced neuroinflammation in cerebellar cultures and induces neuroprotection associated to the modulation of astrocyte response and expression of neurotrophic and inflammatory factors. International Immunopharmacology. 2019;70:302-312.
135. Klis FM, Sosinska GJ, de Groot PWJ, Brul S. Covalently linked cell wall proteins of *Candida albicans* and their role in fitness and virulence. FEMS Yeast Research. 2009;9(7):1013-1028.
136. Staab Janet F, Bradway Steven D, Fidel Paul L, Sundstrom P. Adhesive and mammalian transglutaminase substrate properties of *Candida albicans HWP1*. Science. 1999;283(5407):1535-1538.
137. Monniot C, Boisramé A, Da Costa G, Chauvel M, Sautour M, Bougnoux M-E, et al. Rbt1 protein domains analysis in *Candida albicans* brings insights into hyphal surface modifications and Rbt1 potential role during adhesion and biofilm formation. PloS One. 2013;8(12):82395-82395.
138. Hoyer LL, Cota E. *Candida albicans* agglutinin-like sequence (Als) family vignettes: a review of Als protein structure and function. Frontiers in Microbiology. 2016;7:280.
139. Cabezón V, Llama-Palacios A, Nombela C, Monteoliva L, Gil C. Analysis of *Candida albicans* plasma membrane proteome. Proteomics. 2009;9(20):4770-4786.
140. UniProtKB. UniProtKB - P0CU38 (ALS2_CANAL). 2022 [updated April 15, 2022]. Available from: https://www.uniprot.org/uniprot/P0CU38.
141. UniProtKB. UniProtKB - Q5AJY5 (PGA4_CANAL). 2022 [updated April 15, 2022]. Available from: https://www.uniprot.org/uniprot/Q5AJY5.
142. Martchenko M, Alarco A-M, Harcus D, Whiteway M. Superoxide dismutases in *Candida albicans*: transcriptional regulation and functional characterization of the hyphal-induced *SOD5* gene. Molecular Biology of the Cell. 2004;15(2):456-467.
143. Sun L, Liao K, Hang C, Wang D. Honokiol induces reactive oxygen species-mediated apoptosis in *Candida albicans* through mitochondrial dysfunction. PloS One. 2017;12(2):172228.
144. Perrone GG, Tan S-X, Dawes IW. Reactive oxygen species and yeast apoptosis. Biochimica et Biophysica Acta (BBA) - Molecular Cell Research. 2008;1783(7):1354-1368.
145. Li S, Zhao Y, Zhang Y, Zhang Y, Zhang Z, Tang C, et al. The δ subunit of F1Fo-ATP synthase is required for pathogenicity of *Candida albicans*. Nature Communications. 2021;12(1):6041.
146. Song J, Pfanner N, Becker T. Assembling the mitochondrial ATP synthase. Proceedings of the National Academy of Sciences of the United States of America. 2018;115(12):2850-2852.
147. Duvezin-Caubet S, Caron M, Giraud M-F, Velours J, di Rago J-P. The two rotor components of yeast mitochondrial ATP synthase are mechanically coupled by subunit delta. Proceedings of the National Academy of Sciences of the United States of America. 2003;100(23):13235-13240.
148. Alarco AM, Raymond M. The bZip transcription factor Cap1p is involved in multidrug resistance and oxidative stress response in *Candida albicans*. Journal of

Bacteriology. 1999;181(3):700-708.
149. Zhang X, De Micheli M, Coleman ST, Sanglard D, Moye-Rowley WS. Analysis of the oxidative stress regulation of the *Candida albicans* transcription factor, Cap1p. Molecular Microbiology. 2000;36(3):618-629.
150. Dai B-D, Wang Y, Zhao L-X, Li D-D, Li M-B, Cao Y-B, et al. Cap1p attenuates the apoptosis of *Candida albicans*. The FEBS Journal. 2013;280(11):2633-2643.
151. Dai B-D, Cao Y-Y, Huang S, Xu Y-G, Gao P-H, Wang Y, et al. Baicalein induces programmed cell death in *Candida albicans*. Journal of Microbiology and Biotechnology. 2009;19(8):803-809.
152. Kelly J, Rowan R, McCann M, Kavanagh K. Exposure to caspofungin activates Cap and Hog pathways in *Candida albicans*. Medical Mycology. 2009;47(7):697-706.
153. Murakami S, Mealey BL, Mariotti A, Chapple ILC. Dental plaque–induced gingival conditions. Journal of Clinical Periodontology. 2018;45(S20):17-27.
154. Safiaghdam H, Oveissi V, Bahramsoltani R, Farzaei MH, Rahimi R. Medicinal plants for gingivitis: a review of clinical trials. Iranian Journal of Basic Medical Sciences. 2018;21(10):978-991.
155. Jiang K, Chen L-L, Wang S-F, Wang Y, Li Y, Gao K. Anti-inflammatory terpenoids from the leaves and twigs of *Dysoxylum gotadhora*. Journal of Natural Products. 2015;78(5):1037-1044.
156. Zhao Q-Q, Wang S-F, Li Y, Song Q-Y, Gao K. Terpenoids with anti-inflammatory activity from *Abies chensiensis*. Fitoterapia. 2016;111:87-94.
157. Costa J, Islam M, Santos P, Ferreira P, Oliveira G, Alancer M, et al. Evaluation of antioxidant activity of phytol using non-and pre-clinical models. Current Pharmaceutical Biotechnology. 2016;17(14):1278-1284.
158. Silva RO, Sousa FBM, Damasceno SRB, Carvalho NS, Silva VG, Oliveira FRMA, et al. Phytol, a diterpene alcohol, inhibits the inflammatory response by reducing cytokine production and oxidative stress. Fundamental & Clinical Pharmacology. 2014;28(4):455-464.
159. Lee W, Woo E-R, Lee DG. Phytol has antibacterial property by inducing oxidative stress response in *Pseudomonas aeruginosa*. Free Radical Research. 2016;50(12):1309-1318.
160. Carvalho AMS, Heimfarth L, Pereira EWM, Oliveira FS, Menezes IRA, Coutinho HDM, et al. Phytol, a chlorophyll component, produces antihyperalgesic, anti-inflammatory, and antiarthritic effects: possible NF-κB pathway involvement and reduced levels of the proinflammatory cytokines TNF-α and IL-6. Journal of Natural Products. 2020;83(4):1107-1117.
161. Abbas MH, Al-Yaseen A, Alhamadi W. Prevalence of *Staphylococcus aureus* among gingivitis in patient with orthodontic wires in Kufa city/Iraq. Pakistan Journal of Biotechnology. 2017;14(1):91-96.
162. McCarney R, Warner J, Iliffe S, van Haselen R, Griffin M, Fisher P. The Hawthorne Effect: a randomised, controlled trial. BMC Medical Research Methodology. 2007;7:30-30.
163. Patil S, Rao RS, Majumdar B, Anil S. Clinical appearance of oral *Candida* infection and therapeutic strategies. Frontiers in Microbiology. 2015;6:1391-1391.

มหาวิทยาลัยนเรศวร

BIOGRAPHY

Name-Surname Watunyoo Buakaew

Date of Birth

Address

Current Position Ph.D. Candidate

Work Experience
1 October 2021 - 31 March 2022
Visiting reseacher at The Brindley laboratory
Department of Microbiology, Immunology & Tropical Medicine
Research Center for Neglected Diseases of Poverty
School of Medicine & Health Sciences
The George Washington University

Education Background
2017 - Present
Ph.D. in Biomedical Sciences, Faculty of Allied Health Sciences, Naresuan University
2013 - 2017
B.Sc. in Medical Technology, Faculty of Allied Health Sciences, Naresuan University

Publication
1. Buakaew W, Pankla Sranujit R, Noysang C, Krobthong S, Yingchutrakul Y, Thongsri Y, Potup P, Daowtak K and Usuwanthim K (2022) Proteomic Analysis Reveals Proteins Involved in the Mode of Action of β-Citronellol Identified From Citrus hystrix DC. Leaf Against Candida albicans. Front. Microbiol. 13:894637. doi: 10.3389/fmicb.2022.894637

2. Buakaew, W.; Sranujit, R.P.; Noysang, C.; Sangouam, S.; Suphrom, N.; Thongsri, Y.; Potup, P.; Usuwanthim, K. Evaluation of Mouthwash Containing Citrus hystrix DC., Moringa oleifera Lam. and Azadirachta indica A. Juss. Leaf Extracts on Dental Plaque and Gingivitis. Plants 2021, 10, 1153. https://doi.org/10.3390/plants10061153

3. Buakaew, W.; Pankla Sranujit, R.; Noysang, C.; Thongsri, Y.; Potup, P.; Nuengchamnong, N.; Suphrom, N.; Usuwanthim, K. Phytochemical Constituents of Citrus hystrix DC. Leaves Attenuate Inflammation via NF-κB Signaling and NLRP3 Inflammasome Activity in Macrophages. Biomolecules 2021, 11, 105. https://doi.org/10.3390/biom11010105

Awards
Research and Researchers for Industries (RRI) Ph.D. Scholarship (PHD60I0053)